

MODEL RISER TEST FOR VORTEX INDUCED
VIBRATION IN A SHEARED CURRENT

LIN ZHU



Model riser test for vortex induced vibration in a sheared current

BY

Lin Zhu, B.Eng.

**A thesis submitted to the school of graduate studies in partial fulfillment
of the requirements for the degree of master of engineering**

March 2006

**Faculty of Engineering and Applied Science
Memorial University of Newfoundland
St. John's, Newfoundland, Canada**

UMI Number: MR30521

INFORMATION TO USERS

The quality of this reproduction is dependent upon the quality of the copy submitted. Broken or indistinct print, colored or poor quality illustrations and photographs, print bleed-through, substandard margins, and improper alignment can adversely affect reproduction.

In the unlikely event that the author did not send a complete manuscript and there are missing pages, these will be noted. Also, if unauthorized copyright material had to be removed, a note will indicate the deletion.

UMI[®]

UMI Microform MR30521

Copyright 2007 by ProQuest Information and Learning Company.

All rights reserved. This microform edition is protected against unauthorized copying under Title 17, United States Code.

ProQuest Information and Learning Company
300 North Zeeb Road
P.O. Box 1346
Ann Arbor, MI 48106-1346

Abstract

This thesis describes a laboratory investigation and a method for analysis of multi-mode vortex induced vibration of a flexible slender riser model which was subjected to a sheared current and a uniform current. The Reynolds number of the tests was in the region from 2127 to 40,171 which belonged to the subcritical range.

The model riser was made of an 8.5 m long and 0.047 m diameter rubber hose. Twenty pairs of accelerometers were spaced inside the rubber hose to monitor the in-line and crossflow vortex induced vibration responses which will be abbreviated as VIV responses later. The simplified shear flow was produced by a 4 m or 3.5 m long and 38 cm diameter PVC pipe. The model riser segment covered by the PVC pipe stayed in still water and the other part was subjected to a uniform velocity.

A total of 120 test runs were conducted in the VIV experiment. The test flow velocity range was from 0.1 to 1.0 m/s and increments were 0.1 m/s. The duration of each run was two minutes. Most tests were done twice for the same velocity profile and same pretension in respectively up run test and down run test. The so-called up run test denotes that test current velocities change from low to high. In contrast, the down run test represents that test current velocities change from high to low. In addition, a thirty minute data acquisition sustained test was performed in a sheared current.

The test analysis was conducted in the time-domain, the frequency-domain and the space-domain. Close attention was paid to investigation of the multi-mode responses, the lock in phenomenon, the difference between the up run test and down run test, and sudden changes occurring in the thirty minute data acquisition sustained test.

In the thesis, a comparison method is used to help understand the behavior of the VIV responses. The riser VIV test results in uniform currents had been completed before. These test results were familiar to us. Through comparing the test results in the sheared currents with the uniform currents, the test results in sheared currents can be understood better. A rough comparison of the two uniform tests in the Ice Tank and in the Flume Tank is done. Here it was found that reduced velocity V^* corresponding to the model VIV maximum amplitude does not change in between these two tests.

Acknowledgments

I would like to particularly thank here:

- 1) Petroleum Research Atlantic Canada; Natural Sciences and Engineering Research Council, Canada; National Research Council, Canada, for their financial assistance to the VIV project.
- 2) Dr. Neil Bose, Professor of ocean and naval architectural engineering, for his supervision, and guidance.
- 3) Mr. George Legge at the Flume Tank of the Marine Institute, for his help with experiments.
- 4) Mr. Don Spencer, Vice-President of Oceanic Consulting Corporation, for his suggestions.
- 5) Mr. Billy Bidgood and other staff in the welding/sheet metal shop, for their help in preparing the experiment devices and setup.
- 6) Diver team in Marine Lab of MUN, for their help to the experiment setup.
- 7) Finally, my husband Xiangqun Li, for his understanding and support, and work term student Michael Stamp, for his help.

Contents

Abstract

Acknowledgement

List of Figures

List of Tables

List of Symbols

1. Introduction

2. Literature Review

2.1 Previous work on VIV experiments

2.1.1 VIV experiments

2.1.2 VIV test in sheared current

2.1.3 Tests comparisons

2.2 Miscellany

3. Experiment

3.1 Experiment aim

3.2 The Flume Tank in the Marine Institute and its facilities

3.3 Shear current

3.4 Riser model

3.4.1 Theory of model design

3.4.2 Model building

3.5 Experiment and experimental apparatus design

3.5.1 Experiment design

3.5.2 Experiment apparatus design

3.6 Calibration

3.6.1 Load cell calibration

3.6.2 Accelerometer calibration

3.7 Installation of the experiment setup

3.8 General procedures of experiments

3.8.1 Shear current produced by the 4 m long pipe

3.8.2 Shear current produced by the 3.5 m long pipe

3.8.3 Uniform current without block pipe

3.8.4 Uniform current test in the Ice Tank

3.9 Discussion or summary

4. Test analysis

4.1 Time-domain analysis

4.1.1 Amplitude versus current velocity

4.1.1.1 Amplitude comparison between shear currents and uniform current

4.1.1.2 Amplitude comparison between different pretensions

4.1.1.3 Amplitude comparison between different positions on the model riser

4.1.1.4 Amplitude comparison between tests in the Ice Tank and the Flume Tank

4.1.2 Frequency versus current velocity

4.1.2.1 Comparison of frequency between different currents

4.1.2.2 Comparison of frequency between different tensions

4.2. Frequency-domain analysis

4.2.1 Comparison of power spectrum between different tensions

4.2.2 Comparison of power spectrum between different velocities

4.2.3 Comparison of power spectrum between different positions over riser length

4.2.4 Power spectrum comparison between different currents

4.3 Space-domain analysis

4.3.1 Modal components in the VIV response at various flow velocity

4.3.2 Modal components vs. current velocity at various modes

4.3.4 Vibration trajectories

4.4 Tension

4.5 Thirty minute sustained data acquisition test

5. Conclusion

Reference

Appendix A

Appendix B

Appendix C

List of Figures

Figure 2-1 The sheared flow consisted of two slabs with different uniform flows

Figure 2-2 Non-uniform cross-section pipe tested in uniform flow

Figure 3-1 The Flume Tank

Figure 3-2 The sketch of the Flume Tank

Figure 3-3 Shear current category

Figure 3-4 The sketch of the model riser

Figure 3-5 The sketch of experiment arrangement

Figure 3-6 Experiment apparatus

Figure 3-7 The calibration testing ground

Figure 3-8 The calibration testing ground

Figure 3-9 No.5 and No. 6 accelerometer fitted sinusoidal curves of calibration

Figure 3-10 No.11 and No.12 accelerometer fitted sinusoidal curves of calibration

Figure 3-11 No.21 and No.22 accelerometer fitted sinusoidal curves of calibration

Figure 3-12 No.27 and No.28 accelerometer fitted sinusoidal curves of calibration

Figure 3-13 Diver installing experiment apparatus

Figure 3-14 Tests under shear current produced by a 4 m block pipe

Figure 3-15 Tests under shear current produced by a 3.5 m block pipe

Figure 3-16 Tests under uniform current without block pipe

Figure 4-1 The average and significant amplitude of in-line in shear current produced by a 4 m block pipe

Figure 4-2 The average and significant amplitude of in-line in shear current produced by a 3.5 m block pipe

Figure 4-3 The average and significant amplitude of in-line in uniform current

Figure 4-4 The average and significant amplitude of the cross-flow in shear current produced by a 4 m block pipe

Figure 4-5 The average and significant amplitude of the cross-flow in shear current produced by a 3.5 m block pipe

Figure 4-6 The average and significant amplitude of the cross-flow in uniform current

Figure 4-7 The average and significant amplitude of the cross-flow at pretension 460 N in shear current produced by a 4 m block pipe

Figure 4-8 The average and significant amplitude of the cross-flow at pretension 520 N in shear current produced by a 4 m block pipe

Figure 4-9 The average and significant amplitude of the cross-flow at pretension 690 N in shear current produced by a 4 m block pipe

Figure 4-10(a) The average in-line vibration amplitude at $x=2.024$ m in shear current produced by a 3.5m block pipe

Figure 4-10(b) The average in-line vibration amplitude at $x=2.833$ m in shear current produced by a 3.5 m block pipe

Figure 4-10(c) The average in-line vibration amplitude at $x=4.452$ m in shear current produced by a 3.5 m block pipe

Figure 4-10(d) The average in-line vibration amplitude at $x=5.262$ m in shear current produced by a 3.5 m block pipe

Figure 4-11(a) The average in-line vibration amplitude at $x=2.024$ m in uniform current

Figure 4-11(b) The average in-line vibration amplitude at $x=2.833$ m in uniform current

Figure 4-11(c) The average in-line vibration amplitude at $x=4.452$ m in uniform current

Figure 4-11(d) The average in-line vibration amplitude at $x=5.262$ m in uniform current

Figure 4-12(a) The average cross-flow vibration amplitude at $x=2.024$ m in shear current produced by a 3.5 m block pipe

Figure 4-12(b) The average cross-flow vibration amplitude at $x=2.833$ m in shear current produced by a 3.5 m block pipe

Figure 4-12(c) The average cross-flow vibration amplitude at $x=4.452$ m in shear current produced by a 3.5 m block pipe

Figure 4-12(d) The average cross-flow vibration amplitude at $x=5.262$ m in shear current produced by a 3.5 m block pipe

Figure 4-13(a) the average cross-flow vibration amplitude at $x=2.024$ m in uniform current

Figure 4-13(b) the average cross-flow vibration amplitude at $x=2.833$ m in uniform current

Figure 4-13(c) the average cross-flow vibration amplitude at $x=4.452$ m in uniform current

Figure 4-13(d) the average cross-flow vibration amplitude at $x=5.262$ m in uniform current

Figure 4-14 The average vibration amplitude in uniform current tested in the Flume Tank

Figure 4-15 The average vibration amplitude in uniform current tested in the Ice Tank

Figure 4-16 The frequency of in-line VIV in shear current produced by a 4 m block pipe

Figure 4-17 The frequency of in-line VIV in shear current produced by a 3.5 m block pipe

Figure 4-18 The frequency of in-line VIV in uniform current

Figure 4-19 The frequency of cross-flow VIV in shear current produced by a 4 m block pipe

Figure 4-20 The frequency of cross-flow VIV in shear current produced by a 3.5 m block pipe

Figure 4-21 The frequency of cross-flow VIV in uniform current

Figure 4-22 The frequency of in-line in shear current produced by a 4 m block pipe and pretension=460 N

Figure 4-23 The frequency of in-line in shear current produced by a 4 m block pipe and pretension=520 N

Figure 4-24 The frequency of in-line in shear current produced by a 4 m block pipe and pretension=690 N

Figure 4-25 The Power spectrum of in-line VIV in shear current produced by a 4 m block pipe

Figure 4-26 The Power spectrum of in-line VIV in shear current produced by a 4 m block pipe

Figure 4-27 The Power spectrum of in-line VIV in shear current produced by a 4 m block pipe

Figure 4-27(a) The power spectrum of in-line VIV in shear current produced by a 3.5 m block pipe at $v^*=2.68$ ($U=0.1$ m/s)

Figure 4-27(b) The power spectrum of in-line VIV in shear current produced by a 3.5 m block pipe

at $v^*=5.36$ ($U=0.2$ m/s)

Figure 4-27(c) The power spectrum of in-line VIV in shear current produced by a 3.5 m block pipe at $v^*=8.05$ ($U=0.3$ m/s)

Figure 4-27(d) The power spectrum of in-line VIV in shear current produced by a 3.5 m block pipe at $v^*=10.73$ ($U=0.4$ m/s)

Figure 4-27(e) The power spectrum of in-line VIV in shear current produced by a 3.5 m block pipe at $v^*=13.41$ ($U=0.5$ m/s)

Figure 4-27(f) The power spectrum of in-line VIV in shear current produced by a 3.5 m block pipe at $v^*=16.09$ ($U=0.6$ m/s)

Figure 4-27(g) The power spectrum of in-line VIV in shear current produced by a 3.5 m block pipe at $v^*=18.77$ ($U=0.7$ m/s)

Figure 4-27(h) The power spectrum of in-line VIV in shear current produced by a 3.5 m block pipe at $v^*=21.46$ ($U=0.8$ m/s)

Figure 4-27(i) The power spectrum of in-line VIV in shear current produced by a 3.5 m block pipe at $v^*=24.14$ ($U=0.9$ m/s)

Figure 4-27(j) The power spectrum of in-line VIV in shear current produced by a 3.5 m block pipe at $v^*=26.82$ ($U=1.0$ m/s)

Figure 4-28(a) The cross-flow VIV power spectrum at $x=0.81$ m in shear current produced by a 3.5 m pipe

Figure 4-28(b) The cross-flow VIV power spectrum at $x=1.214$ m in shear current produced by a 3.5 m pipe

Figure 4-28(c) The cross-flow VIV power spectrum at $x=1.619$ m in shear current produced by a 3.5 m pipe

Figure 4-28(d) The cross-flow VIV power spectrum at $x=2.024$ m in shear current produced by a 3.5 m pipe

Figure 4-28(e) The cross-flow VIV power spectrum at $x=2.833$ m in shear current produced by a 3.5 m pipe

Figure 4-28(f) The cross-flow VIV power spectrum at $x=3.238$ m in shear current produced by a 3.5 m pipe

Figure 4-28(g) The cross-flow VIV power spectrum at $x=3.643$ m in shear current produced by a 3.5 m pipe

Figure 4-28(h) The cross-flow VIV power spectrum at $x=4.048$ m in shear current produced by a 3.5 m pipe

Figure 4-28(i) The cross-flow VIV power spectrum at $x=4.452$ m in shear current produced by a 3.5 m pipe

Figure 4-28(j) The cross-flow VIV power spectrum at $x=4.857$ m in shear current produced by a 3.5 m pipe

Figure 4-28(k) The cross-flow VIV power spectrum at $x=5.262$ m in shear current produced by a 3.5 m pipe

Figure 4-28(l) The cross-flow VIV power spectrum at $x=6.476$ m in shear current produced by a 3.5 m pipe

Figure 4-28(m) The cross-flow VIV power spectrum at $x=6.881$ m in shear current produced by a 3.5 m pipe

Figure 4-28(n) The cross-flow VIV power spectrum at $x=7.286$ m in shear current produced by a 3.5 m pipe

Figure 4-28(o) The cross-flow VIV power spectrum at $x=7.691$ m in shear current produced by a 3.5 m pipe

Figure 4-29 The Power spectrum of in-line VIV in shear current produced by a 4 m pipe

Figure 4-30 The Power spectrum of in-line VIV in shear current produced by a 3.5 m pipe

Figure 4-31 The Power spectrum of in-line VIV in uniform current

Figure 4-32(a) The in-line VIV modal component distribution in shear current produced by a 4 m pipe and reduced velocity from 2.68 to 10.73

Figure 4-32(b) The in-line VIV modal component distribution in shear current produced by a 4 m pipe and reduced velocity from 13.41 to 21.46

Figure 4-32(c) The in-line VIV modal component distribution in shear current produced by a 4 m pipe and reduced velocity 24.14 and 26.82

Figure 4-33(a) The cross-flow VIV modal component distribution in shear current produced by a 4 m pipe and reduced velocity from 2.68 to 10.73

Figure 4-33(b) The cross-flow VIV modal component distribution in shear current produced by a 4 m pipe and reduced velocity from 13.41 to 21.46

Figure 4-33(c) The cross-flow VIV modal component distribution in shear current produced by a 4 m pipe and reduced velocity 13.41 and 21.46

Figure 4-34(a) The in-line VIV modal component distribution in shear current produced by a 3.5 m pipe and reduced velocity from 2.68 to 10.73

Figure 4-34(b) The in-line VIV modal component distribution in shear current produced by a 3.5 m pipe and reduced velocity from 13.41 to 21.46

Figure 4-34(c) The in-line VIV modal component distribution in shear current produced by a 3.5 m pipe and reduced velocity 24.14 and 26.82

Figure 4-35(a) The cross-flow VIV modal component distribution in shear current produced by a 3.5 m pipe and reduced velocity from 2.68 to 10.73

Figure 4-35(b) The cross-flow VIV modal component distribution in shear current produced by a 3.5 m pipe and reduced velocity from 13.41 to 21.46

Figure 4-35(c) The cross-flow VIV modal component distribution in shear current produced by a 3.5 m pipe and reduced velocity 24.14 and 26.82

Figure 4-36 The in-line VIV modal component distribution in uniform current and reduced velocity from 2.68 to 10.73

Figure 4-37 The cross-flow VIV modal component distribution in uniform current and reduced velocity from 2.68 to 10.73

Figure 4-38 The component of in-line mode 1 in shear current produced by a 3.5 m pipe

Figure 4-39 The component of in-line mode 2 in shear current produced by a 3.5 m pipe

Figure 4-40 The component of in-line mode 3 in shear current produced by a 3.5 m pipe

Figure 4-41 The component of in-line mode 4 in shear current produced by a 3.5 m pipe

Figure 4-42 The component of in-line mode 5 in shear current produced by a 3.5 m pipe

Figure 4-43 The component of in-line mode 6 in shear current produced by a 3.5 m pipe

Figure 4-44 The component of in-line mode 7 in shear current produced by a 3.5 m pipe

Figure 4-45 The component of in-line mode 8 in shear current produced by a 3.5 m pipe

Figure 4-46 The component of in-line mode 9 in shear current produced by a 3.5 m pipe

Figure 4-47 The component of in-line mode 10 in shear current produced by a 3.5 m pipe

Figure 4-48 The component of cross-flow mode 1 in shear current produced by a 3.5 m pipe

Figure 4-49 The component of cross-flow mode 2 in shear current produced by a 3.5 m pipe

Figure 4-50 The component of cross-flow mode 3 in shear current produced by a 3.5 m pipe

Figure 4-51 The component of cross-flow mode 4 in shear current produced by a 3.5 m pipe

Figure 4-52 The component of cross-flow mode 5 in shear current produced by a 3.5 m pipe

Figure 4-53 The component of cross-flow mode 6 in shear current produced by a 3.5 m pipe

Figure 4-54 The component of cross-flow mode 7 in shear current produced by a 3.5 m pipe

Figure 4-55 The component of cross-flow mode 8 in shear current produced by a 3.5 m pipe

Figure 4-56 The component of cross-flow mode 9 in shear current produced by a 3.5 m pipe

Figure 4-57 The component of cross-flow mode 10 in shear current produced by a 3.5 m pipe

Figure 4-58 Trajectories of VIV under pretension=690 N, shear current produced by 3.5 m pipe, and reduced velocity $V^*=8.05$

Figure 4-59 Trajectories of VIV under pretension=690 N, shear current produced by a 3.5 m pipe, and reduced velocity $V^*=16.09$

Figure 4-60 Trajectories of VIV under pretension=690 N, shear current produced by a 3.5 m pipe, and reduced velocity $V^*=18.77$

Figure 4-61 Average tension under pretension=690 N in different current

Figure 4-62 Average tension under various pretensions in shear current produced by a 4 m pipe

Figure 4-63 Comparison of in-line VIV amplitude of thirty minutes data acquisition sustained test

Figure 4-64 Comparison of cross-flow VIV amplitude of thirty minutes data acquisition sustained test

Figure 4-65 Comparison of in-line VIV frequency of thirty minutes data acquisition sustained test

Figure 4-66 Comparison of cross-flow VIV frequency of thirty minutes data acquisition sustained test

List of Tables

Table 3-1 Accelerometer locations in the model riser

Table 3-2 Scale factors of accelerometers

Table 3-3 Orientation angles of accelerometers

Table 4-1 Average current velocity versus V^*

Table 4-2 Natural frequencies of various modes

Table 4-3 Time segment number versus time

Chapter 1

Introduction

Presently, oil and natural gas are playing a crucial role in society. They contribute over 60 % of the globe's total energy needs [Hearn, 2005]. Since the 19th century, the first oil well was found in the U.S.A; the offshore became continuously considered because offshore structures were always in a harsh environment. Recently, oil and gas exploration and development on the ocean has been moving into deep-sea and ultra-deep sea zones; this brings more challenges and risks not only to offshore structures but also to platform mooring systems and the drill oil systems which include pipelines and risers.

In deep water oil operation, more floating platforms are used instead of the jacket-tower type platforms. With these changes, the riser system property, which is a critical part of a floating production system, is further focused. Unlike risers in a jacket-tower type platform that can be fixed in platform structural members and follows them up vertically to the water surface, most risers for a floating platform are free, non-vertical catenary with big top tension and sometimes encounter touch down points. In these cases, the uses

of a rigid riser are limited and flexible risers, which differ from the rigid riser in its low bending stiffness, are widely employed.

Both rigid and flexible risers are circular cylinders. If a cylinder is in a water current and orthogonal to the current, current-induced vortex-induced vibrations (VIV) occur. Actually, VIV is a major reason to cause marine riser fatigue damage. The current flow over the cylinder causes vortices to be shed, which consequently produce periodic oscillations. The oscillations are separated into vibration in the in-line and cross flow directions.

As water depth increases, the riser becomes longer and more slender. Comparing VIV in shallow water, the feature for VIV of a deep water riser is several mode vibrations, which is called multi-modal vibration. Multi-modal vibration responses depend on the characteristic of vortex-shedding, which is of great interest to the industry and academia now. Understanding the characteristics of vortex-shedding well is an essential condition of numerical imitation of multi-modal vibration [Li, 2005].

Currents in deep water may be caused by tidal motions, wind-stress, atmospheric pressure gradients, wave-induced forces, river out-flows, large-scale quasi-steady water surface slopes and associated horizontal density gradient. They contribute to the current in different magnitude and direction. Because of being composed of many components, the current is rarely uniform in deep ocean. Current velocities and current directions may vary over the riser length. The varying current is defined as a shear current. VIV of flexible riser in uniform current has been researched and conclusions have been presented

in many from multitudinous papers; but VIV of a flexible riser in a shear current is less well known.

This thesis presents experimental studies on a flexible riser VIV in a sheared current and compares the test results with VIV in a uniform current. The organization of the thesis is made in the following manner:

Literature review of previous research on VIV tests, in particular VIV tests in a shear current are described in Chapter 2. The introduction of the model riser and the design of the experiment and experiment apparatus are reviewed in Chapter 3. They include the theoretical basis of the riser model design and construction, difficulties and problems in the experiment, experimental apparatus design, and solutions to these issues are presented. Finally, the test procedure is introduced. Experimental data and result analysis is introduced in Chapter 4. The analysis is respectively processed in time-domain, frequency-domain and space-domain to investigate high mode response, lock-in phenomena, and movement in the in-line and cross current directions. Conclusions from the research are presented in Chapter 5.

Chapter 2

Literature review

2.1 Previous work on VIV experiments

2.1.1 VIV experiments

Over the past several decades, both small scale model experiments tested in tanks and full scale model experiments tested in rivers or the sea have been initiated to investigate marine riser VIV responses. Models can be categorized as rigid and flexible. Tests can be categorized as half-and-half tests followed by a numerical simulation and complete test. Half-and-half tests followed by a numerical simulation means that unknowns or parts that are difficult to simulate are measured by tests, such as some hydrodynamic coefficients. The rest are simulated by numerical simulation. The advantages of this method are saving funds and more accurate simulation.

A half-and-half test followed by a numerical simulation was done by Chen et al. [1996]. A shaker, strain gauges and displacement transducer were used directly to measure fluid damping which are not understood well and are hard to numerically simulate accurately. Then, numerical simulation was used to investigate tube vibration response induced by the vortices.

A VIV experiment on a flexible cylinder was carried out by Fujarra et al. [1998] in Naval and Ocean Engineering Laboratory Facilities (NOELF) at the S. Paulo State Technological Research Institute. The test purpose was to investigate parameters which affect vibration such as damping and added mass. The model was a cantilever model which was vertically clamped on the tank carriage. The tested Reynolds number range was 6×10^3 to 4×10^4 and a lock-in phenomenon was found in that test.

A VIV experiment was done by Wilde and Huijsmans [2001] in MARIN's high speed towing tank. The model was a 206 mm diameter, 3.84 m long cylinder. The tested Reynolds number was from 2×10^5 to 5×10^5 . The test purpose was to compare the high Reynolds number (Rn) results with the lower Rn data and to measure the drag and lift coefficients [Sarpkaya, 1979].

A 14.11 cm diameter ABS pipe was used to carry out the VIV test by Allen and Henning [1997] in the Naval Surface Warfare Center's David Taylor Model Basin in Carderock, Maryland. The tested Reynolds number was from 2×10^5 to 6×10^5 . Drag force measurement was the test object.

A laboratory investigation for VIV of catenary risers was carried out by Lie et al. [2001] in the towing tank at MARINTEK in Trondheim, Norway. The model was a 58 m long and 0.026 m diameter cylinder. It was fixed to the carriage vertically. The tests were performed in a combination of uniform current and waves. The force and torque at the riser upper end were measured. The test purpose was to better understand hydrodynamics of catenary risers including Strouhal number, added mass and lift coefficients. A new non-linear time domain analysis was developed to apply in the test analysis.

In Oct. 2004, Li managed a flexible model riser VIV test in the Ice Tank of the National Research Council- Institute for Ocean Technology. That test included three parts, shaker-excitation test in air, shaker-excitation test in water, and VIV test in uniform current. In the shaker-excitation test, added mass, damping, stiffness, and natural frequencies from mode 1 to mode 10 were investigated. The uniform current VIV test purpose is to understand multi-modal vibration of the flexible riser. The test data analysis method and corresponding software were developed for previous tests in the Ice Tank and this test.

In Li's research [Li, 2005], the riser model was an 8.5 m long, 0.047 m diameter flexible riser model. The riser model was installed horizontally on a steel structure which was connected to the tank carriage. Lock-in phenomenon was found in the tests. So-called lock-in phenomenon occurs when the VIV response frequencies remain constant, which is usually cylinder natural frequency, so that the linear relation between the response frequencies and the current velocities is violated.

This same flexible riser model was used in the tests which are described in this thesis. A detailed description of the riser will be presented in Chapter 3.

2.1.2 VIV test in sheared current

A cylinder test in sheared current was done by Vandiver and Mazel [1976] in Castine, Maine. From the test, they found that lock-in phenomena appeared at very high mode vibration. The vibration response amplitudes were around $\pm 1/2$ to ± 1 diameter. In 1981, Vandiver and his colleagues completed two cylinder tests at the same place [Vandiver, 1993]. The first cylinder was made of cable and had a length of 22.86 m and a diameter of 3.18 cm. The second was made of steel pipe and was 22.86 m and had a diameter of

4.13 cm. Tension, acceleration, current and drag were measured in the tests. In-line and cross-flow amplitudes were obtained through double integration of the acceleration. Lock-in occurred in the test. They found lock-in occurred around the cylinder modal natural frequency which can be estimated using the following formula:

$$f_{nk} = \frac{k}{2L} \sqrt{\frac{T}{m_T}} \quad (2 - 1)$$

where f_{nk} are the natural frequencies with the unit of Hz, and m_T is the total mass per unit length including structural mass and added mass, k is the modal number.

In 1983, two more VIV tests were done on slender cables in the Arctic and St. Croix in the U.S. Virgin Islands [Vandiver, 1993]. One of the test's purposes was to determine which drag coefficient was more appropriate to use in engineering design: the drag coefficients under lock-in conditions or the reduced drag coefficient under random vibration. Another purpose was to investigate if lock-in occurs in strong shear currents. The test results showed that lock-in never occurred in the tested conditions.

Sheared flow experiments were conducted at Lawrence, Massachusetts by Vandiver and Chung [1986]. The test cable was 17.68 m in length and 2.86 cm in diameter. Six pairs of accelerometers were placed in the cable. In the test, the highest excited mode number was five. Lock-in was not found. Later, Vandiver [1992] summarized that lock-in will not occur for risers with a large length to diameter ratio and vibrations with a high mode number. He also considered that lock-in occurs more easily in uniform flow than in shear flow.

All of the above sheared current tests took advantage of natural shear flows in rivers.

Vandiver et al. [1996] did a series of VIV shear current tests. The tests were conducted in a 3.66 m deep circulating channel with a 17.7 m deep pit. The test purpose is to

understand how two dimensionless parameters are used to predict lock-in in sheared flow conditions. A result from the tests was that a high lock-in possibility exists in low modal vibrations.

A series of tests with 90 m long, 30 mm diameter and 2 mm wall thickness model risers were performed at an open air test site in a Norwegian fjord by Huse et al. [1998]. The test was designed to investigate the riser VIV situation in a sheared current. They drew the conclusions as follows: The axial vibration could lead to large stress in the riser and hydrodynamic damping was insufficient to reduce the axial vibration problem significantly. Some types of dampers were suggested to reduce the axial vibrations.

A test for a 1300 m long full-scale riser was performed by Furnes et al. [1998] in a non-uniform current to measure acceleration and displacement in the coast of mid Norway. Five pairs of accelerometers with two linear accelerometers in each pair and two rotational rate sensors were used. The test's purpose was to improve the analysis tools to predict the VIV response.

A VIV test in sheared current was performed by Chaplin and Bearman [2004] in the DELTA FLUME. The model's diameter was 28 mm; length was 13.12 m; and mass ratio was 3. The model consisted of a steel cylinder and some layers of tape wrapped outside the steel cylinder. Thirty two bending strain gauges were arranged along the steel cylinder to measure strain of the steel cylinder; then vibration frequency and mode can be gained from the strain data. The model was installed vertically. The shear current profile was a block current. Incident current at the lower end of the 7 m riser was a uniform current; the rest of the riser was in still water. The maximum uniform current was 1m/s.

The vibration amplitude, which was measured in the test, was about 0.8 of the riser's diameter. Lock-in phenomenon was found in the test.

A long flexible cylinder was used by Marcollo and Hinwood [2005] to monitor riser VIV response in a spatially sheared flow. Five accelerometers were spaced along the riser to measure the riser motion. The sheared flow consisted of two slabs with different uniform flows, as shown in figure 2-1. A conclusion from the test results is that in-line vibration is more important than cross flow vibration in predicting single mode cross-flow lock-in in a sheared current.

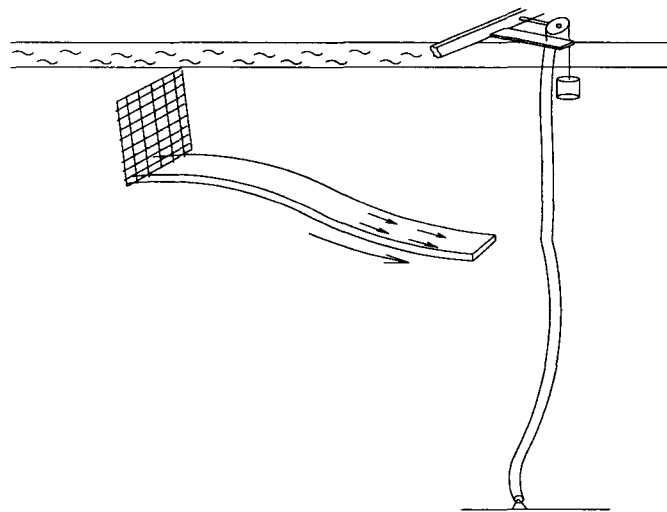


Figure 2-1 The sheared flow consisted of two slabs with different uniform flows

2.1.3 Tests comparisons

Test comparisons are usually done for two purposes. One of them is to help to understand unfamiliar results through the comparison between familiar test results and unfamiliar test results. This method was used in this thesis. As VIV tests in uniform current have been understood, test results in sheared currents can be understood better through comparison with test results in uniform currents. Another is to help understand the effects of the improvements through comparison tests between the original model and the

improved model, such as the bare riser VIV test and the VIV test of riser with suppressive coverage. So-called suppressive coverage is some special shape surface layer which encircles the cylinder to reduce VIV responses, such as strakes. In this test apparatus design, a rope strake was used; detail was described in Chapter 3.5.2. The comparison purpose for this case is to verify the suppressive coverage effectiveness or to further improve the suppressive coverage.

A series of VIV comparison tests were carried out by Hong and Choi [2001] in a towing water tank. Two 6 m long steel pipes with uniform cross-section and non-uniform cross-section were used to perform tests. The so-called non-uniform cross-section pipe was a pipe in which the cross-section changed. It is shown in Figure 2-2 and diameter D and diameter d were different. Five strain gauges were installed on each pipe to measure the vibration. Uniform cross-section pipe VIV responses were typical and relatively simple. Through comparing the results from two pipes with uniform cross-section and non-uniform cross-section, non-uniform cross-section pipe VIV response can be understood better, although it is relatively difficult to understand. Hong and Choi believe that uniform and non-uniform cross-section pipe VIV characteristics are the same as the uniform pipe VIV characteristics in uniform current and shear current. In other words, non-uniform cross-section pipe can be tested in a towing tank to simulate VIV conditions in a shear current.

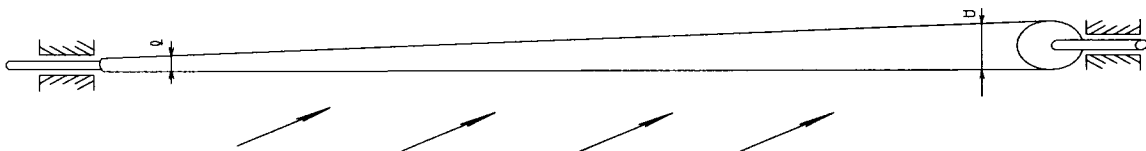


Figure 2-2 Non-uniform cross-section pipe tested in uniform flow

Another comparison test is that a bare and a staggered riser were tested in a uniform current and a sheared current. This test was completed by Lie et al. [1998]. The bare riser test result was typical and relatively simple, especially in a uniform current condition. Through comparing the test results of a bare and staggered riser model, the difficult and unfamiliar staggered riser model test results become easier to understand. The VIV frequencies of both a bare and staggered riser observe $St = 0.15$ well. The riser shifted between lock-in and non-lock-in; in other words, lock-in occurs in some cases, and no-lock-in is observed in the remaining cases.

2.2 Miscellany

So far, many small scale and full scale riser tests have been completed for different purposes which are described above. From recent literature, the multi-mode vibration investigations are popular; but the number of accelerometers installed in the riser model is usually not enough to measure high modes. Many researchers used strain gauges in their tests to measure multi-mode vibration because strain gauges have the advantages of a small body and of being easily installed. Simultaneously, strain gauge usage has many limits, especially when used with a flexible riser. In the tests done in the NRC-IOT Ice tank and the test done in the MI Flume Tank, enough accelerometers were installed in the model to measure the flexible riser up to the 10th mode of vibration.

Chapter 3

Experiment

Experimental research is a chief method in the investigation of long span riser VIV; especially now, riser VIV properties are still not completely understood. Experiments can help researchers obtain some insight into the problems and to gain an understanding of the properties.

In this chapter, an experiment for pipe riser in a shear current is described. The key to the experiment is how to make a sheared current in the Flume Tank at the Marine Institute. The riser model used was an 8.5 m long existing model. It was once used to carry out shaker exciting tests in air and water, and the VIV test in a uniform current in the Ice Tank of the National Research Council of Canada - The Institute for Ocean Technology in Oct. 2004 [Li, 2005].

In the subsequent sections, the model, experiment apparatus design, and experimental design will be introduced respectively. Description of model test procedures will also be given.

3.1 Experiment aim

1) Investigate flexible riser VIV in a sheared current and compare the VIV response between uniform and sheared currents.

2) Investigate the high mode vibration situation induced by a sheared current and observe if the lock-in phenomena exists.

3) Develop basic understanding of VIV for slender structures in deep water sheared currents.

3.2 The Flume Tank in the Marine Institute and its facilities

The test was performed in the Flume Tank of the Marine Institute from Nov 14-18, 2005. Figure 3-1 is a photo of the Flume Tank. This tank is the largest indoor flume tank in the world. Its length is 22 m; width is 8 m; and depth is 4 m. Maximum flow velocity is 1 m per second. Water holding capacity is around 700,000 liters. The Data Acquisition System has 32 High Speed Channels.

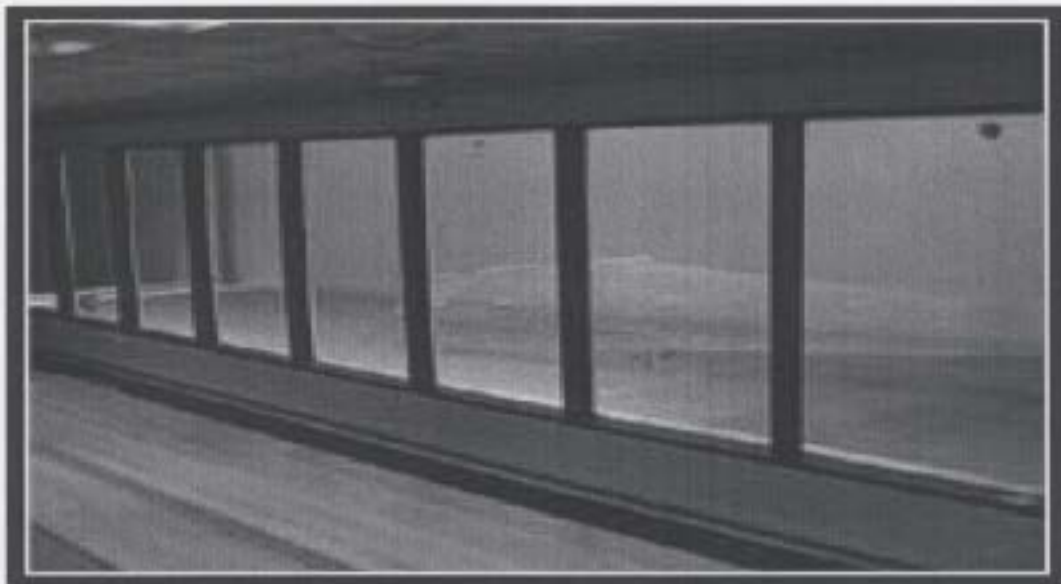
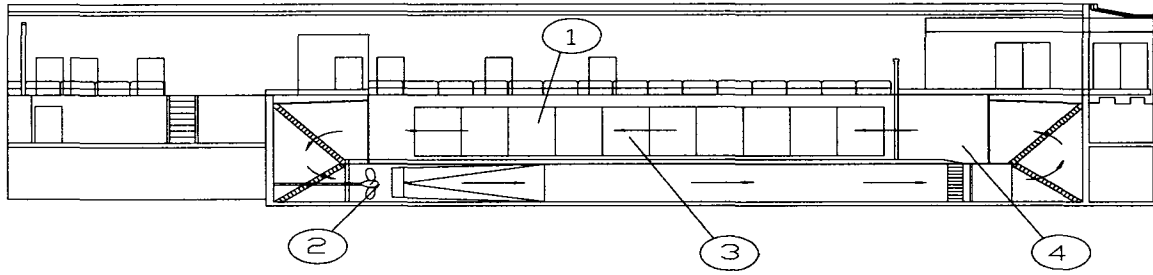


Figure 3-1 The Flume Tank

In the Flume Tank, water is driven by three Hydraulic Motors. Going through a rectifying section, a closely uniform current is produced in the working section. Moreover, several glass windows can provide favorable sight for observing a test, as shown in Figure 3-2.



- | | |
|--------------------|-----------------------|
| 1. glass windows | 2. hydraulic motors |
| 3. working section | 4. rectifying section |

Figure 3-2 The sketch of the Flume Tank

3.3 Shear current

If strength or direction of current, or both, vary along the riser length, the current is called a sheared current. Shear currents can be separated into two-dimensional and three-dimensional shear currents; and two-dimensional sheared currents also have various patterns. These patterns include positive shear currents, negative shear currents and block currents, as shown in Figure 3-3.

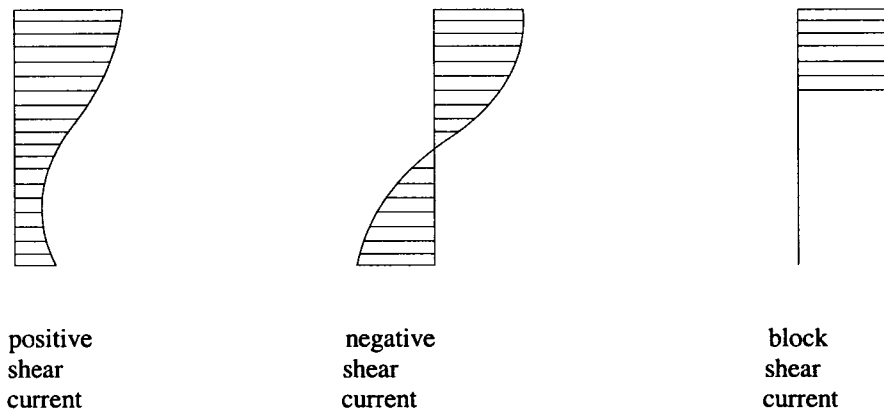


Figure 3-3 Shear current category

In the thesis, the VIV for a riser in block shear currents was the investigation objective.

3.4 Riser model

3.4.1 Theory of model design

A simplified theory description was used as a basis of the riser model design; but the detailed derivation of governing equations for risers is not shown here. It is introduced directly from Li's thesis [Li, 2005].

A Cartesian coordinate system is specified for a horizontal riser stretched across the width of the tank. The origin of the coordinate system is located at one end of the riser. The x-axis points along the direction of the riser model axial direction. The y-axis points in a horizontal direction parallel to the direction of flow, and, the z-axis points downward. On the x-z plane, the governing equation is:

$$m_T \frac{\partial^2 z(t, x)}{\partial t^2} + c_T \frac{\partial z(t, x)}{\partial t} - \frac{\partial}{\partial x} \left[T(t, x) \frac{\partial z(t, x)}{\partial x} \right] + EI \frac{\partial^4 z(t, x)}{\partial x^4} = f_v(t, x) \quad (3-1)$$

where m_T is the total mass per unit length, which can be written as $m_s + m_a$; m_a is added mass per unit length and m_s is structure mass per unit length. c_T is the total damping; $f_v(t, x)$ is the vortex-shedding force in the cross-flow direction, which can be written as $f_0 \sin(\omega t)$; $T(t, x)$ is the tension; E is elastic modulus and I is the moment of inertial of riser's cross-section (m^4).

The boundary conditions for the governing equation are

$$\left. \begin{array}{l} z(t, 0) = 0 \\ z(t, L) = 0 \\ M_y(t, 0) = 0 \\ M_y(t, L) = 0 \end{array} \right\} \quad (3-2)$$

From the hydrodynamic coefficient definition, added mass coefficient C_m , hydrodynamic damping coefficient C_d , and lift coefficient C_l can be written as

$$\left. \begin{aligned} m_a &= \frac{\pi}{4} \rho C_m D^2 \\ c_h &= \frac{1}{\pi} \rho C_d \omega z_0 \\ f_0 &= \frac{1}{2} \rho C_l D U^2 \end{aligned} \right\} \quad (3-3)$$

where, c_h is hydrodynamic damping which is a horizontal oscillation obstruction contributed by the fluid around riser. The total damping c_T in equation (3-1) equals c_h plus structure damping c_s . z_0 is the amplitude of an assumed sine vibration.

Substituting equations (3-2) and (3-3) into (3-1), a simplified governing equation for the cross-flow VIV and its boundary conditions is as follows:

$$\left. \begin{aligned} \left[m_s + \frac{\pi}{4} \rho C_m D^2 \right] \frac{\partial^2 z}{\partial t^2} + \left(c_s + \frac{1}{\pi} \rho C_d D \omega z_0 \right) \frac{\partial z}{\partial t} - T \frac{\partial^2 z}{\partial x^2} + k_b \frac{\partial^4 z}{\partial x^4} &= f_0 \sin(\omega t) \\ z(t, 0) &= 0 \\ \frac{\partial^2 z(t, 0)}{\partial x^2} &= 0 \\ z(t, L) &= 0 \\ \frac{\partial^2 z(t, L)}{\partial x^2} &= 0 \end{aligned} \right\} \quad (3-4)$$

where ω is the vortex-shedding forcing frequency. It satisfies the Strouhal formula.

$$\omega = 2\pi St \frac{U}{D} \quad (3-5)$$

Assuming the modal solution of equation (3-4) is

$$z(t, x) = \sum_{k=1}^{\infty} z_k(t) \sin\left(\frac{k\pi}{L} x\right) \quad (3-6)$$

where z_k are the modal vibration responses, substitute the solution into equation (3-4), and then integrate and put in order. The modal vibration governing equation becomes

$$\begin{aligned} A_k \ddot{z}_k(t) + B_k \dot{z}_k(t) + C_k z_k(t) &= f_{k0} \sin(\omega t) \\ k &= 1, 2, 3, \dots \end{aligned} \quad (3-7)$$

where A_k , B_k and C_k represent the modal mass, the modal damping and riser stiffness; and they can be expressed as

$$\left. \begin{aligned} A_k &= \frac{L}{2} \left(m_s + \frac{\pi}{4} \rho C_m D^2 \right) \\ B_k &= \frac{L}{2} \left(c_s + \frac{1}{\pi} \rho C_d D \omega z_0 \right) \\ C_k &= \frac{L}{2} \left[k_b \left(\frac{k\pi}{L} \right)^4 + T \left(\frac{k\pi}{L} \right)^2 \right] \\ f_{k0} &= \frac{2L}{k\pi} f_0 \end{aligned} \right\} \quad (3-8)$$

From vibration theory [Clough and Penzien, 1993], natural frequency of modal vibration can be gained from the governing equation (3-7) as follows:

$$\omega_{nk} = \sqrt{\frac{C_k}{A_k}} = \sqrt{\frac{k_b \left(\frac{k\pi}{L} \right)^4 + T \left(\frac{k\pi}{L} \right)^2}{m_s + \frac{\pi}{4} \rho C_m D^2}} \quad (3-9)$$

In addition, the non-dimensional parameter of modal response amplitude can be denoted from dimensional analysis as follows:

$$\frac{z_k}{D} = \phi \left(\frac{f_{k0}}{\rho g L D^2}, \frac{\omega}{\omega_{nk}}, \frac{A_k}{\rho L D^2}, \frac{B_k}{\rho L D \omega z_0} \right) \quad (3-10)$$

On the basis of similarity theory, to make the model riser and prototype riser similar, the following condition should be satisfied: all non-dimensional parameters for the model riser and the prototype riser in equation (3-10) must be equal. Thus, the following formulae can be obtained (detail derivation is shown in Appendix C):

$$\left[\frac{C_l U^2}{D} \right]^{(m)} = \left[\frac{C_l U^2}{D} \right]^{(p)} \quad (3-11)$$

$$\left[\frac{StUL^2}{\sqrt{k_b(k\pi)^2 + TL^2}} \right]^{(m)} = \left[\frac{StUL^2}{\sqrt{k_b(k\pi)^2 + TL^2}} \right]^{(p)} \quad (3-12)$$

$$\left[\frac{m_s}{\rho D^2} + \frac{\pi}{4} C_m \right]^{(m)} = \left[\frac{m_s}{\rho D^2} + \frac{\pi}{4} C_m \right]^{(p)} \quad (3-13)$$

$$\left[\frac{c_s}{2\rho St Uz_0} + C_d \right]^{(m)} = \left[\frac{c_s}{2\rho St Uz_0} + C_d \right]^{(p)} \quad (3-14)$$

where the superscripts (m) and (p) , respectively, indicate the values of the model riser and the prototype riser. In equations (3-11), (3-12), (3-13), and (3-14), assuming the hydrodynamic coefficients C_b , St , C_m and C_d for the model and prototype are equal, these equations can be further simplified to:

$$\left[\frac{U^2}{D} \right]^{(m)} = \left[\frac{U^2}{D} \right]^{(p)} \quad (3-15)$$

$$\left[\frac{UL^2}{\sqrt{k_b(k\pi)^2 + TL^2}} \right]^{(m)} = \left[\frac{UL^2}{\sqrt{k_b(k\pi)^2 + TL^2}} \right]^{(p)} \quad (3-16)$$

$$\left[\frac{m_s}{\rho D^2} \right]^{(m)} = \left[\frac{m_s}{\rho D^2} \right]^{(p)} \quad (3-17)$$

$$\left[\frac{c_s}{Uz_0} \right]^{(m)} = \left[\frac{c_s}{Uz_0} \right]^{(p)} \quad (3-18)$$

Equation (3-15) indicates Froude number similarity between the model and prototype.

In VIV research, the most important similarity is Reynolds number similarity. Obviously, simultaneous Froude and Reynolds similarities are impossible. Equation (3-15) has to be abandoned. Two unknown parameters k_b and T exist in equation (3-16). To solve equation (3-16), a non-dimensional parameter about bending stiffness k_b similarity is considered as replenishment. Thus, the equation (3-19) leads into:

$$\left[\frac{k_b}{\rho g D^5} \right]^{(m)} = \left[\frac{k_b}{\rho g D^5} \right]^{(p)} \quad (3-19)$$

According to geometrical similarity, the ratio of z_0 between the model and prototype in equation (3-18) is identical to the ratio of diameter D between the model and prototype. Equation (3-20) is the final model riser designing formulae.

$$\begin{aligned} \left[\frac{k_b}{\rho g D^5} \right]^{(m)} &= \left[\frac{k_b}{\rho g D^5} \right]^{(p)} \\ \left[\frac{UL^2}{\sqrt{k_b (k\pi)^2 + TL^2}} \right]^{(m)} &= \left[\frac{UL^2}{\sqrt{k_b (k\pi)^2 + TL^2}} \right]^{(p)} \\ \left[\frac{m_s}{\rho D^2} \right]^{(m)} &= \left[\frac{m_s}{\rho D^2} \right]^{(p)} \\ \left[\frac{c_s}{UD} \right]^{(m)} &= \left[\frac{c_s}{UD} \right]^{(p)} \end{aligned} \quad (3-20)$$

Our riser model was designed and made according to the designing formula (3-20); details are shown in Li's research [Li, 2005].

3.4.2 Model building

The riser is composed of an 8.5 m long and 0.047 m diameter flexible rubber pipe and several smaller diameter plastic pipes, as shown in Figure 3-4. These pipes were split

along their length to install forty uniaxial ADXL150JQC accelerometers, which were supplied by ANALOG DEVICES Inc, U.S.A. The website is www.analog.com. These accelerometers were chosen not only because they are less expensive, but also because they have good sensitivity, $\pm 2\%$. They were glued into twenty orthogonal pairs and were evenly distributed along the riser length; thirty-one of the forty accelerometers survived when the tests were carried out; table 3-1 shows their location on the model riser. The values of location are measured from the riser top. For example, the position of No.5 & No.6 accelerometers is $x=0.81\text{ m}$; this denotes that the two accelerometers are at 0.81 m from the riser top during the tests.

The surviving accelerometers were non-uniformly spaced on the riser model. The signal wires for the accelerometers go out from a hole on the aluminum ends and were connected to a data acquisition system. Thirty-one data acquisition channels were used for the thirty-one surviving accelerometers; one channel was used for the load cell to measure the top tensions. A layer of metal foil was used to shield and protect accelerometers from noise. An anti-magnetic steel cable connecting two aluminum connection ends was also placed in the pipes to carry the axial tension load.



Figure 3-4 The sketch of the model riser

In order to meet the required mass of the riser, lead weights were evenly arranged over the riser length.

Table 3-1 Accelerometer locations in the model riser

Accelerometer Number	No.5 & No.6	No.7 & No.8	No.9 & No.10	No.11 & No.12	No.13	No.15 & No.16	No.17 & No.18	No.19 & No.20
location(m)	0.810	1.214	1.619	2.024	2.429	2.833	3.238	3.643
Accelerometer Number	No. 21 & No.22	No.23 & No.24	No.25 & No.26	No.27 & No.28	No.33 & No.34	No.35 & No.36	No.37 & No.38	No.39 & No.40
location(m)	4.048	4.452	4.857	5.262	6.476	6.881	7.286	7.691

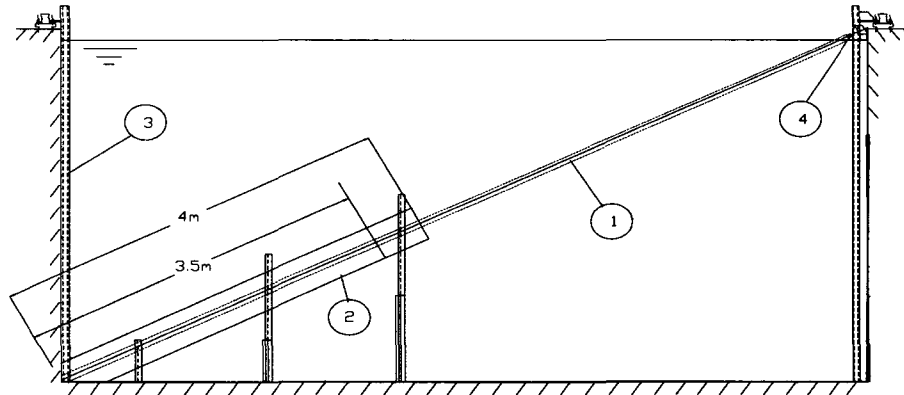
One important parameter about riser models is mass ratio; the model mass ratio for this riser model is 0.986. Mass ratio was the ratio of riser mass to the mass of displaced water. The ratio of the model length to the diameter is 180.85 for the riser model used.

3.5 Experiment and experimental apparatus design

3.5.1 Experiment design

New model testing methods and advanced data analysis techniques were used to improve our understanding of the complex behavior of riser VIV in a shear current.

The 8.5 m long model riser was installed in a diagonal line of the tank section, as shown in figure 3-5. During the test, pretensions were exerted along the model axis. A load cell was used to measure the top tension of the riser. The frequency of data acquisition was 50 Hz. The time of data acquisition was 2 minutes for each run.



- | | |
|--------------------|----------------------------------|
| 1. Model riser | 2. Pipe to produce shear current |
| 3. Steel apparatus | 4. Load cell |

Figure 3-5 The sketch of the experiment arrangement

A 38 cm diameter, 4 m long PVC pipe was used to produce shear current. The PVC pipe can keep water calm over the riser model segment covered by the PVC pipe. Using this method can make it so that a segment of the riser model encounters uniform current and the rest of the segments stay in the still water. A 3.5 m long and a 4 m long PVC pipe were used to produce shear currents. For comparison, a uniform test without PVC pipe was also done.

The tested Reynolds number, defined as $Rn=UD/\nu$, was changed from 2127 to 40,171. Rn is an important dimensionless parameter of inertia to viscosity effects. The range from $Rn=300$ to 3×10^5 is called the subcritical range, where the vortex street is fully turbulent [Blevins, 1977]. But vortex shedding frequencies in both in-line and cross-flow are close to the frequencies calculated from the following Strouhal formula:

$$f_s = \frac{St U}{D} \quad (3-21)$$

where, f_s is the frequency of vortex shedding, U is the current velocity, and D is width of value.

In addition, there are several important non-dimensional parameters used in the experiment analysis, namely frequency ratio ω^* , reduced velocity V^* , non-dimensional vibration amplitude A^* , non-dimensional power spectrum B^* , non-dimensional modal VIV response C^* , and damping ratio ζ ; they are respectively represented as follows:

$$\omega^* = \frac{\omega}{\omega_n} \quad (3-22)$$

where ω is the vortex shedding frequency and the natural frequency of mode 1 is chosen as a representation of ω_n to calculate ω^* . ω_n can be obtained from equation (3-9) provided a value for k_b is known.

$$V^* = \frac{U}{f_k D} \quad (3-23)$$

where U is the current velocity, D is the riser diameter, and f_k is the natural frequency of the k^{th} mode in the calm water

$$A^* = \frac{A}{D} \quad (3-24)$$

where A is the average peak-pick-up amplitude

$$B^* = \frac{B}{D^2} \quad (3-25)$$

where B is the power spectrum, which is the Fourier transform of the correlation function and indicates how the power (energy per unit time) is distributed with frequency.

$$C^* = \frac{z_{k0}}{D} \quad (3-26)$$

where z_{ko} is defined as the average amplitudes of the modal response components $z_k(t)$, which is mentioned in equation (3-6)

$$\zeta = \frac{C}{C_{crit}} \quad (3-27)$$

where ζ is the damping ratio, C is vibration system damping, including structure damping and hydrodynamic damping, and C_{crit} is critical damping.

3.5.2 Experiment apparatus design

A test apparatus was built for the test, as shown in appendix A. In order to solve the bottom fixing problem of the model riser, a row of steel plates from one tank wall to the other was placed on the tank floor; these steel plates were bolted together and were connected to four support bars. These support bars were connected to the carriage track. This apparatus was a frame type of steel structure. For the frame steel apparatus, considerable axial tension of the riser is an inner force. The inner force can't move the steel plates to ram the tank glass wall. This design ensures the tank glass was safe. Before building the apparatus, a check of the strength of the steel apparatus was done, as shown in Appendix B. In terms of the evaluation, the size and materials of the structure components were finally determined.

VIV also occurs when the water flow passes the 38 cm diameter PVC pipe and the VIV is considerably big. To reduce the VIV, a one inch diameter rope strake was used. The pitch of the strake was 0.68 m. Figure 3-6 is a photo of the apparatus.

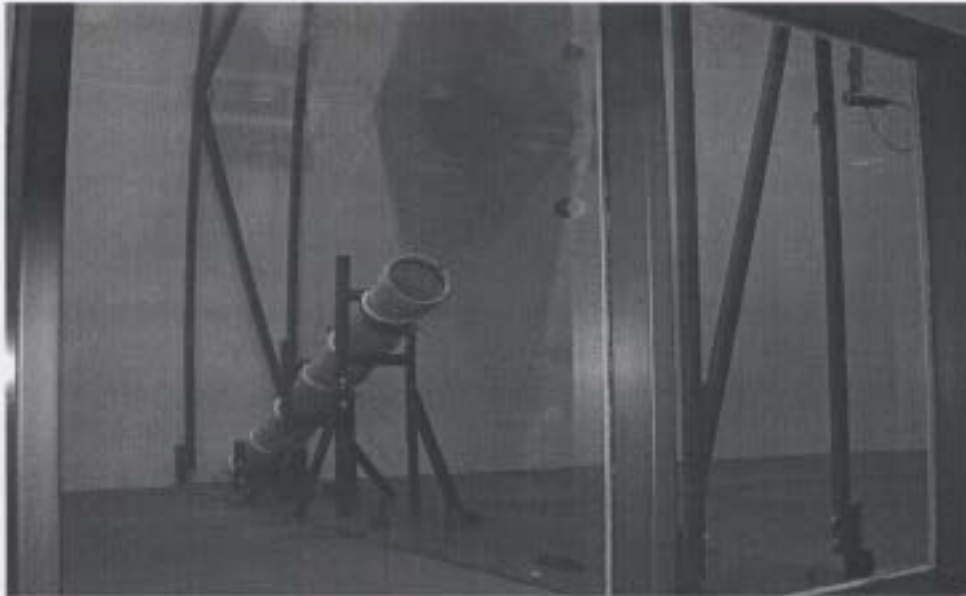


Figure 3-6 Experiment apparatus

3.6 Calibration

The calibration of the measurement system included two parts. One was the load cell calibration. Another was the accelerometer calibration.

3.6.1 Load cell calibration

A load cell was a transducer for force and load measurement. In the tests, a load cell with the maximum weight of 500 pounds (2200 N) was used to measure the top tension of the riser. For calibration, the load cell was hung; then, a weight basket was hung on the load cell. The present calibration of the load cell was carried out by simply changing the weight on the basket; the data acquisition system recorded the corresponding voltage output for different weights on the basket. The calibration coefficient was obtained from fitting a straight line to a graph of the output voltage versus the applied load.

3.6.2 Accelerometer calibration

The setup for accelerometer calibration is shown in Figure 3-7 and Figure 3-8:



Figure 3-7 The calibration testing ground

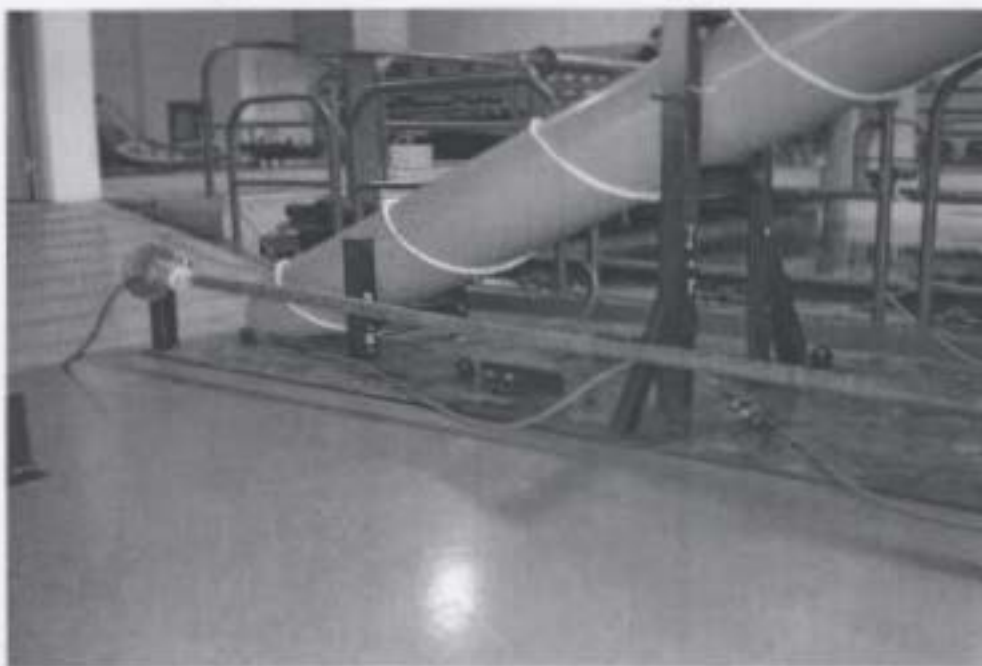


Figure 3-8 The calibration testing ground

The model riser was horizontally mounted on two support rods. Two metal plates with graduation from 0 to 360° on the plate surface were fixed to the rods. When the model riser was rotated, its longitudinal axis had thirteen rotating angles ranging from zero to 360°, and the voltages from the accelerometers altered; the alteration was output and recorded by the data acquisition system. The voltage outputs were then fitted with proper sinusoidal curves, as shown in figure 3-9, 3-10, 3-11 and 3-12. In these figures, the transverse axes are the angle of the model riser rotation, and the vertical axes are the voltage output values. The calibration parameter, including the scale factors and the orientation angles of the accelerometers inside the model riser, were evaluated from the amplitudes and phases of the fitted sinusoidal curves. Scale factors and orientation angles are shown in Table 3-2 and Table 3-3.

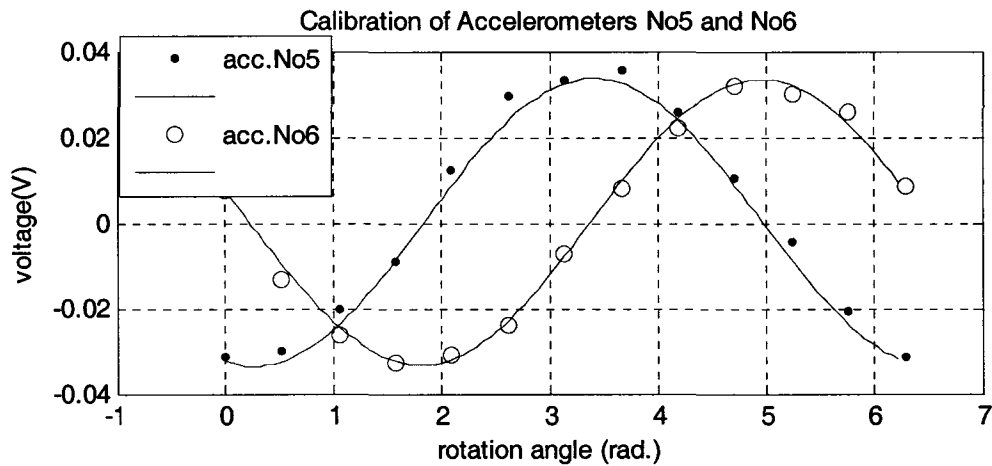


Figure 3-9 No. 5 and No. 6 accelerometer fitted sinusoidal curves of calibration

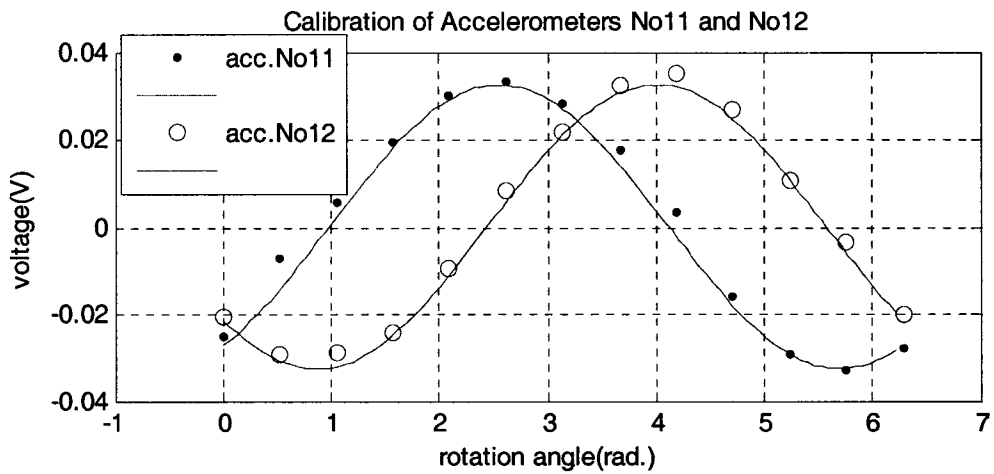


Figure 3-10 No.11 and No.12 accelerometer fitted sinusoidal curves of calibration

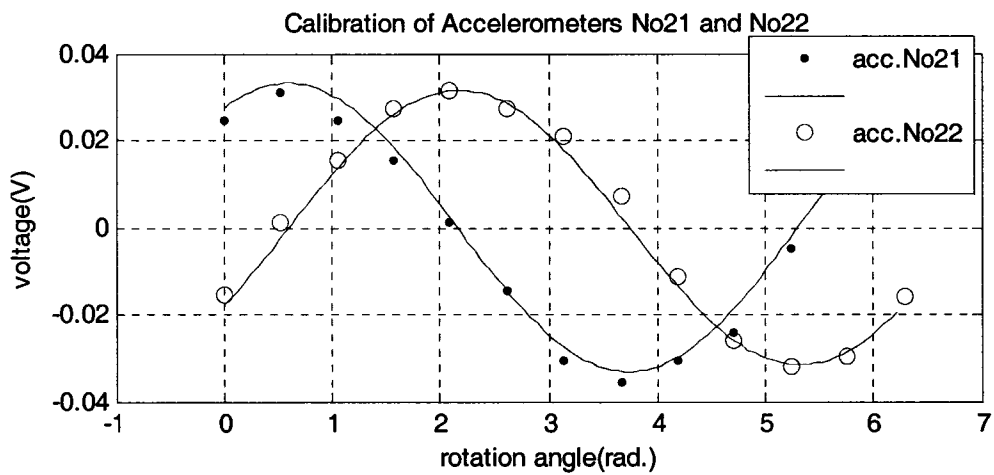


Figure 3-11 No.21 and No.22 accelerometer fitted sinusoidal curves of calibration

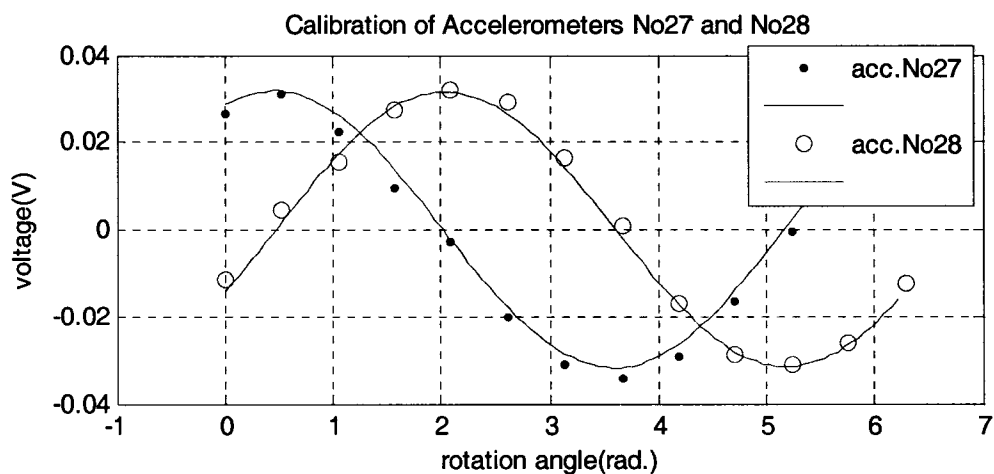


Figure 3-12 No.27 and No.28 accelerometer fitted sinusoidal curves of calibration

Table 3-2 Scale factors of accelerometers

accel. No.	5	6	7	8	9	10	11	12
factor(V/g)	0.0337	0.0334	0.0946	0.0328	0.0331	0.0335	0.0325	0.0326
accel. No.	13	15	16	17	18	19	20	21
factor(V/g)	0.0323	0.0334	0.0294	0.0385	0.0362	0.0409	0.0330	0.0331
accel. No.	22	23	24	25	26	27	28	33
factor(V/g)	0.0316	0.0324	0.0317	0.0341	0.0320	0.0318	0.0316	0.0318
accel. No.	34	35	36	37	38	39	40	
factor(V/g)	0.0301	0.0311	0.0292	0.0320	0.0312	0.0318	0.0311	

Table 3-3 Orientation angles of accelerometers

accel. No.	5	6	7	8	9	10	11	12
angle(rad.)	4.4489	2.9088	4.9941	3.1557	5.1982	3.6785	5.3058	3.8477
accel. No.	13	15	16	17	18	19	20	21
angle(rad.)	5.5813	5.6112	4.6464	0.5565	5.2774	1.7642	6.2256	0.9789
accel. No.	22	23	24	25	26	27	28	33
angle(rad.)	5.6816	1.6620	6.2646	1.1093	0.0127	1.1197	5.8132	2.0942
accel. No.	34	35	36	37	38	39	40	
angle(rad.)	0.5888	2.3891	0.8668	2.8287	1.3723	3.2687	1.6777	

In the Table 3-3, the angles are with respect to the horizontal.

The vibration acceleration in in-line and cross-flow directions can be calculated using equations (3-28) to (3-30). The detailed derivation of them can be found in Li's research [Li, 2005]. First, substituting scale factors and the orientation angle into equation (3-28), the measured acceleration magnitudes $|A_1|$ and $|A_2|$ for each pair of accelerometers are gained as follows:

$$|A_j| = \frac{A_j'}{\lambda_j} \quad j = 1, 2, 3 \dots$$

$$\theta_j = \alpha_j \quad (3-28)$$

where, λ_j is the scale factor of the j th accelerometer; A_j is acceleration magnitudes; A_j' is the voltage value measured by the j th accelerometer; θ_j is the measured acceleration phase; and α_j is the orientation angle of the j th accelerometer.

Then, substituting $|A_1|$ and $|A_2|$, θ_1 and θ_2 into equation (3-29), the magnitude $|A|$ and phase θ of the total acceleration can be obtained as follows:

$$\left. \begin{aligned} \tan \theta &= \frac{|A_2| \cos \theta_1 - |A_1| \cos \theta_2}{|A_1| \sin \theta_2 - |A_2| \sin \theta_1} \\ |A| &= \frac{|A_1|}{\cos(\theta - \theta_1)} \end{aligned} \right\} \quad (3-29)$$

Thus, the accelerations in the in-line and the cross-flow directions can be obtained from

$$\left. \begin{aligned} a_y &= |A| \cos \theta \\ a_z &= |A| \sin \theta \end{aligned} \right\} \quad (3-30)$$

3.7 Installation of the experiment setup

The installation of the experiment setup is shown in Figure 3-13. This task was carried out by the diver team of the Marine Lab at MUN. First, the plates on the tank floor were installed. Then, the support bars were assembled. Finally, the support bars were bolted to the connectors on the tracks.

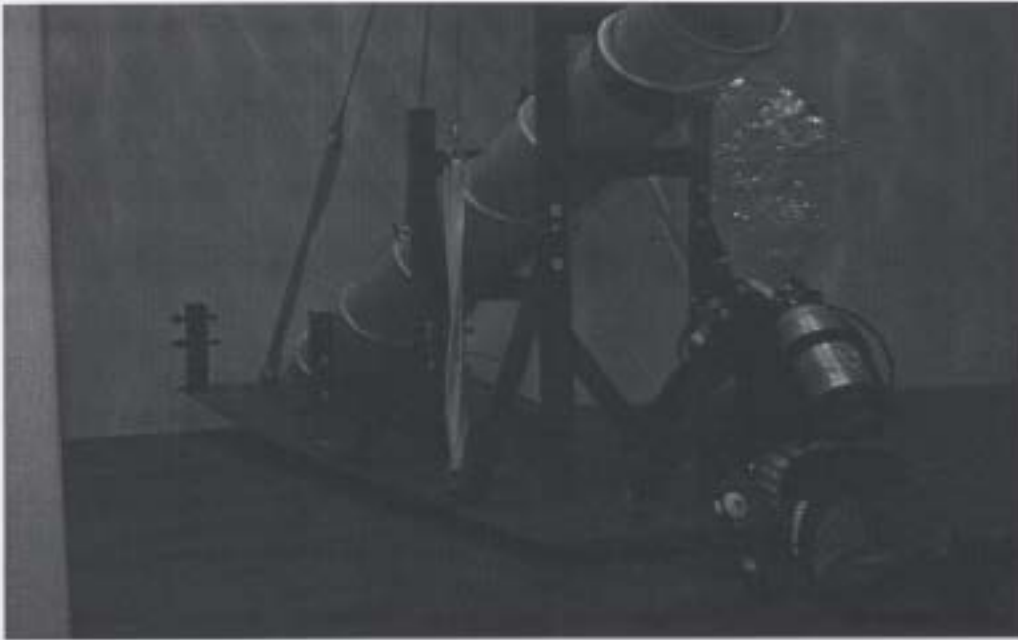


Figure 3-13 Diver installing experiment apparatus

3.8 General procedures of experiments

For the simplicity of the setup installation, the experiments were first performed in the shear currents produced by the 4 m long pipe, and then the experiments in the shear current produced by the 3.5 m long pipe. Finally, the test in uniform current was conducted without block pipe. A total of 120 test runs were carried out.

3.8.1 Shear current produced by the 4 m long pipe

In these tests, three top pretensions were used. They were 460 N, 520 N and 690 N. Under 460 N pretension, first the current velocity was changed from the lowest velocity 0.1 m/s to the highest velocity 1m/s, which was called the up run tests, then back down to the lowest velocity 0.1 m/s, which was called the down run tests; the velocity interval was 0.1 m/s. The waiting water time between two current velocity alternations was 5 minutes. Figure 3-14 is a picture for the test case. Under 690 N pretension, only the up

run tests were done; the velocity was from 0.1m/s to 1m/s. Under 520 N pretension, only the down run tests were done; the velocity was from 1m/s to 0.1 m/s.

In addition, a thirty-minute data acquisition sustained test was performed in this current case, using 720 N top pretension and 0.7 m/s current velocity.

In these tests, six pairs of accelerometer positions were inside PVC pipe. They were No.25, No.26, No.27, No.28, No.33, No.34, No.35, No.36, No.37, No.38, No.39, and No.40.

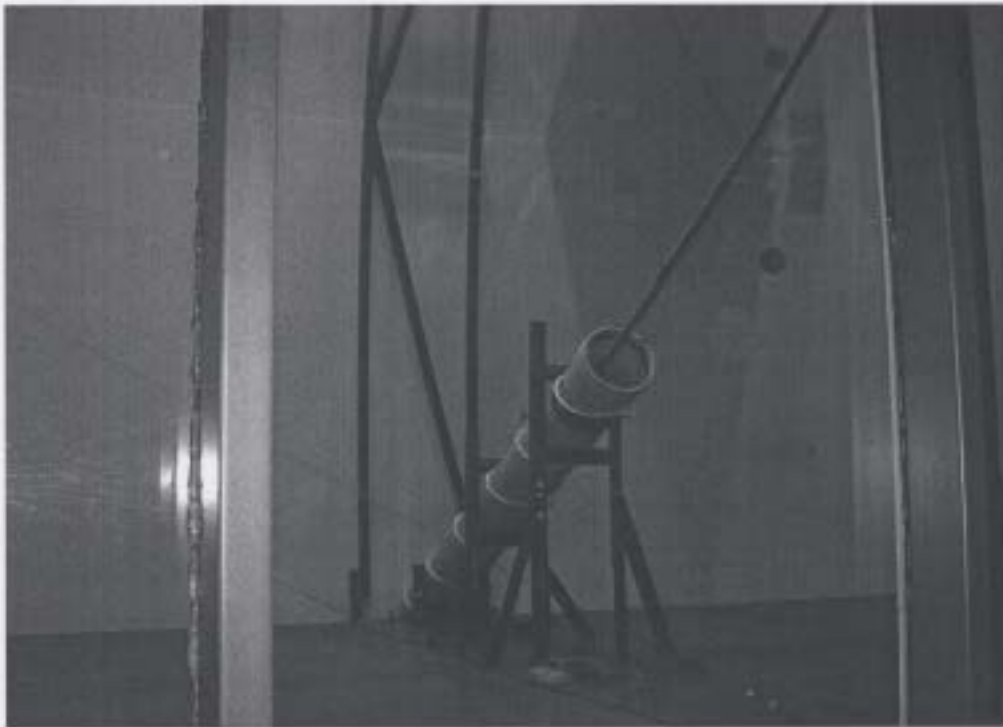


Figure 3-14 Tests under shear current produced by a 4 m block pipe

3.8.2 Shear current produced by the 3.5 m long pipe

In these tests, two top pretensions were used. They were 460 N and 690 N. Under each pretension, current velocity was designed starting from 0.1 m/s to 1m/s, and then down

to 0.1 m/s again; the current velocity interval is 0.1 m/s. Figure 3-15 is a picture of the test case.

In these tests, five pairs of accelerometer positions were inside PVC pipe. They were No.27, No.28, No.33, No.34, No.35, No.36, No.37, No.38, No.39, and No.40.

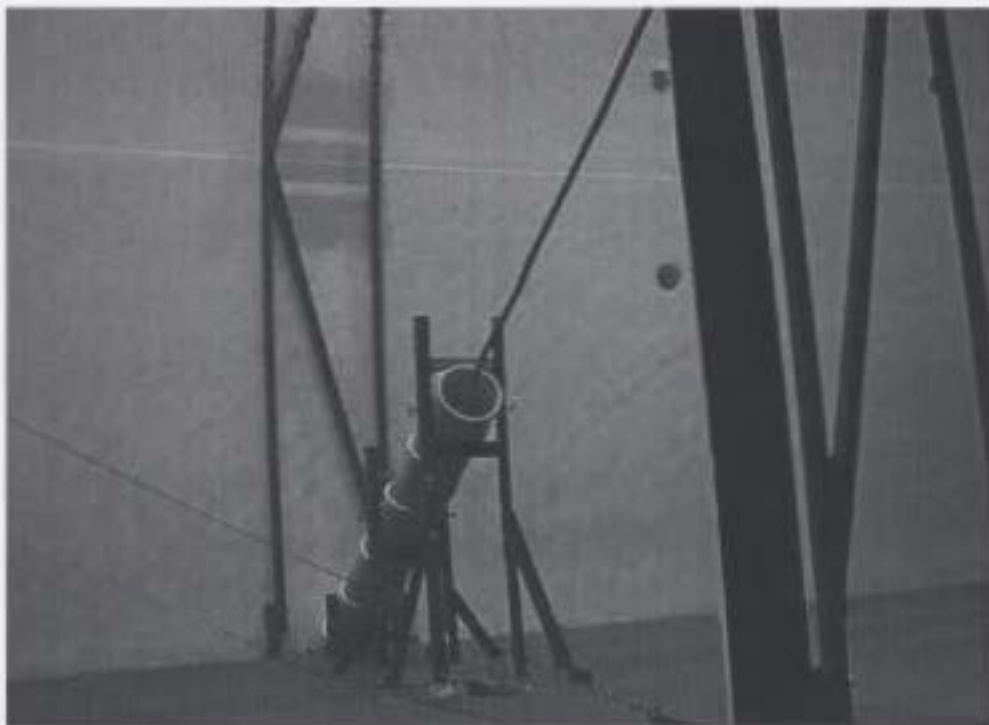


Figure 3-15 Tests under shear current produced by a 3.5 m block pipe

3.8.3 Uniform current without block pipe

This is a uniform current test. Two top pretensions were used. They were 460 N and 690 N. Under 460 N pretension, current velocity was designed starting from 0.1 m/s to 0.9 m/s, and then back down to 0.1 m/s again. When the flow velocity attained 1m/s, due to the drag force and lift force, the top tension of riser exceeded 2227 N, which was the

limit value of the load cell. To avoid damaging the load cell, the test for flow velocity 1 m/s was cancelled.

Under 690 N pretension, current velocity was designed from 0.1 m/s to 0.8 m/s, and then back down to 0.1 m/s again; the current velocity interval is 0.1 m/s. In Figure 4-58, extending the test curve for uniform current, it is easy to see that the top tension exceeds 2227 N, which is the load cell limit value. Therefore, the tests for flow velocity 0.9 m/s and 1 m/s under the top pretension were cancelled.

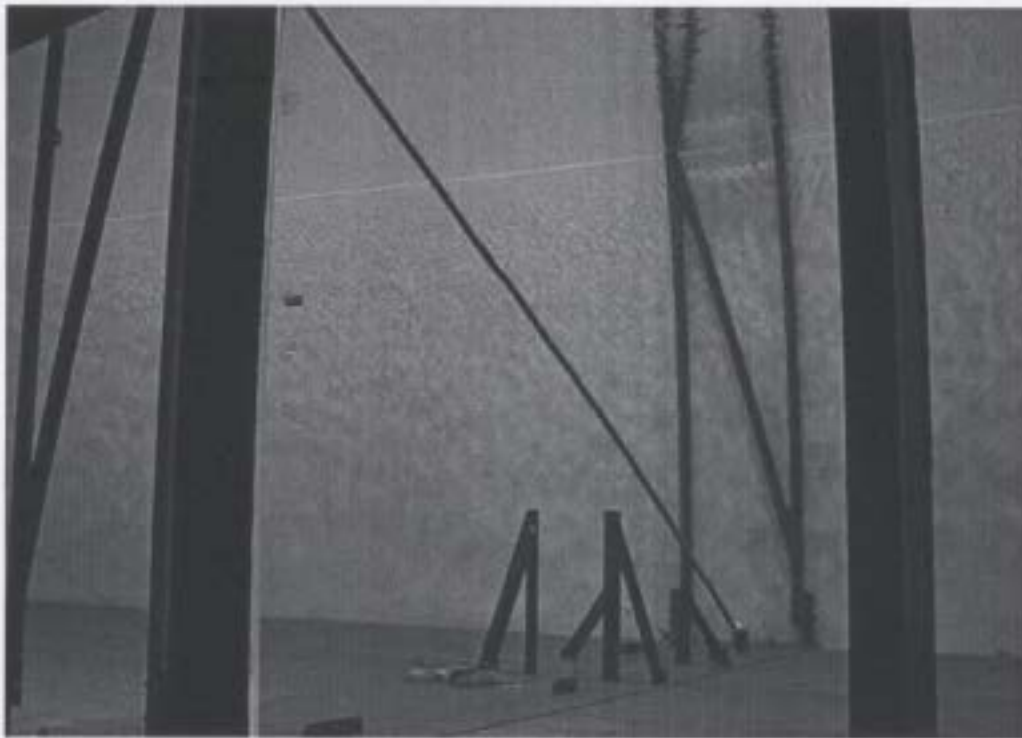


Figure 3-16 Tests under uniform current without block pipe

Figure 3-16 is a picture of these tests.

3.8.4 Uniform current test in the Ice Tank

The VIV tests for uniform current were performed in the Ice Tank in Oct. 2004. The model riser was horizontally installed on a steel frame, which was fixed to the towing

carriage. The uniform current was produced by the carriage moving. Two pretensions were used; they were 200 N and 600 N. Under these pretensions, twenty seven current velocities were tested starting from 0.1 m/s to 1.5 m/s.

3.9 Discussion or summary

The key factor to successfully conducting the tests is safety.

A careful check of the apparatus strength and the stability of the apparatus should be considered. Because the block pipe suffers a large drag force, it causes the apparatus to have a stability problem. To solve this problem, some weights were put on the plates of the apparatus to avoid the turnover of the apparatus. In addition, two pieces of steel wire were used to ensure apparatus safety.

Chapter 4

Test analysis

The analytical code, which was used to analyze the tests, was written in Matlab by Li [2005]; its validation was done in “Identification of Linear and Non-linear Multi-Modal VIV Responses for Flexible Deepwater Risers”, which was Xiangqun Li’s thesis for his PhD degree. The test data were analyzed and compared in the time-domain, the frequency-domain and the space-domain. The measured VIV responses are the waves in the time-domain, and analyzing directly vibration amplitude and frequency is called time-domain analysis. In the time-domain analysis, the velocity and displacement can be obtained by integrating the acceleration. However, analysis should be done from different angles of view. There are some limitations in the analysis of time-domain such as hard-to-analyze intermodulation vibrations which contain both high- and low-frequency components and high-frequency vibrations containing long-time constants; frequency-domain analysis is also widely used in vibration analysis. Spectral analysis is the procedure of transforming the vibration information in the time domain into that of the frequency domain. A major transformation method is the Fourier transform. When the Fourier transform is used for block data that is not periodic, leakage error will occur. To reduce the leakage error, a window function is employed. In frequency-domain analysis, the resultant graph is called the spectrum. Its horizontal axis is frequency or dimensionless frequency; its vertical axis denotes power spectral values. Frequency components in VIV responses can be clearly shown in the spectrum.

Modal analysis of the oscillating body is called the space-domain analysis. The results of the space-domain analysis are modal response frequency, modal response amplitude, and mode shape. These mode features are related to vibration body mass, stiffness and boundary conditions. In this chapter, non-dimensional parameters defined in chapter 3 are used to express test results. For convenience, the maximum current velocity over riser length is substituted into the formula to calculate reduced velocity V^* and the Strouhal number.

Table 4-1 Average current velocity versus V^*

V^*			Average current velocity (m/s)		
Pretension =460 N	Pretension =520 N	Pretension =690 N	shear current produced 4 m block pipe	shear current produced 3.5 m block pipe	Uniform current
3.28	3.09	2.68	0.0529	0.0588	0.1
6.57	6.16	5.36	0.1059	0.1176	0.2
9.86	9.27	8.05	0.1588	0.1765	0.3
13.14	12.36	10.73	0.2118	0.2353	0.4
16.42	15.45	13.41	0.2647	0.2941	0.5
19.71	18.54	16.09	0.3176	0.3529	0.6
22.99	21.63	18.77	0.3706	0.4118	0.7
26.28	24.72	21.46	0.4235	0.4706	0.8
29.57	27.81	24.14	0.4765	0.5294	0.9
32.85	30.90	26.82	0.5294	0.5882	1.0

4.1 Time-domain analysis

4.1.1 Amplitude versus current velocity

Two definitions are introduced first. One of them is average peak-pick-up amplitude; it indicates the average value of all amplitude peaks. Another is significant value of amplitude; it represents the average height of the one-third highest amplitudes of a given vibration group or sample.

4.1.1.1 Amplitude comparison between shear current and uniform current

Figure 4-1, Figure 4-2 and Figure 4-3 respectively show the average peak-pick-up in-line amplitudes in shear flow and uniform flow. They have the same pretension of 690 N.

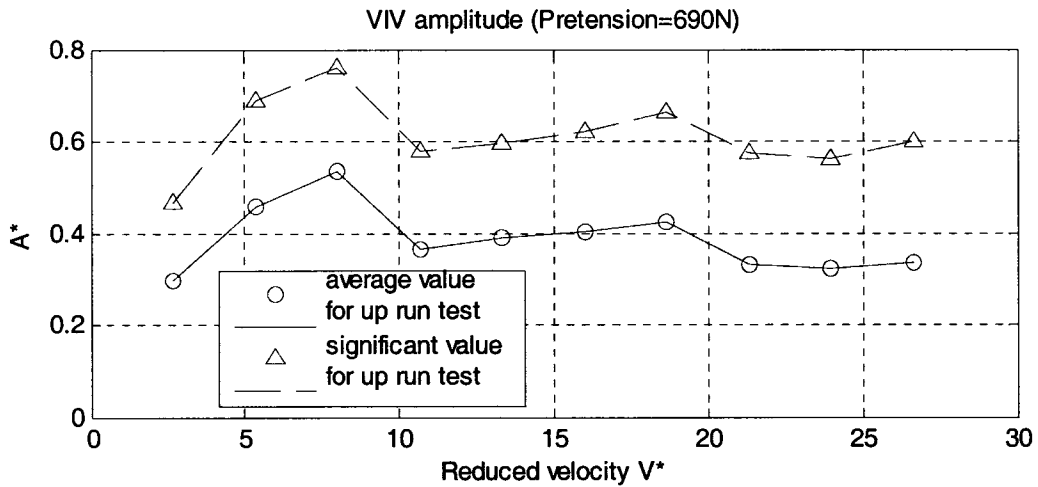


Figure 4-1 The average and significant amplitude of in-line in shear current produced by a 4 m block pipe

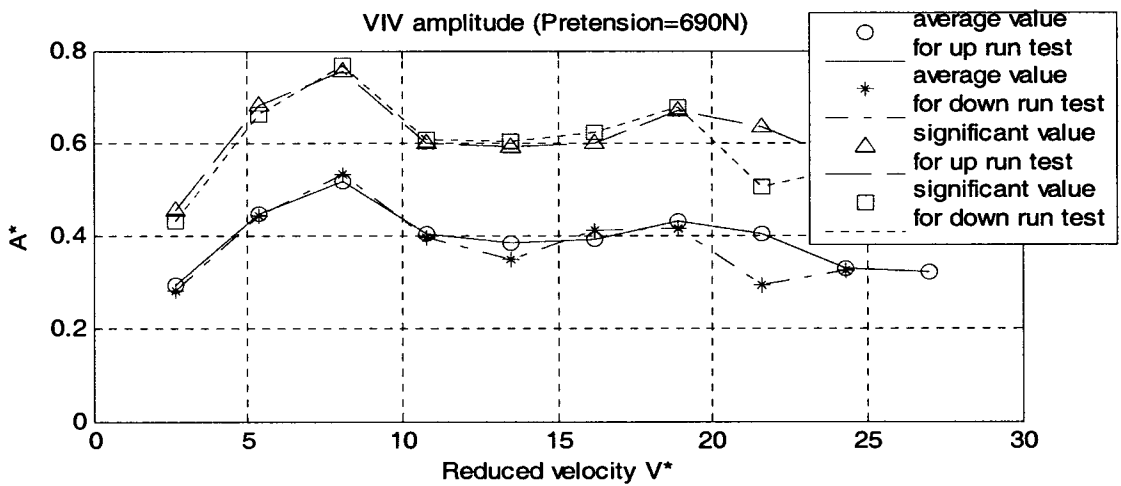


Figure 4-2 The average and significant amplitude of in-line in shear current produced by a 3.5 m block pipe

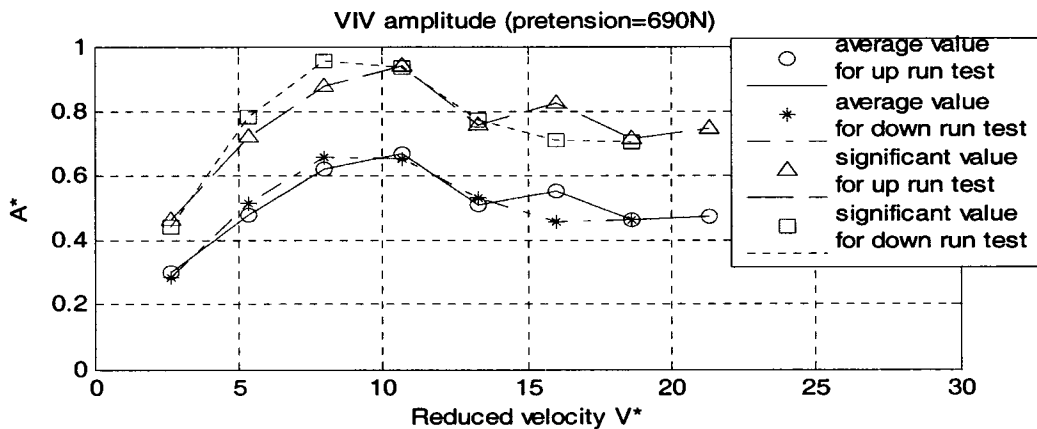


Figure 4-3 The average and significant amplitude of in-line in uniform current

The horizontal axes in these figures are reduced velocity V^* and vertical axes are non-dimensional vibration amplitude A^* . These non-dimensional numbers are defined in chapter 3. As seen in these figures, \circ displays the average amplitude for the up run test; $*$ displays the average amplitude for the down run test; Δ displays the significant amplitude for the up run test, and \square displays the significant amplitude for the down run test. The curves for the significant value of amplitude and the average value of amplitude are parallel. This means that the ratio between the significant value of the amplitude and the average value of the amplitude for the same vibration group is one constant.

In these figures, V^* ranges from 2.5 to 27, A^* of average amplitude ranges from 0.3D to 0.7D, and A^* of significant amplitude ranges from 0.4D to 0.9D. Figure 4-1 and Figure 4-2 display the test results in two kinds of shear current. They are very similar, including peak positions and peak values. The first peaks are at low velocity $V^*=8.05$ with values of about 0.5D and 0.75D. The second peaks are at high velocity $V^*=18.77$ with values of about 0.42D and 0.63D. The reason for the two tests is that the two kinds of shear current are slightly different. Figure 4-3 displays the test results in uniform flow. The peak is at low velocity $V^*=10.73$ with a value of about 0.67D and 0.92D. Obviously, higher peak values exist in the uniform current than in the shear currents because the block pipe reduced the energy producing vibration in the shear current tests. Along with the shrinking of the block pipe, V^* corresponding to the peak get bigger. Since a model riser in a uniform current experiences a larger overall downstream deflection than does the model riser when it is inside the block pipe, the tension in the riser is always higher when the riser is exposed to a uniform current than when inside the block pipe. Thus the natural frequencies for each mode are always higher when the riser is exposed to a uniform current than when inside the block pipe. It then follows that a higher current speed is required in the uniform current than when inside the block pipe in order to produce resonance in each mode.

The natural frequency of the model riser can be found from equation (2-1).

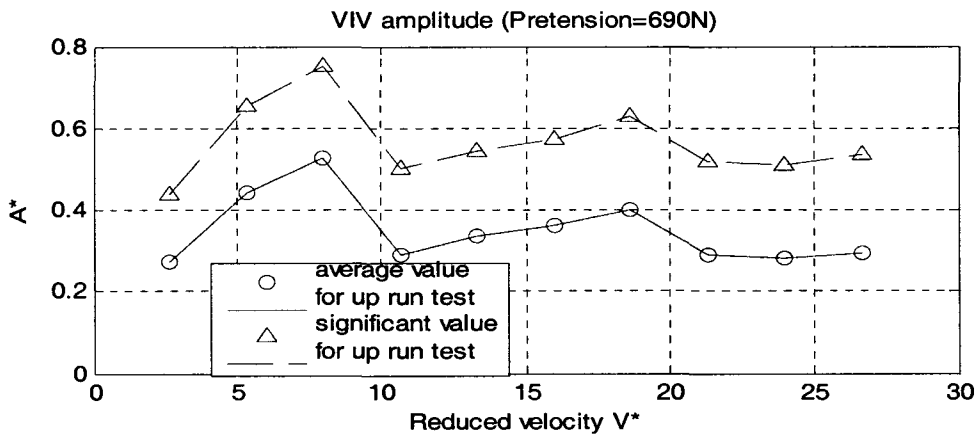


Figure 4-4 The average and significant amplitude of the cross-flow in shear current produced by a 4 m block pipe

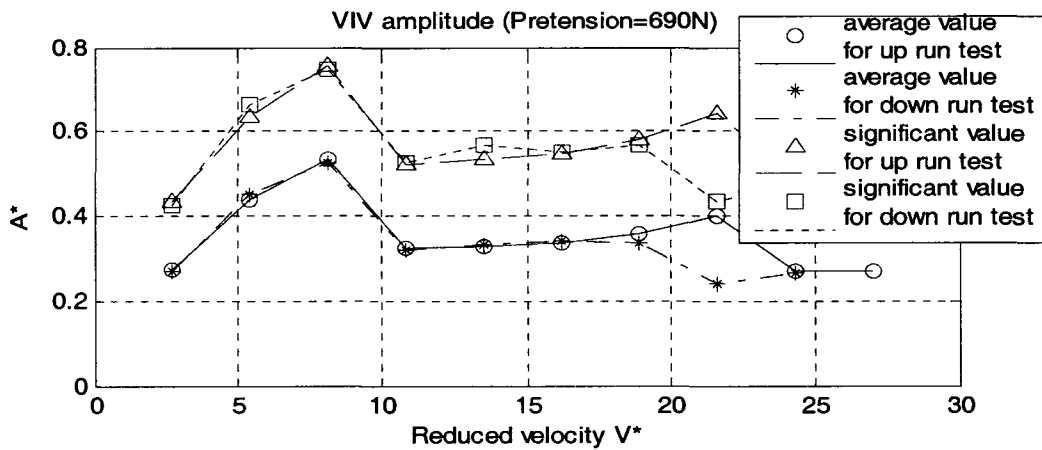


Figure 4-5 The average and significant amplitude of the cross-flow in shear current produced by a 3.5 m block pipe

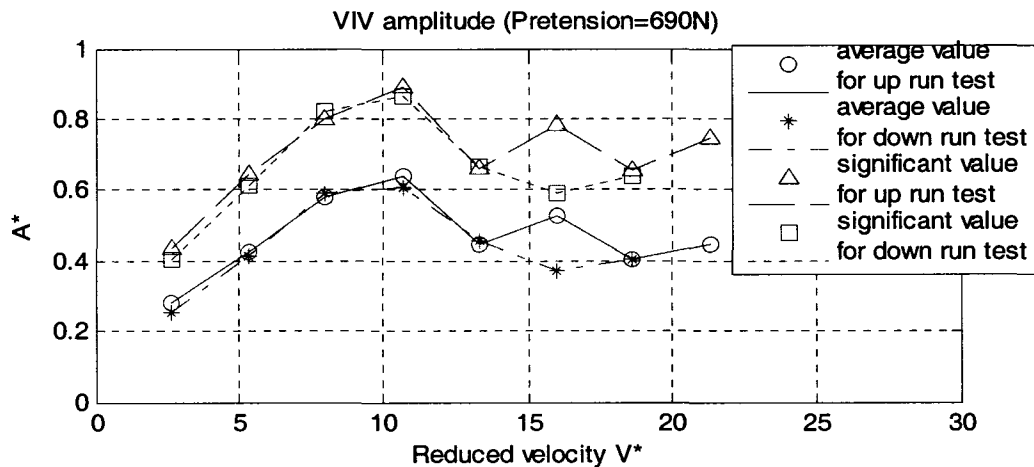


Figure 4-6 The average and significant amplitude of the cross-flow in uniform current

Like Figure 4-1, Figure 4-2 and Figure 4-3, Figure 4-4, Figure 4-5 and Figure 4-6, respectively, show the significant peak-pick-up cross-flow amplitudes and average peak-pick-up cross-flow amplitudes in shear and uniform flows. Comparing Figure 4-1 to Figure 4-4, in-line and cross-flow peak displacements under the same current configuration are basically the same. The maximum peaks are 0.75D for significant amplitudes and 0.5D for average amplitudes. The same results can be gained from comparing Figure 4-2 to Figure 4-5 and Figure 4-3 to Figure 4-6. For a rigid riser, in-line and cross-flow vibration amplitudes have different values; for example, 0.4D amplitude in in-line and 1.2D amplitude in cross-flow [Chaplin et al., 2004]. In addition, test values of the up-run and the down-run coincide well based on the figures. This implies that test results should not be related to the test schedule so long as the waiting water time is long enough.

4.1.1.2 Amplitude comparison between different pretensions

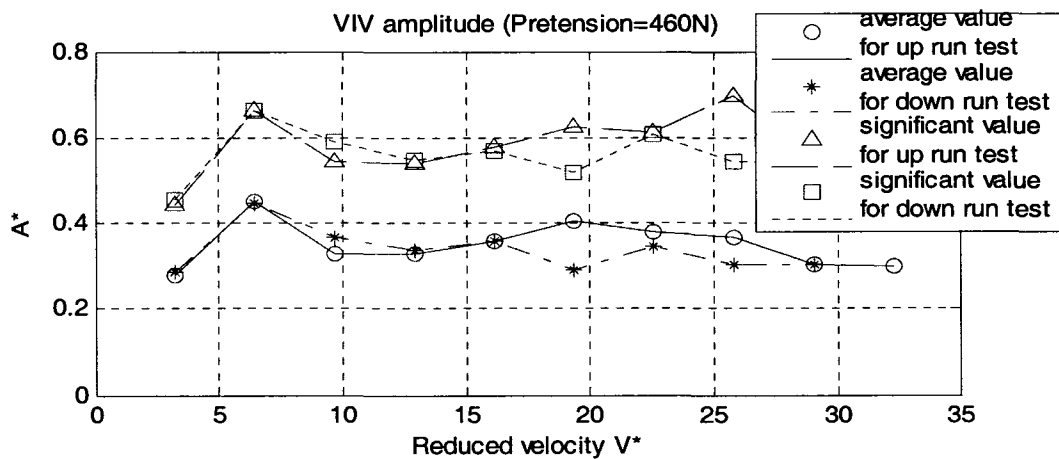


Figure 4-7 The average and significant amplitude of the cross-flow at pretension 460 N in shear current produced by a 4 m block pipe

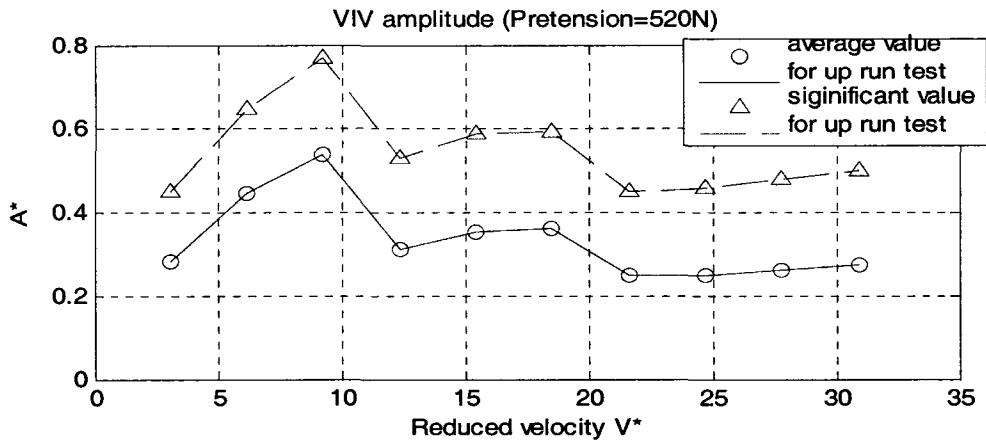


Figure 4-8 The average and significant amplitude of the cross-flow at pretension 520 N in shear current produced by a 4 m block pipe

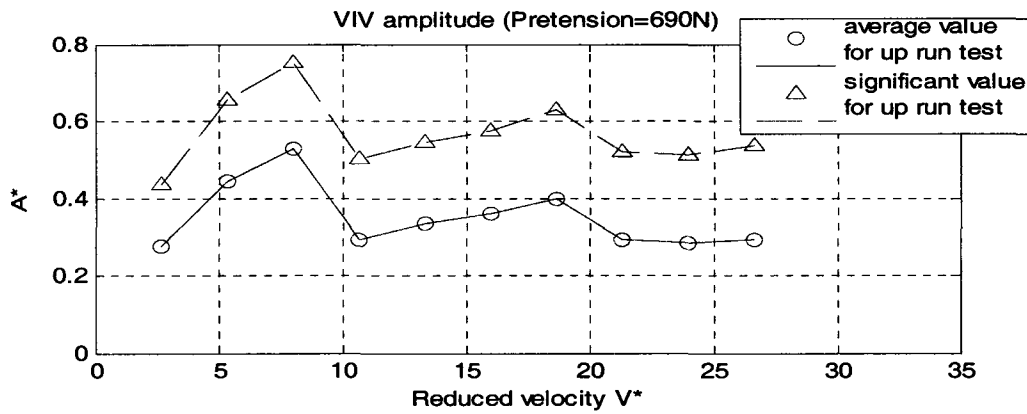


Figure 4-9 The average and significant amplitude of the cross-flow at pretension 690 N in shear current produced by a 4 m block pipe

Figure 4-7, Figure 4-8 and Figure 4-9 show the average cross-flow vibration amplitude. They are the test results from the same shear current, but different pretensions. The horizontal axes in the figures are reduced velocity V^* and the vertical axes are the non-dimensional vibration amplitude A^* . The average peak-pick-up vibration amplitudes in the cross-flow direction range from 0.25D to 0.55D.

Figure 4-7 displays the vibration amplitude under pretension=460 N. The first peak is at $V^*=6.57$, and the peak values are 0.45D and 0.67D. Figure 4-8 displays the vibration amplitude under pretension=520N. The peak value is 0.52D and 0.77D. Figure 4-9 displays the vibration

amplitude under pretension=690 N. The peak value is 0.53D and 0.78D. From equation (2-1), increasing tension can directly cause the model natural frequency to increase. The resonances occur at higher velocities in Figure 4-8 and Figure 4-9 than in Figure 4-7.

Tension acting on the riser can affect its stiffness. The larger the tension, the larger the stiffness. The peak value of the vibration should be proportional to the inverse of stiffness; but the test results are the opposite. For example, the vibration amplitude peak under pretension=520 N is larger than that under pretension=460 N. This fact implies that two of the other parameters, damping ratio, defined in chapter 3, and vortex-shedding forces, have a larger effect on the peak values than the tension.

4.1.1.3 Amplitude comparison between different positions on the model riser

In order to further understand VIV in the shear current, vibration amplitude at several relative special positions were chosen to compare with those in uniform current. These positions are at about 1/4, 1/3, 1/2, and 2/3 riser length, which correspond with the positions of $x=2.024$ m, $x=2.833$ m, $x=4.452$ m, and $x=5.262$ m, respectively.

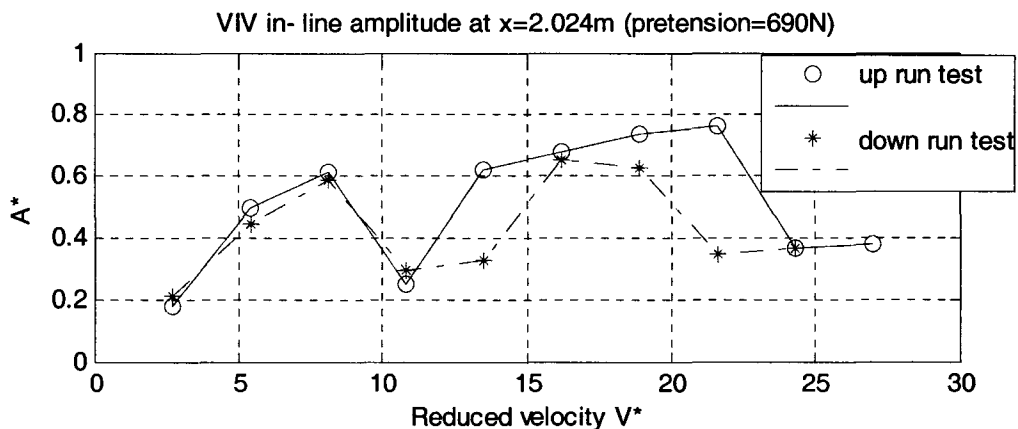


Figure 4-10(a) The average in-line vibration amplitude at $x=2.024$ m in shear current produced by a 3.5 m block pipe

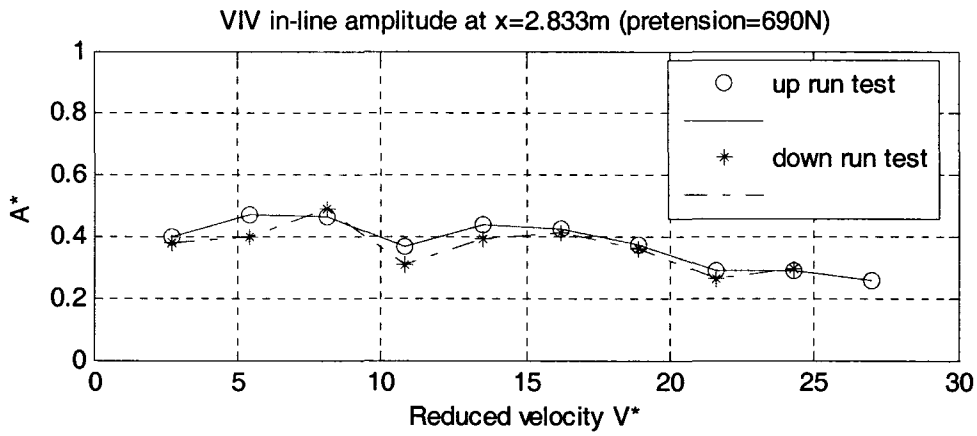


Figure 4-10(b) The average in-line vibration amplitude at $x=2.833$ m in shear current produced by a 3.5 m block pipe

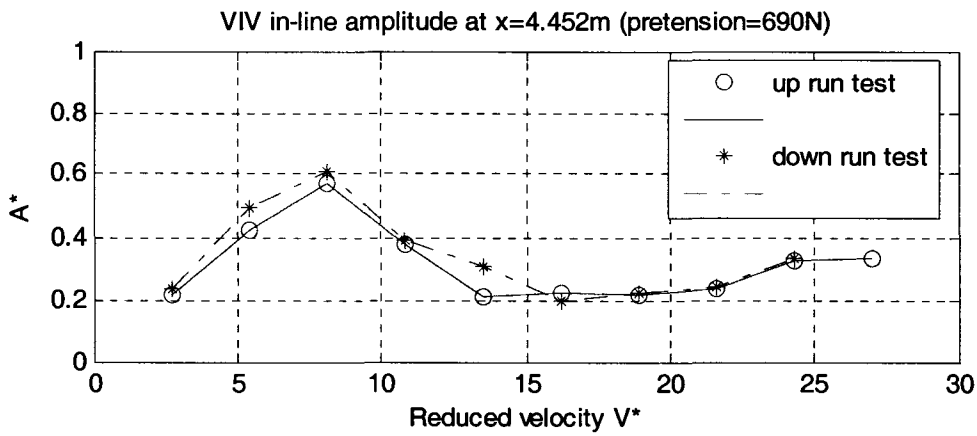


Figure 4-10(c) The average in-line vibration amplitude at $x=4.452$ m in shear current produced by a 3.5 m block pipe

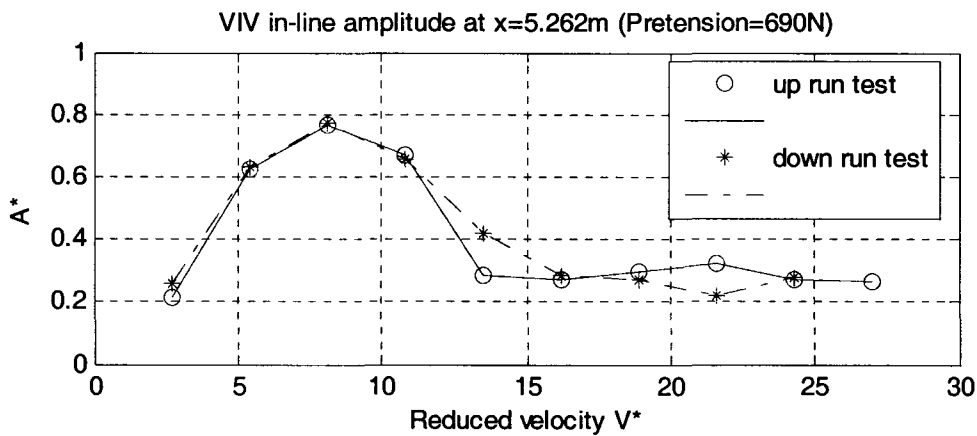


Figure 4-10(d) The average in-line vibration amplitude at $x=5.262$ m in shear current produced by a 3.5 m block pipe

Figure 4-10(a), Figure 4-10(b), Figure 4-10(c), and Figure 4-10(d) show average peak-pick-up in-line vibration amplitudes at these positions under the same shear current and same pretension. The horizontal axes in the figures are the reduced velocity V^* and the vertical axes are the non-dimensional vibration amplitude A^* .

The feature of figure 4-10(a) is that it has two peaks. The second peak is higher than the first peak. The two peak values are between $0.6D$ and $0.8D$ of the riser diameter. The feature of figure 4-10(b) is that it is a flat curve; it has no obvious peak. The feature of figure 4-10(c) is that a small peak is at $V^*=8.05$; the peak value is $0.6D$. The feature of figure 4-10(d) is that a relatively high peak is at $V^*=8.05$; the peak value is $0.8D$.

Figure 4-11(a), Figure 4-11(b), Figure 4-11(c), and Figure 4-11(d) show the average in-line vibration amplitude in uniform current. Like Figure 4-10(a), Figure 4-11(a) has two peaks. The difference is that reduced velocities V^* corresponding to the peaks become larger in Figure 4-11(a). The reason for this is the increasing model natural frequency, as discussed earlier. The curve of Figure 4-11(b) is as flat as that in Figure 4-10(b). It is noted that there is only one peak in Figure 4-11(c) and 4-10(c). Not only do the reduced velocity V^* corresponding to the peaks get bigger, but also the peak value increases to $0.8D$. The difference between Figure 4-11(d) and Figure 4-10(d) is that reduced velocities V^* corresponding to the peak are different. Yet, peak values in the two figures are the same.

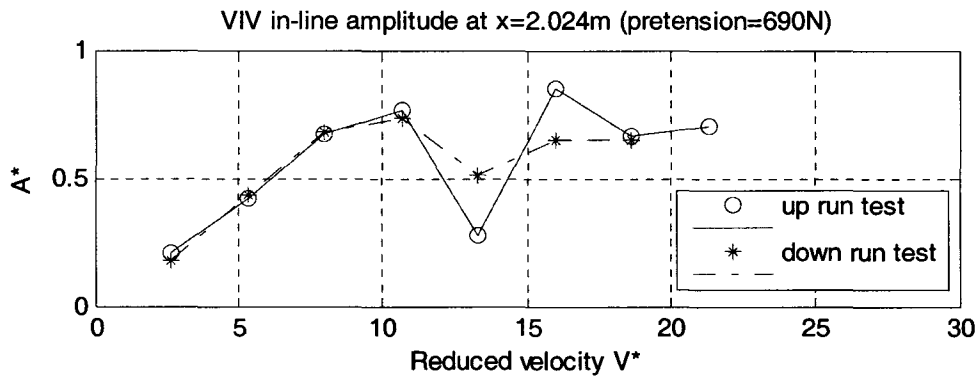


Figure 4-11(a) The average in-line vibration amplitude at $x=2.024\text{ m}$ in uniform current

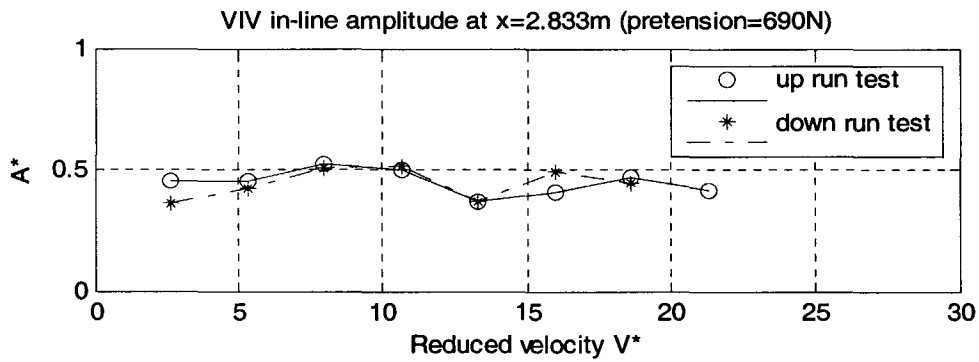


Figure 4-11(b) The average in-line vibration amplitude at $x=2.833\text{ m}$ in uniform current

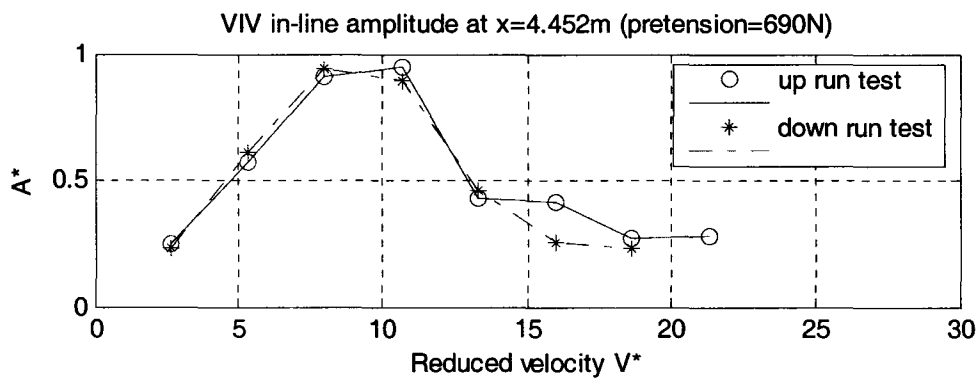


Figure 4-11(c) The average in-line vibration amplitude at $x=4.452\text{ m}$ in uniform current

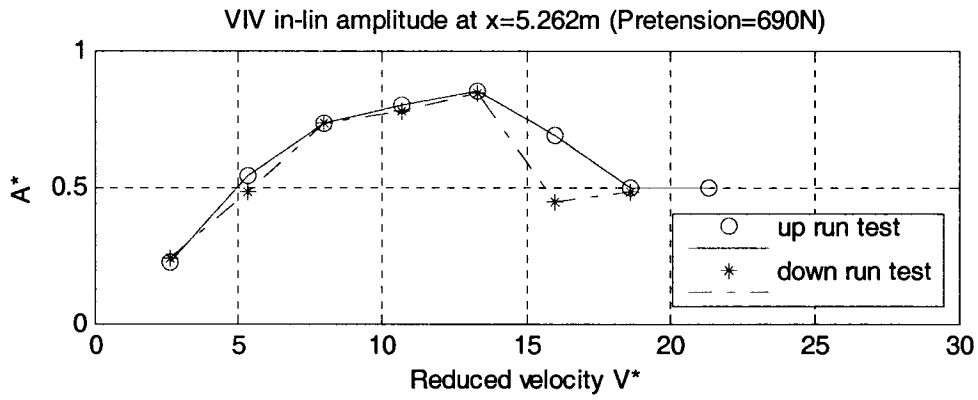


Figure 4-11(d) The average in-line vibration amplitude at $x=5.262\text{ m}$ in uniform current

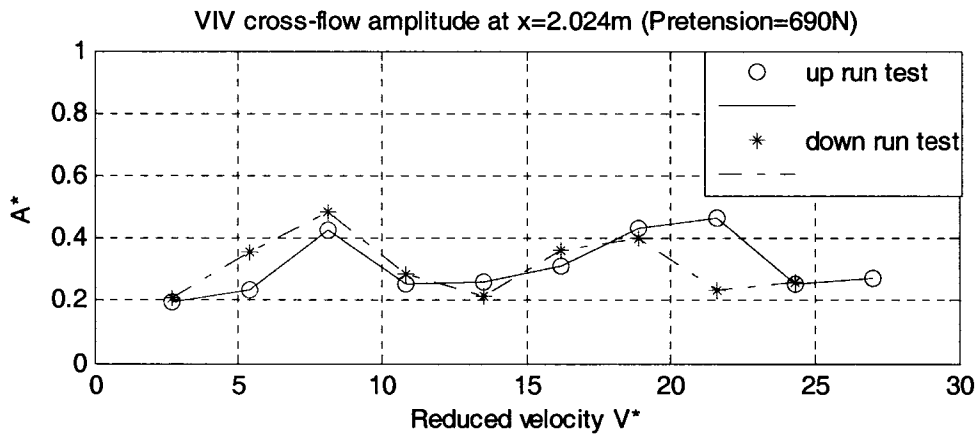


Figure 4-12(a) The average cross-flow vibration amplitude at $x=2.024\text{ m}$ in shear current produced by a 3.5 m block pipe

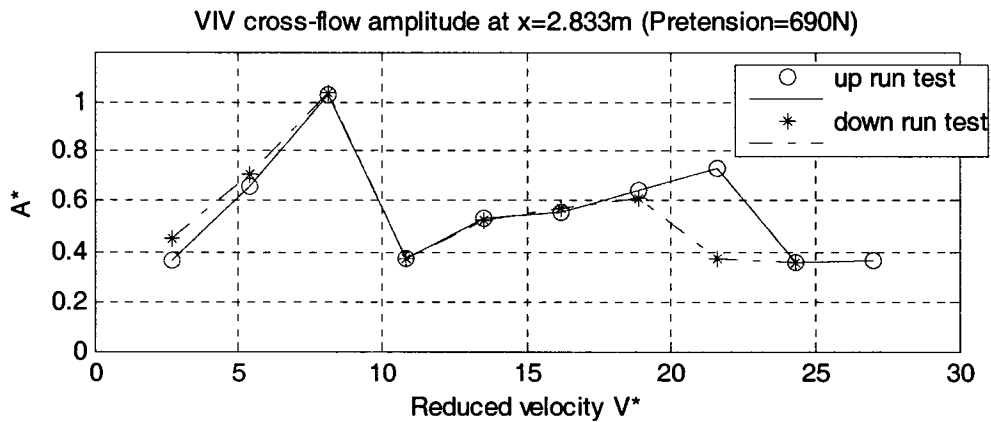


Figure 4-12(b) The average cross-flow vibration amplitude at $x=2.833\text{ m}$ in shear current produced by a 3.5 m block pipe

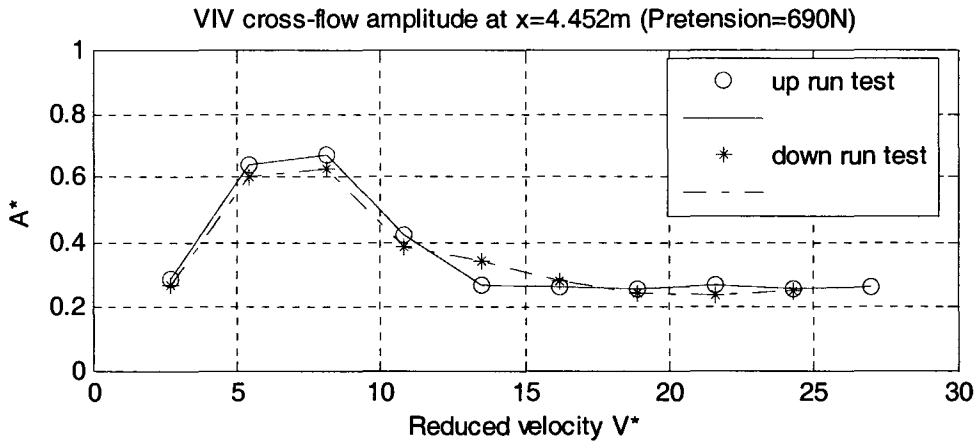


Figure 4-12(c) The average cross-flow vibration amplitude at $x=4.452$ m in shear current produced by a 3.5 m block pipe

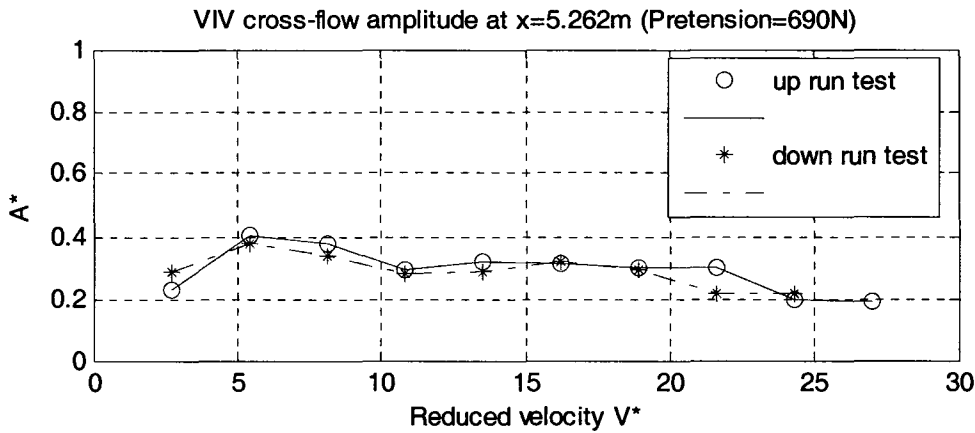


Figure 4-12(d) The average cross-flow vibration amplitude at $x=5.262$ m in shear current produced by a 3.5 m block pipe

Figure 4-12(a), Figure 4-12(b), Figure 4-12(c), and Figure 4-12(d) show average cross-flow vibration amplitude in the same shear current and at the same pretension but at different positions on the riser. The horizontal axes are the reduced velocity V^* and the vertical axes are non-dimensional vibration amplitude A^* .

The feature of figure 4-12(a) is that it has two flat peaks. The peak values are about 0.4D. The feature of figure 4-12(b) is that it has an obvious peak at reduced velocity $V^*=8.05$. The peak

value is 1. The feature of figure 4-12(c) is that a small peak is at $V^*=8.05$. The peak value is 0.6D. The feature of figure 4-12(d) is that it is a flat curve. It has no obvious peak.

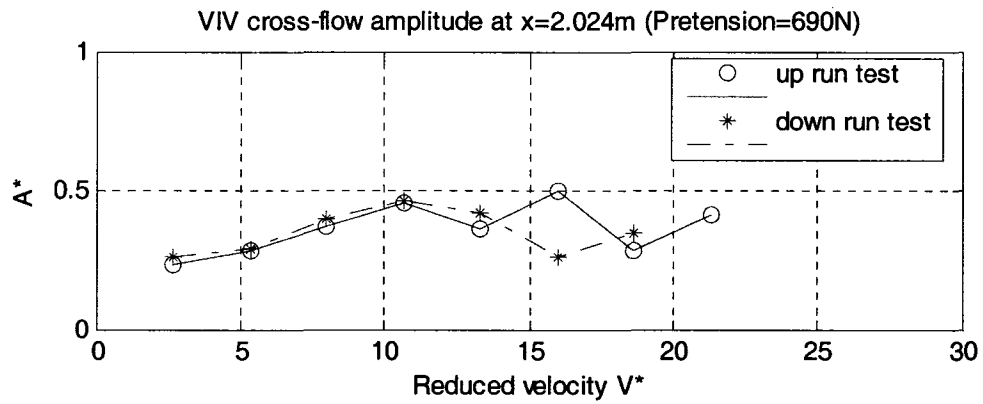


Figure 4-13(a) The average cross-flow vibration amplitude at $x=2.024$ m in uniform current

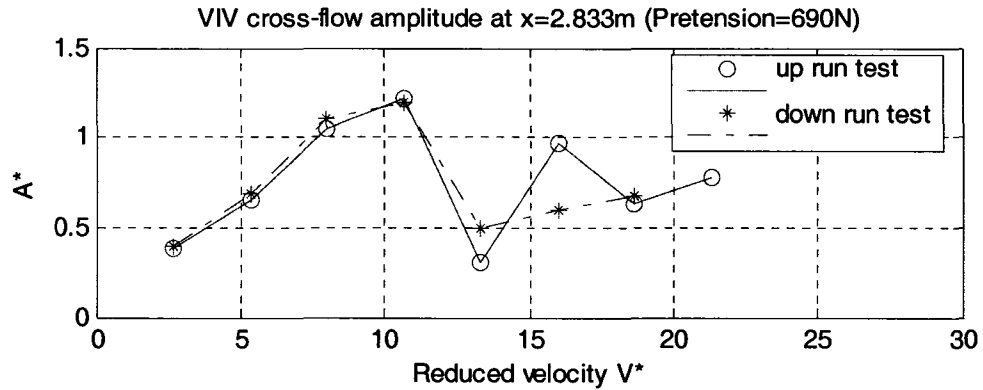


Figure 4-13(b) The average cross-flow vibration amplitude at $x=2.833$ m in uniform current

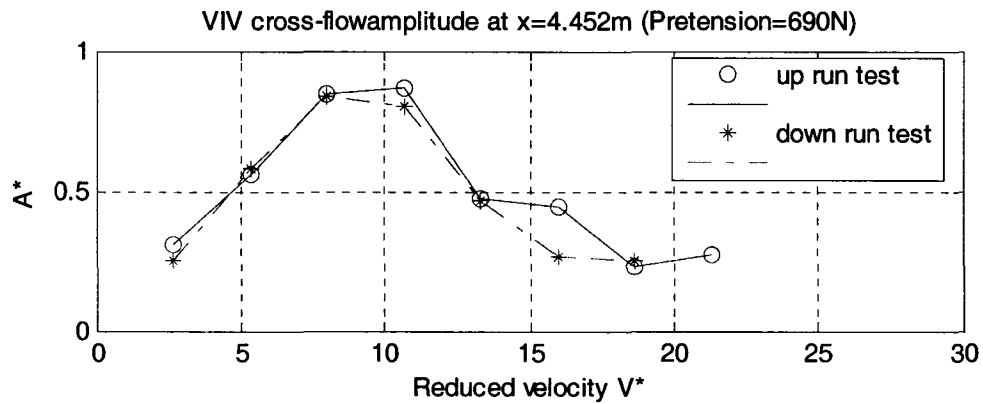


Figure 4-13(c) The average cross-flow vibration amplitude at $x=4.452$ m in uniform current

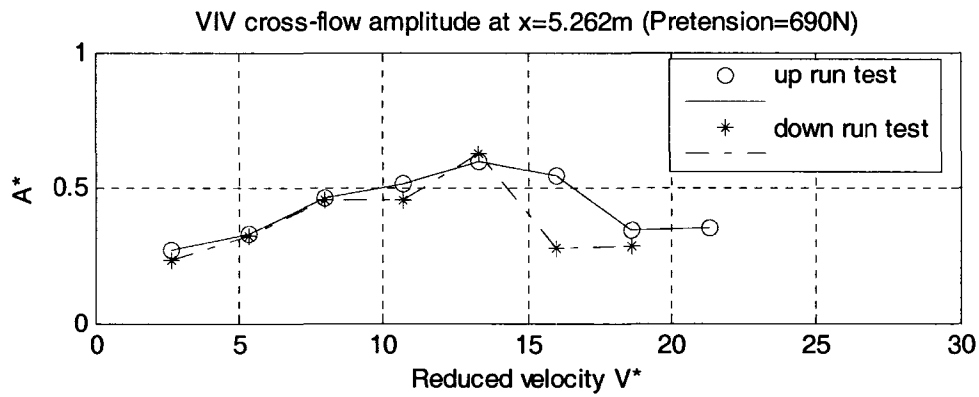


Figure 4-13(d) The average cross-flow vibration amplitude at $x=5.262\text{ m}$ in uniform current

Figure 4-13(a), Figure 4-13(b), Figure 4-13(c), and Figure 4-13(d) show average cross-flow vibration amplitude in uniform current. Like Figure 4-12(a), Figure 4-13(a) should have two peaks, but the second peak does not show up because current velocity cannot increase any more due to the limit of the current generator. The difference is that reduced velocities V^* corresponding to peaks become bigger in Figure 4-13(a). Also there is only one peak in Figure 4-13(b) and Figure 4-12(b). The reduced velocities V^* corresponding to the peak in Figure 4-13(b) is larger than that in Figure 4-12(b); and the peak value in Figure 4-13(b) is also larger than that in Figure 4-12(b). The difference between Figure 4-13(c) and Figure 4-12(c) is that reduced velocity V^* corresponding to peak becomes larger in Figure 4-13(c). The curve of Figure 4-13(d) is as flat as that in Figure 4-12(d).

At the same position, the amplitude of the in-line and cross-flow VIV versus reduced velocity are different pattern, while the amplitude curves versus reduced velocity in the sheared currents and the uniform flow are similar pattern.

4.1.1.4 Amplitude comparison between tests in the Ice Tank and the Flume Tank

Because the model surface was re-processed between the test in the Ice Tank and the test in the Flume Tank, uncertainty was brought into the comparison.

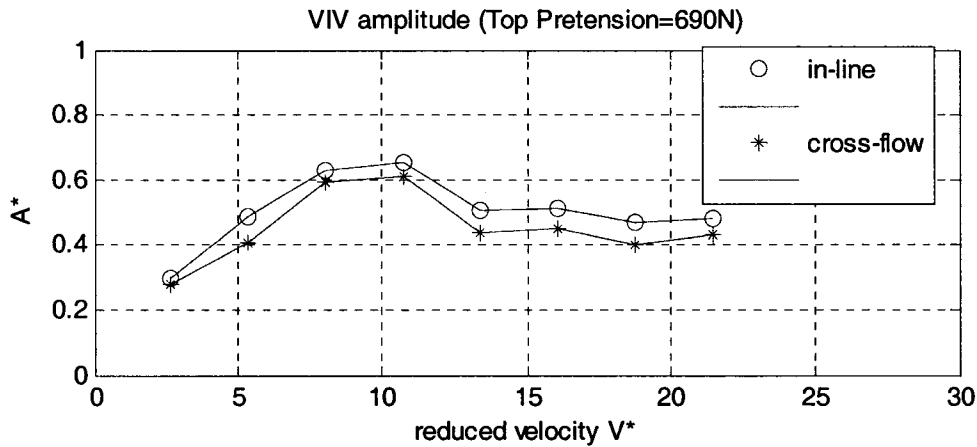


Figure 4-14 The average vibration amplitude in uniform current tested in the Flume Tank

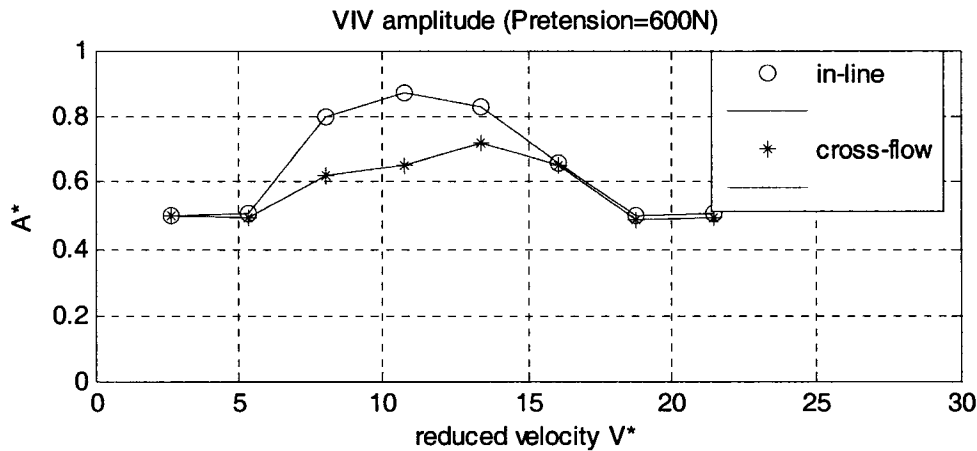


Figure 4-15 The average vibration amplitude in uniform current tested in the Ice Tank

Figure 4-14 and Figure 4-15 show average vibration amplitude in uniform current from the different tanks. The horizontal axes are the reduced velocity V^* and the vertical axes are non-dimensional vibration amplitude A^* . During the test in the Flume Tank, the model riser was installed on an incline; and top pretension was 690 N. The in-line and cross-flow results in Figure 4-14 are the average value of up run tests and down run tests. During the test in the Ice

Tank, the model riser was installed horizontally, and pretension was 600 N. Comparing the two figures, it is observed that in-line vibration amplitudes are a little larger than these of cross-flow vibration and in both figures, amplitude peaks appear at $V^*=10.73$.

Summarizing the two figures, amplitude peaks do not change significantly between the tests.

4.1.2 Frequency versus current velocity

One definition is introduced here; it is the significant value of frequencies. It represents the average value of the one-third largest frequencies of a given sample.

4.1.2.1 Comparison of frequency between different currents

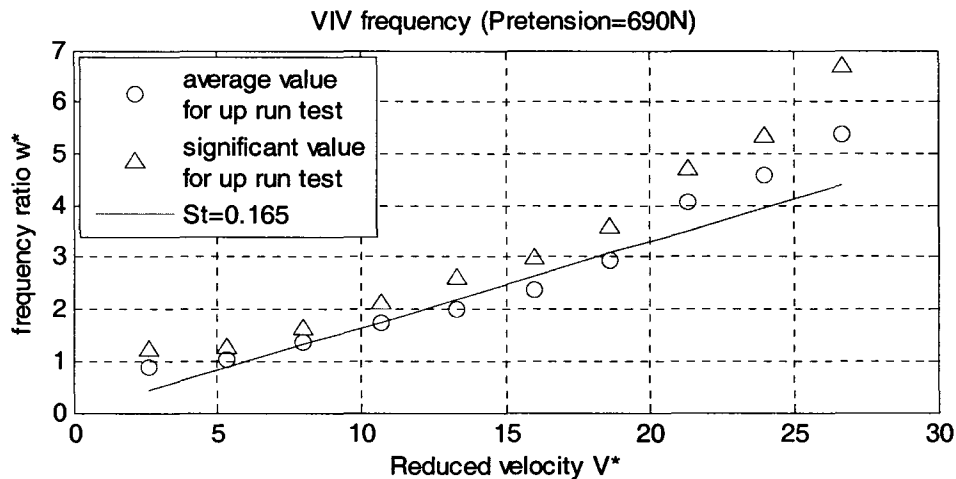


Figure 4-16 The frequency of in-line VIV in shear current produced by a 4 m block pipe

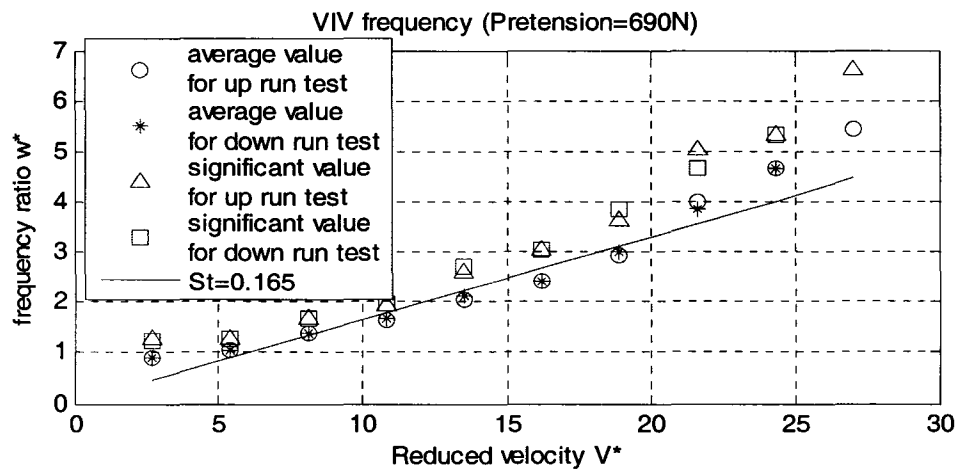


Figure 4-17 The frequency of in-line VIV in shear current produced by a 3.5 m block pipe

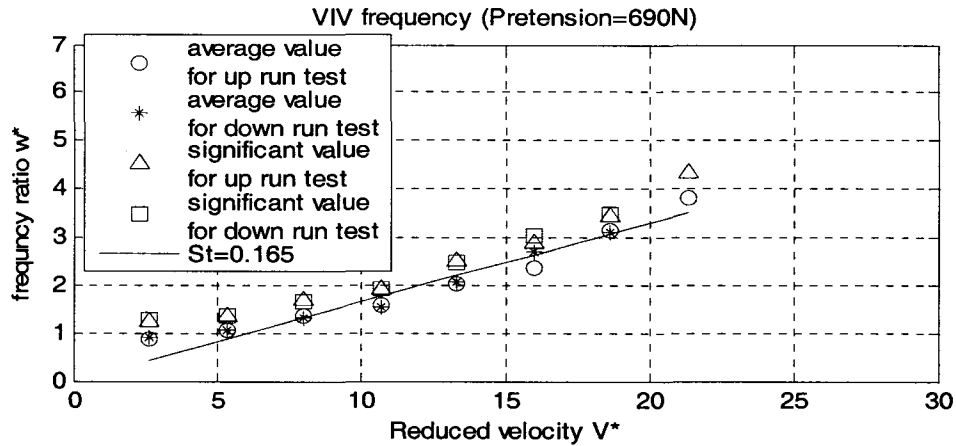


Figure 4-18 The frequency of in-line VIV in uniform current

Figure 4-16, figure 4-17 and figure 4-18 show in-line vibration frequencies in various currents. The horizontal axes are reduced velocity V^* and the vertical axes are frequency ratio ω^* . As seen in these figures, \circ displays the average frequencies for up run tests; $*$ displays the average frequencies for down run tests; Δ displays the significant frequencies for up run tests, and \square displays the significant frequencies for down run tests. Although the values of the significant frequency are a little larger than those of the average frequency, they are close to the Strouhal frequency, which can be calculated using equation (3-21). The estimated value equals 0.165 here.

The Reynolds numbers of the tests belong to the range of 300 to 3×10^5 in which vortex shedding frequencies should be compliant with the Strouhal frequencies, [Blevin, 1977]. The above three figures show that vortex shedding frequencies measured in the tests meet the Strouhal frequencies; this does not change for different current profiles. In addition, no obvious lock-in phenomena were observed.

Observing lock-in phenomena from significant frequencies and average frequencies, the result is the same. In other words, lock-in phenomena appear on the curve of significant frequencies and the curve of average frequencies simultaneously.

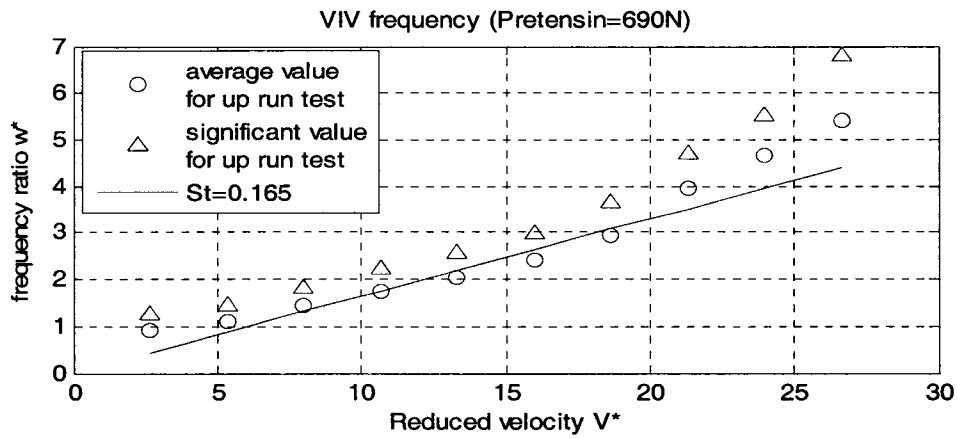


Figure 4-19 The frequency of cross-flow VIV in shear current produced by a 4 m block pipe

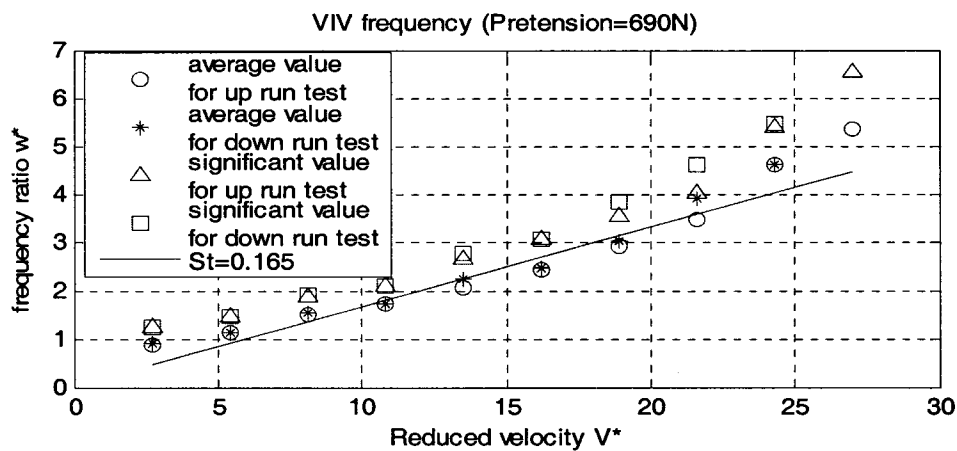


Figure 4-20 The frequency of cross-flow VIV in shear current produced by a 3.5 m block pipe

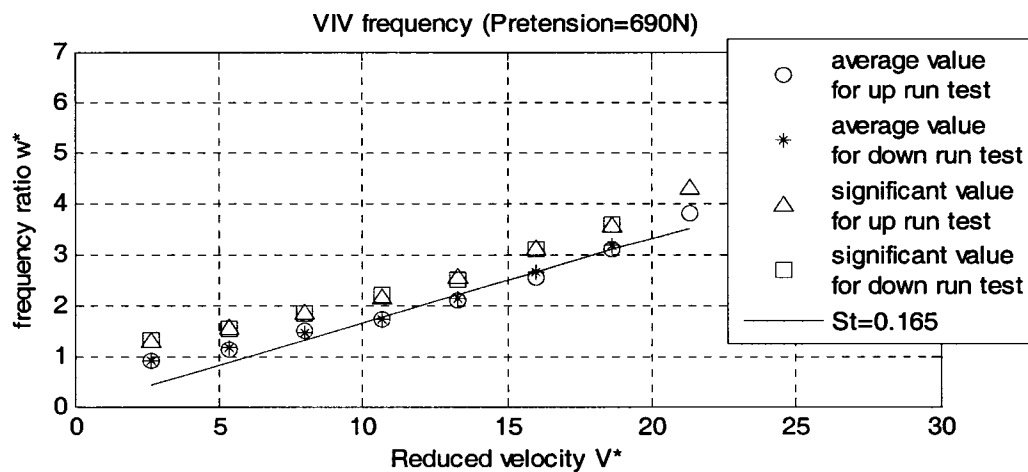


Figure 4-21 The frequency of cross-flow VIV in uniform current

Figure 4-19, figure 4-20 and figure 4-21 show the cross-flow vibration frequency in various currents. Like Figure 4-16, figure 4-17 and figure 4-18, these frequencies are compliant with the Strouhal number $St=0.165$. This does not change for different current profiles. In addition, no obvious lock-in phenomena were observed here. Frequencies from up run tests almost coincided with those from down run tests. This implies that test results should not relate to test order so long as waiting water time is enough long.

4.1.2.2 Comparison of frequency between different tensions

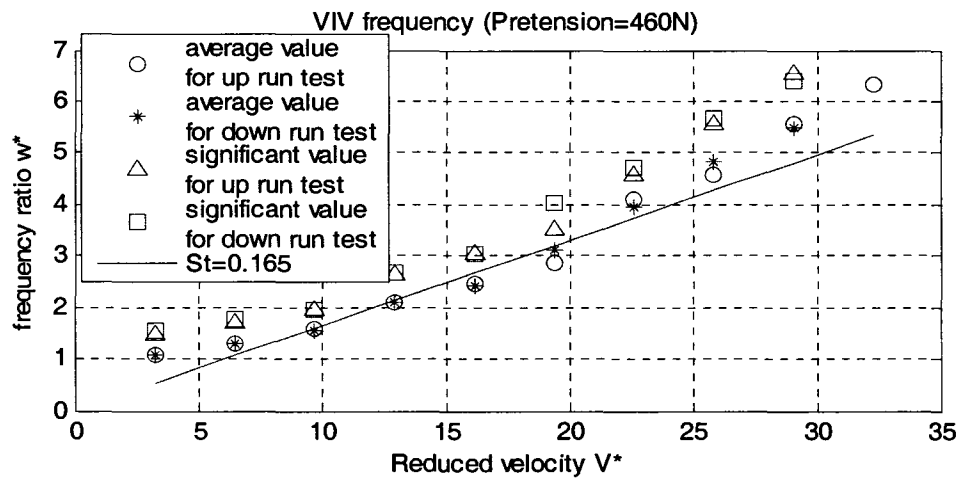


Figure 4-22 The frequency of in-line in shear current produced by a 4 m block pipe and pretension=460 N

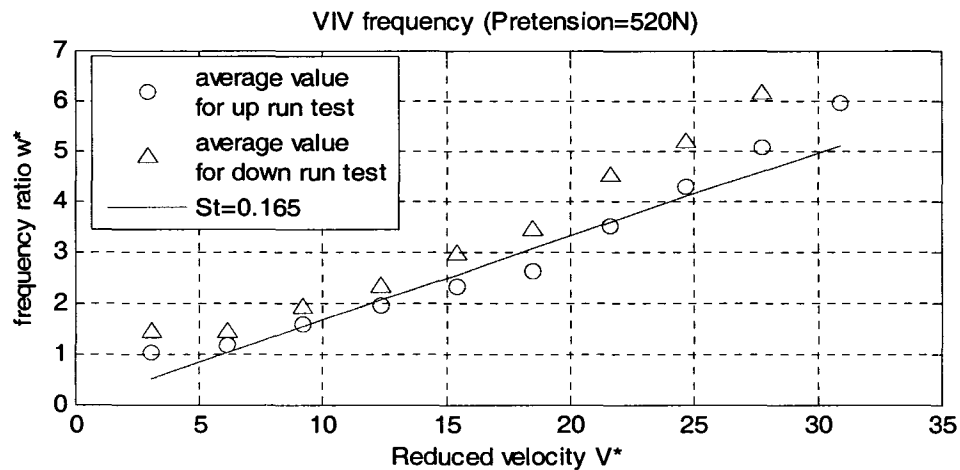


Figure 4-23 The frequency of in-line in shear current produced by a 4 m block pipe and pretension=520 N

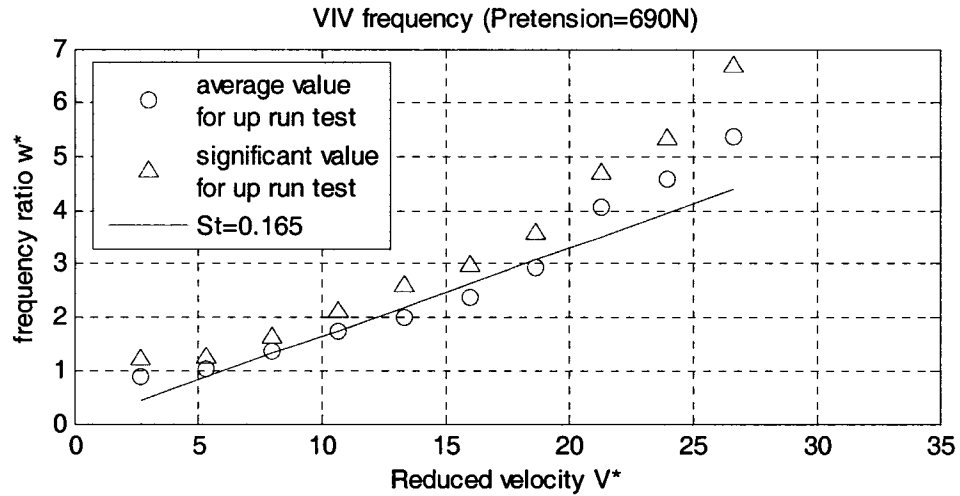


Figure 4-24 The frequency of in-line in shear current produced by a 4 m block pipe and pretension=690 N

Figure 4-22, Figure 4-23, and figure 4-24 show in-line vibration frequencies in the same current but at different pretensions. The horizontal axes are reduced velocity V^* and the vertical axes are frequency ratio ω^* . As seen in the figures, the vibration frequencies also follow the Strouhal frequencies. This does not change when the pretension changes. No obvious lock-in phenomena was observed.

4.2. Frequency-domain analysis

To assist with the interpretation of following contents, the table about modal frequencies is shown here. These values are calculated using equation (2-1).

Table 4-2 Natural frequencies of various modes

Mode	T=460 N	T=520 N	T=690 N	T=800 N
1	0.6806	0.7236	0.8336	0.8976
2	1.3612	1.4473	1.6672	1.7951
3	2.0419	2.1709	2.5008	2.6927
4	2.7225	2.8946	3.3343	3.5903
5	3.4031	3.6182	4.1679	4.4879
6	4.0837	4.3419	5.0015	5.3854
7	4.7643	5.0657	5.8351	6.2830
8	5.4494	5.7892	6.6687	7.1806
9	6.1256	6.5128	7.5023	8.0782
10	6.8062	7.2365	8.3358	8.9757

4.2.1 Comparison of power spectrum between different tensions

Flexible model riser vortex induced vibration always consists of multiple frequency components. The measured frequency components in these tests ranged from zero Hertz to approximately ten Hertz. The figures of power spectrum versus frequency ratio reveal the power distribution energy over various frequencies.

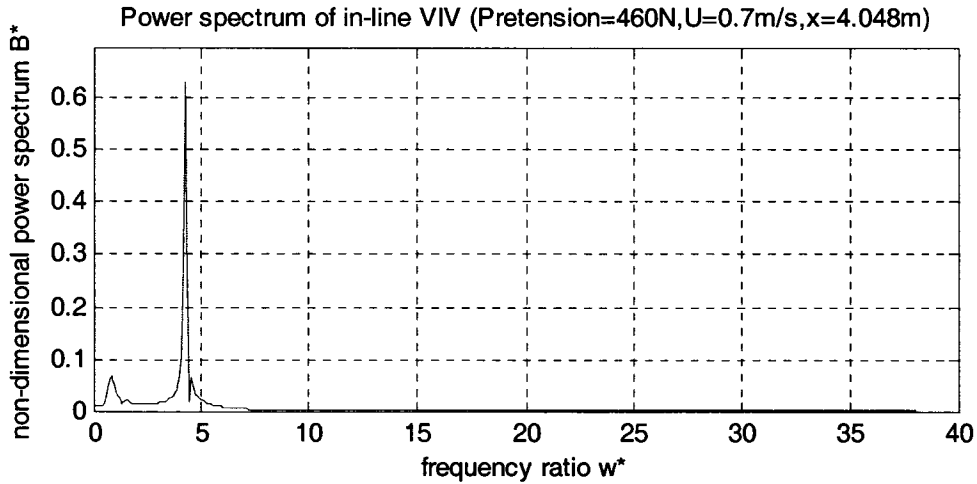


Figure 4-25 The power spectrum of in-line VIV in shear current produced by a 4 m block pipe

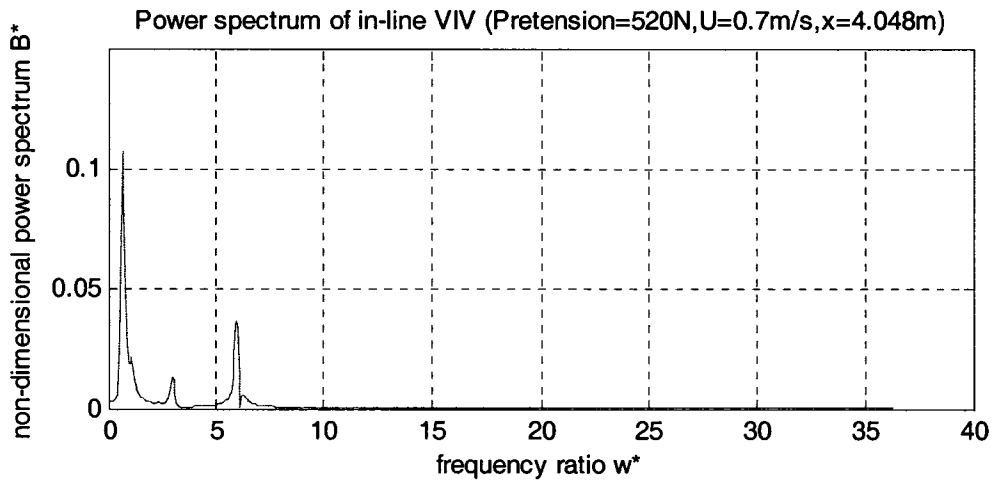


Figure 4-26 The power spectrum of in-line VIV in shear current produced by a 4 m block pipe

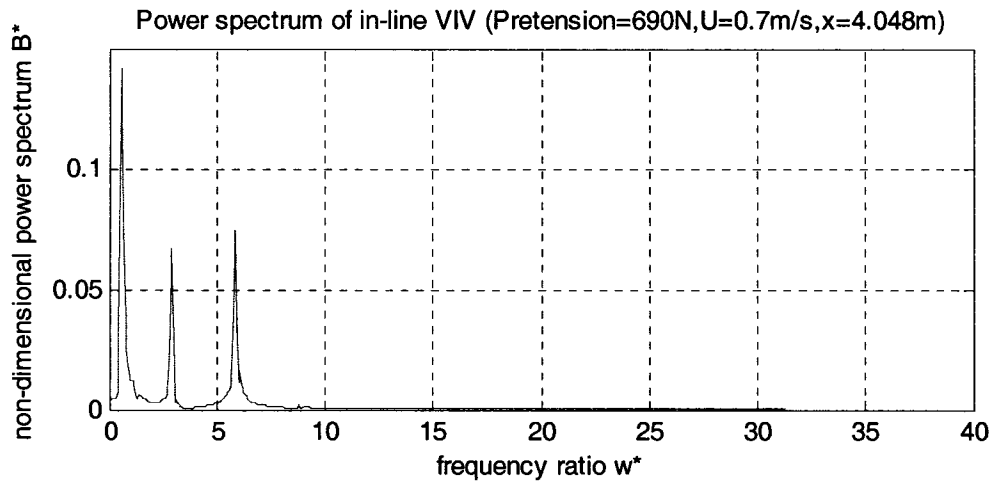


Figure 4-27 The power spectrum of in-line VIV in shear current produced by a 4 m block pipe

Figure 4-25, Figure 4-26 and Figure 4-27 are the power spectrum of in-line VIV under all of the same conditions except for pretensions. The horizontal axes are frequency ratio ω^* and the vertical axes are non-dimensional power spectrum B^* . When $U = 0.7$ m/s, V^* is respectively 22.99, 21.63, and 18.77 under the pretensions of 460 N, 520 N, and 690 N. From Figure 4-25, a strong dominant spectrum peak appears at frequency ratio=4. In other words, the majority of VIV energy is concentrated at this frequency. The results from spectral analysis have a good agreement with the results from the time-domain analysis because the frequency ratio is also 4 in Figure 4-22 when V^* is 22.99. A relatively flat second-dominant peak is at frequency ratio=0.8. It shows that there is much less energy of vibration at this lower frequency. In Figure 4-26, there are three spectrum peaks. From Figure 4-23, the frequency ratio is also 3.5 when V^* is 21.63. It is close to the average value of the three peak frequency ratios in Figure 4-26. Similarly, in Figure 4-27, the average value of the three peak frequencies are close to the frequency ratio at $V^*=18.77$ in Figure 4-24.

4.2.2 Comparison of power spectrum between different velocities

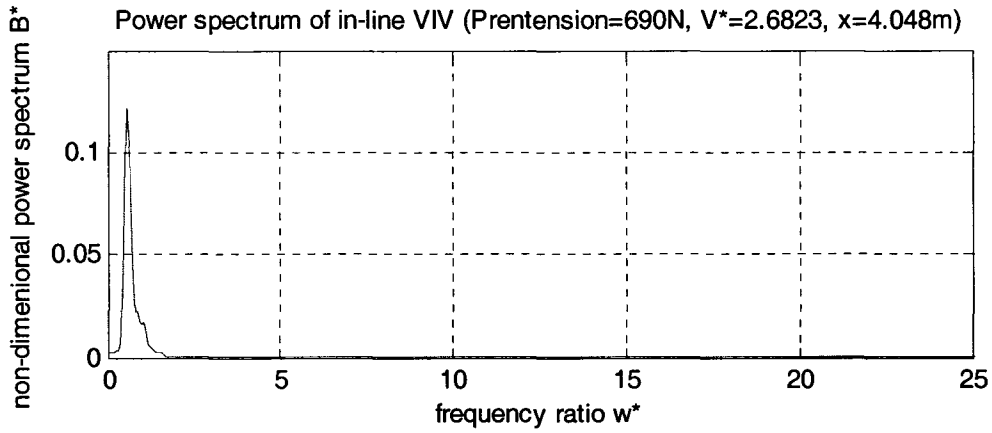


Figure 4-27(a) The power spectrum of in-line VIV in shear current produced by a 3.5 m block pipe at $v^*=2.68$ ($U=0.1$ m/s)

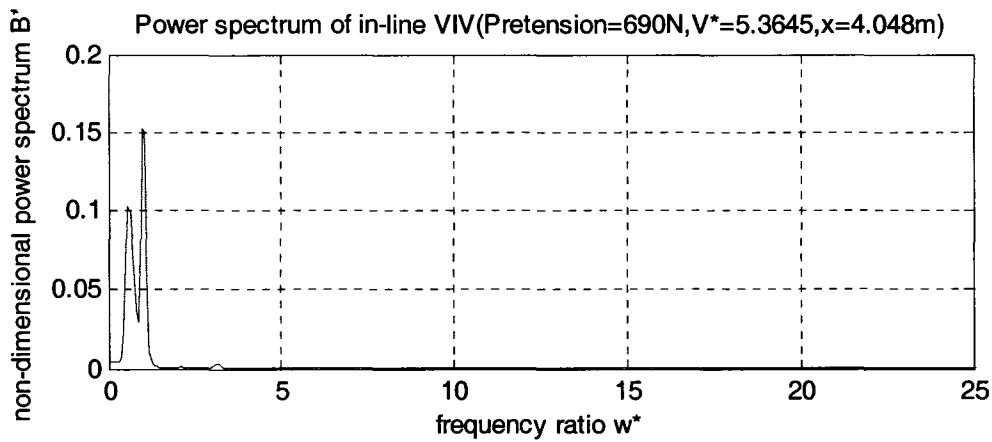


Figure 4-27(b) The power spectrum of in-line VIV in shear current produced by a 3.5 m block pipe at $v^*=5.36$ ($U=0.2$ m/s)

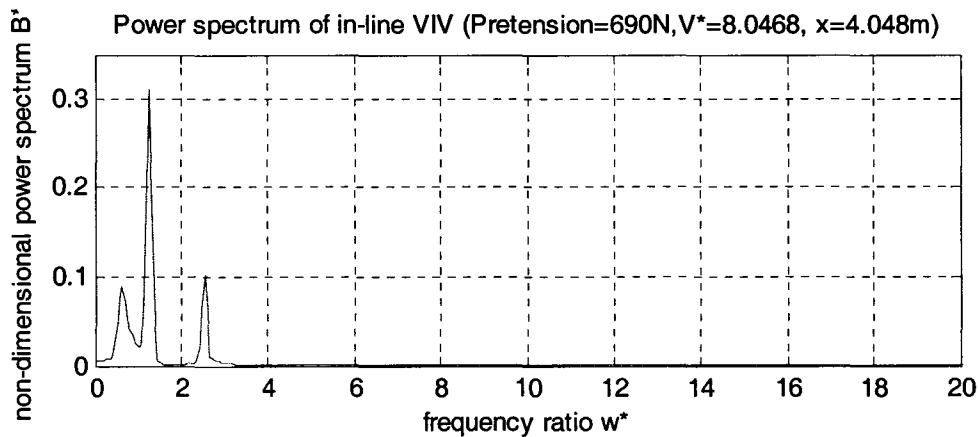


Figure 4-27(c) The power spectrum of in-line VIV in shear current produced by a 3.5 m block pipe at $v^*=8.05$ ($U=0.3$ m/s)

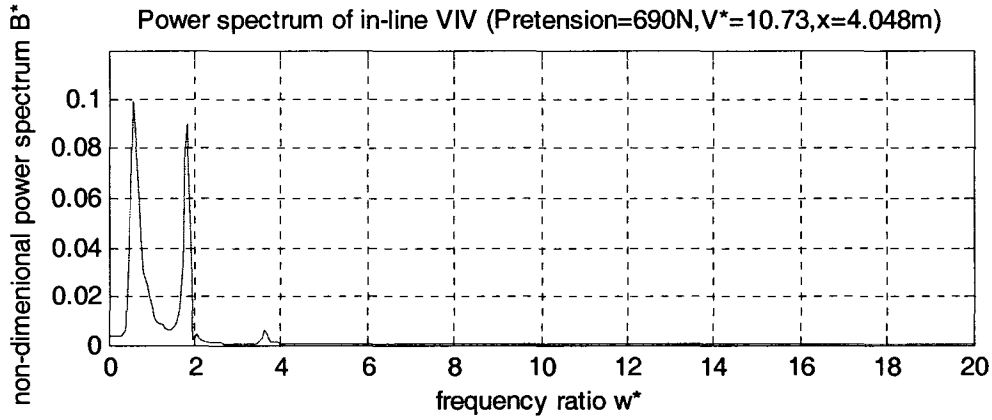


Figure 4-27(d) The power spectrum of in-line VIV in shear current produced by a 3.5 m block pipe at $v^*=10.73$ ($U=0.4$ m/s)

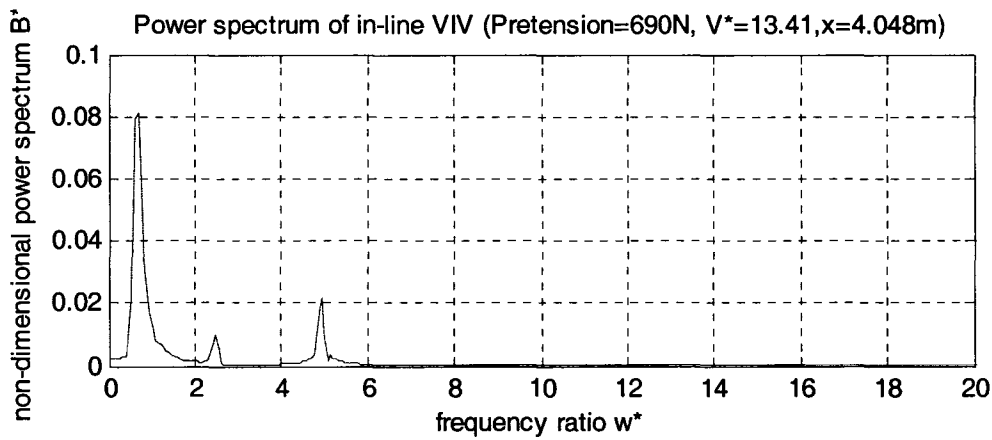


Figure 4-27(e) The power spectrum of in-line VIV in shear current produced by a 3.5 m block pipe at $v^*=13.41$ ($U=0.5$ m/s)

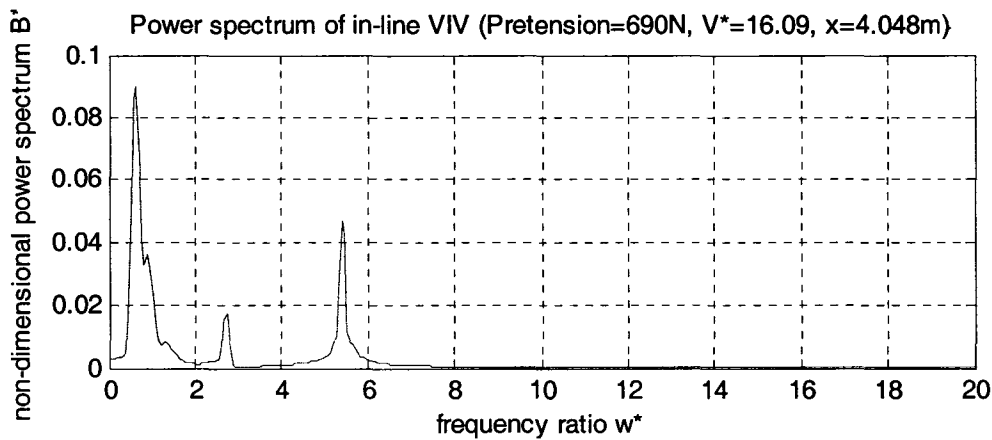


Figure 4-27(f) The power spectrum of in-line VIV in shear current produced by a 3.5 m block pipe at $v^*=16.09$ ($U=0.6$ m/s)

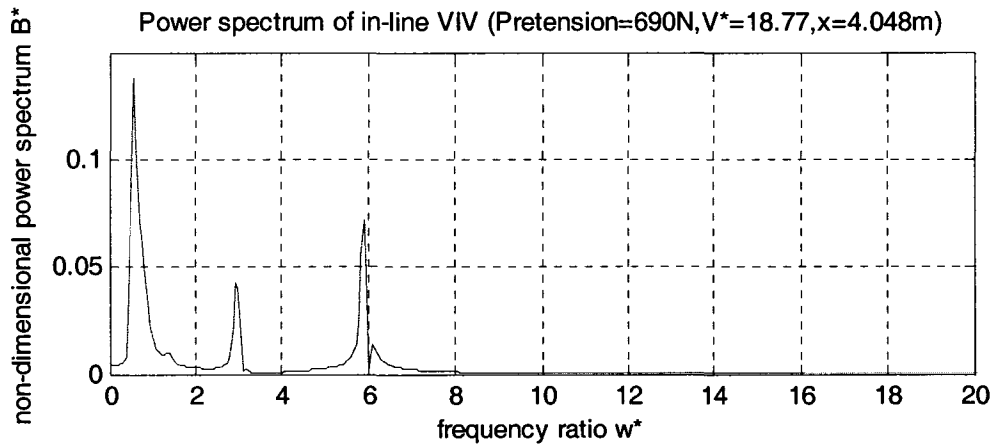


Figure 4-27(g) The power spectrum of in-line VIV in shear current produced by a 3.5 m block pipe at $v^*=18.77$ ($U=0.7$ m/s)

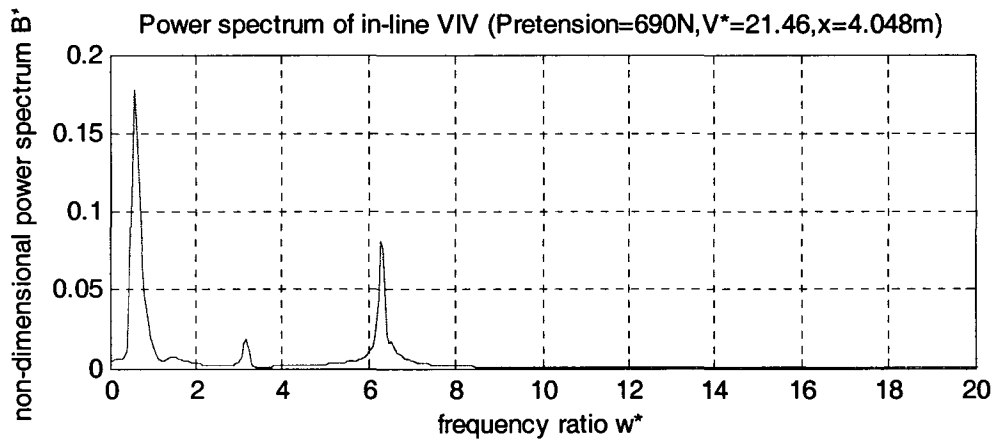


Figure 4-27(h) The power spectrum of in-line VIV in shear current produced by a 3.5 m block pipe at $v^*=21.46$ ($U=0.8$ m/s)

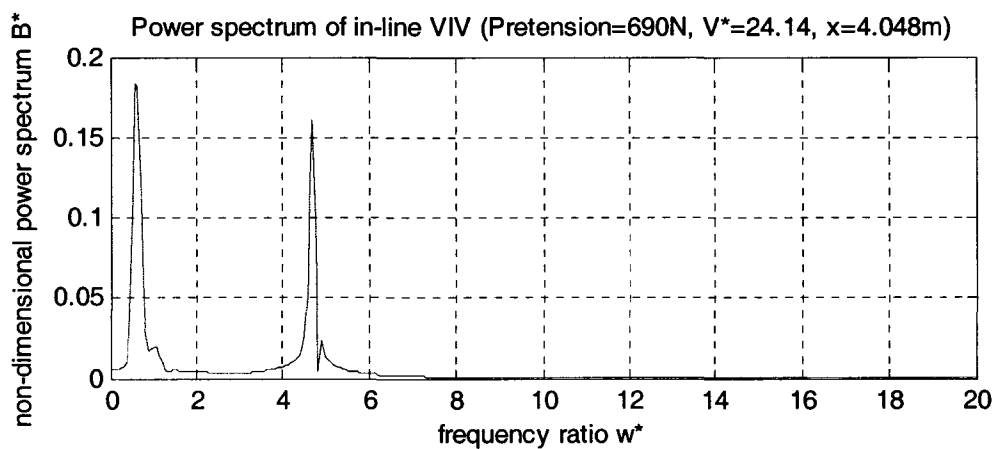


Figure 4-27(i) The power spectrum of in-line VIV in shear current produced by a 3.5 m block pipe at $v^*=24.14$ ($U=0.9$ m/s)

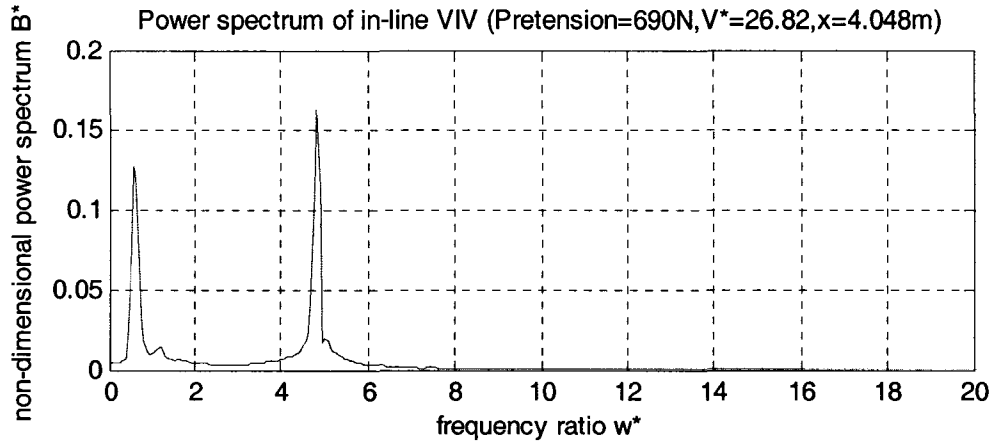


Figure 4-27(j) The power spectrum of in-line VIV in shear current produced by a 3.5 m block pipe at $v^*=26.82$ ($U=1.0$ m/s)

Ten figures in Figure 4-27 show the power spectrum at various current velocities. The horizontal axes are frequency ratio ω^* and the vertical axes are non-dimensional power spectrum B^* . In Figure 4-27(a), current velocities are very low; the power spectrum shows a single peak. The frequency ratio corresponding to the peak is 1. It coincides with a frequency ratio of $V^*=2.68$ in Figure 4-17. In Figure 4-27(b), the power spectrum shows two close peaks. The second peak is higher than the first one. In Figure 4-27(c), the curve contains three peaks. The dominant peak stands in the middle; and the corresponding frequency ratio is 1.5. So the average value of the three peak frequencies corresponds to the frequency ratio at $V^*=8.05$ in Figure 4-17. In Figure 4-27(d), the curve contains two peaks. The average value of the two peak frequencies is lower than the frequency represented by the frequency ratio at $V^*=10.73$ in Figure 4-17. This is because frequency ratios at different riser positions are different, but average frequency ratios over the riser length are the same as the frequency ratio at $V^*=10.73$ in Figure 4-17. In Figure 4-27(e), a dominant peak is at frequency ratio $\omega^* = 0.8$ with two more small peaks. Figure 4-27(f), Figure 4-27(g), and Figure 4-27(h) are similar to Figure 4-27(e). One difference is that the peak at the

high frequency becomes higher as current velocity increases. Figure 4-27(i) and Figure 4-27(j) look similar. They have two dominant peaks. Summarizing the results, it is known that when current velocity is low, the power spectrum has one or several close peaks. When current velocity is in the middle such as $U=0.5$ m/s to 0.7 m/s, the power spectrum has three separating peaks. When current velocity is high, such as 0.9 m/s to 1 m/s, the power spectrum has two separating peaks.

4.2.3 Comparison of power spectrum between different positions over riser length

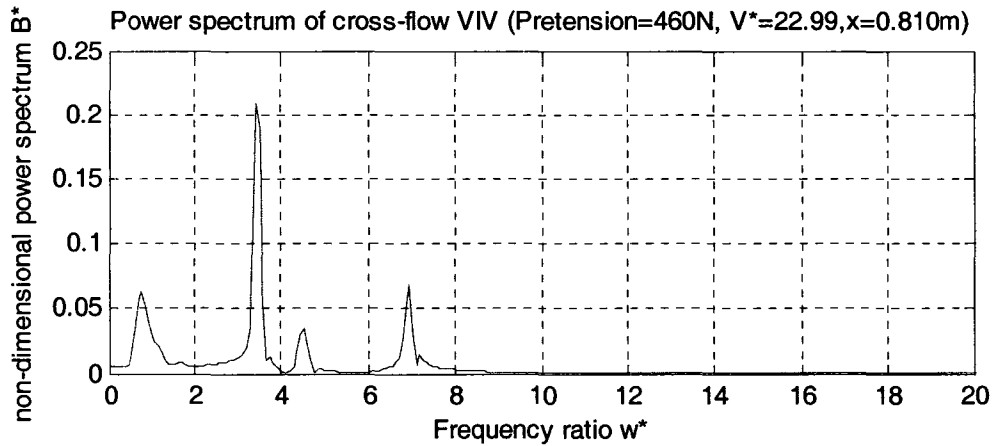


Figure 4-28(a) The cross-flow VIV power spectrum at $x=0.81$ m in shear current produced by a 3.5 m pipe

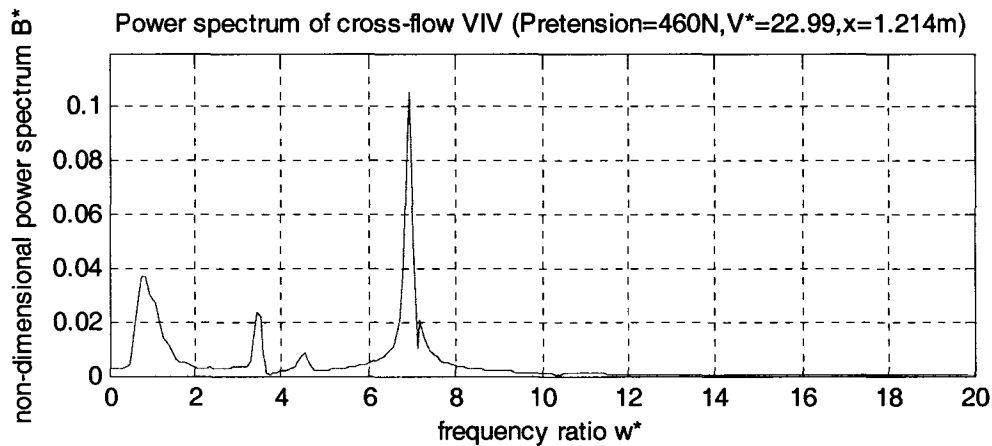


Figure 4-28(b) The cross-flow VIV power spectrum at $x=1.214$ m in shear current produced by a 3.5 m pipe

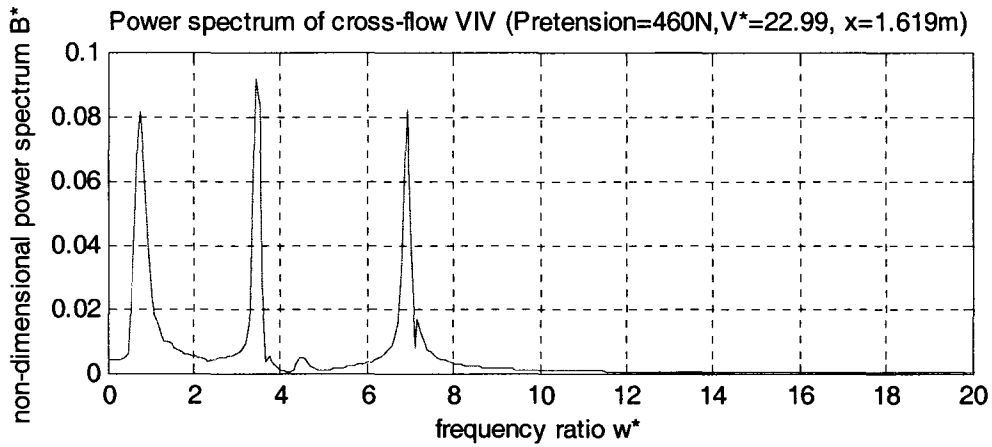


Figure 4-28(c) The cross-flow VIV power spectrum at $x=1.619$ m in shear current produced by a 3.5 m pipe

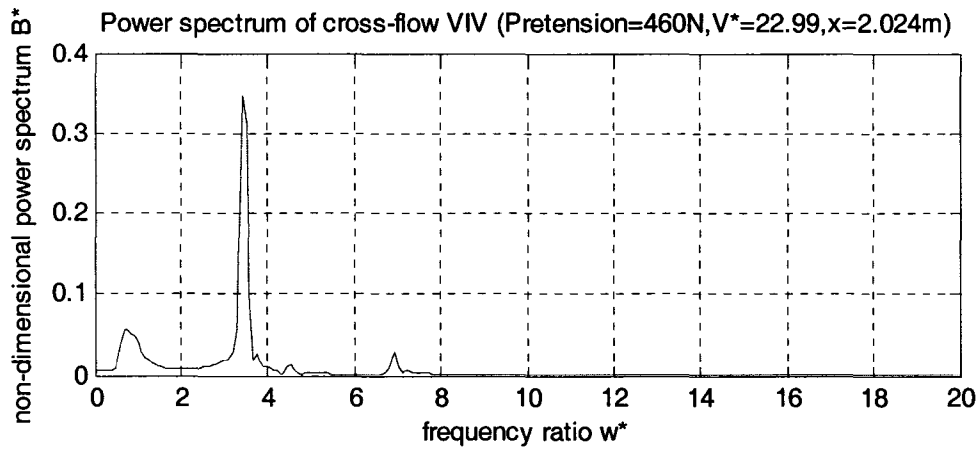


Figure 4-28(d) The cross-flow VIV power spectrum at $x=2.024$ m in shear current produced by a 3.5 m pipe

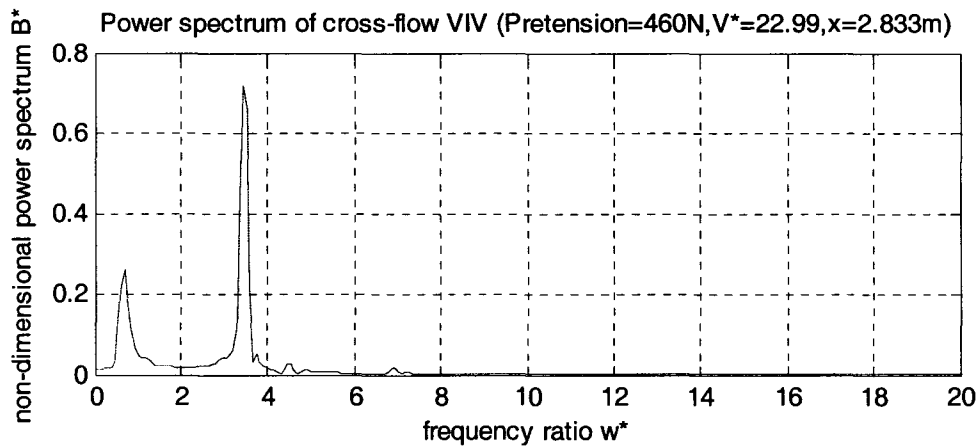


Figure 4-28(e) The cross-flow VIV power spectrum at $x=2.833$ m in shear current produced by a 3.5 m pipe

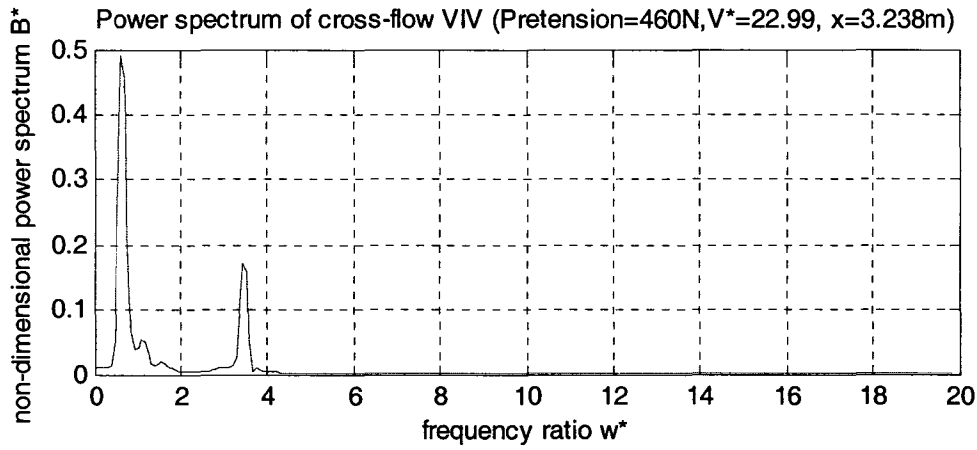


Figure 4-28(f) The cross-flow VIV power spectrum at $x=3.238\text{ m}$ in shear current produced by a 3.5 m pipe

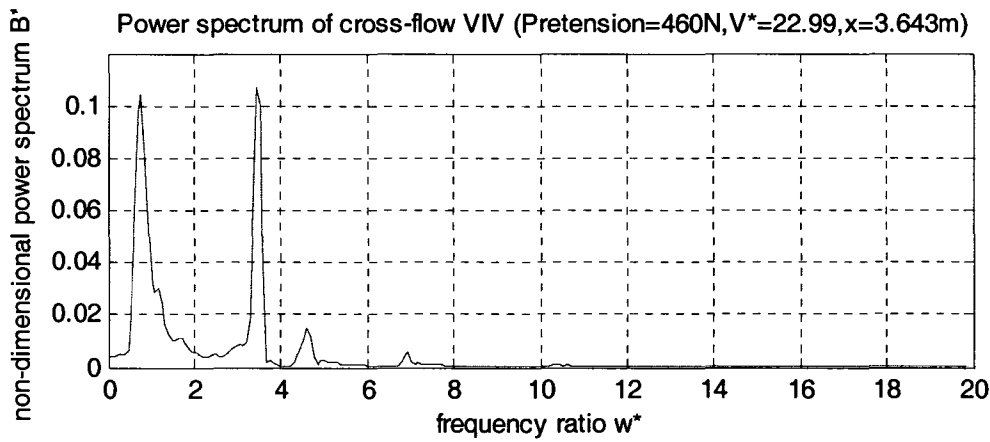


Figure 4-28(g) The cross-flow VIV power spectrum at $x=3.643\text{ m}$ in shear current produced by a 3.5 m pipe

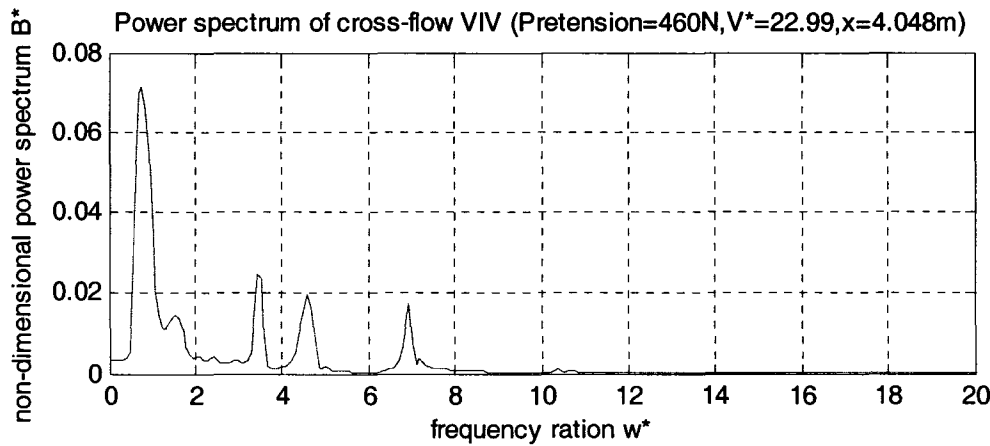


Figure 4-28(h) The cross-flow VIV power spectrum at $x=4.048\text{ m}$ in shear current produced by a 3.5 m pipe

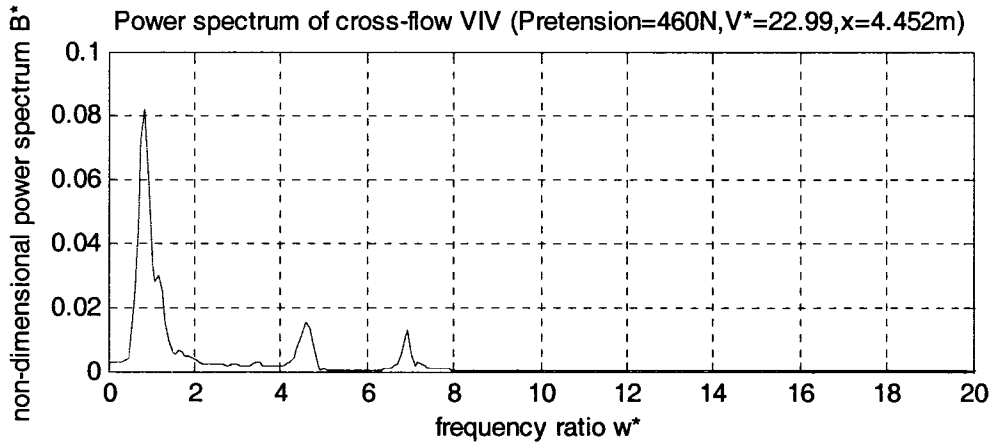


Figure 4-28(i) The cross-flow VIV power spectrum at $x=4.452\text{ m}$ in shear current produced by a 3.5 m pipe

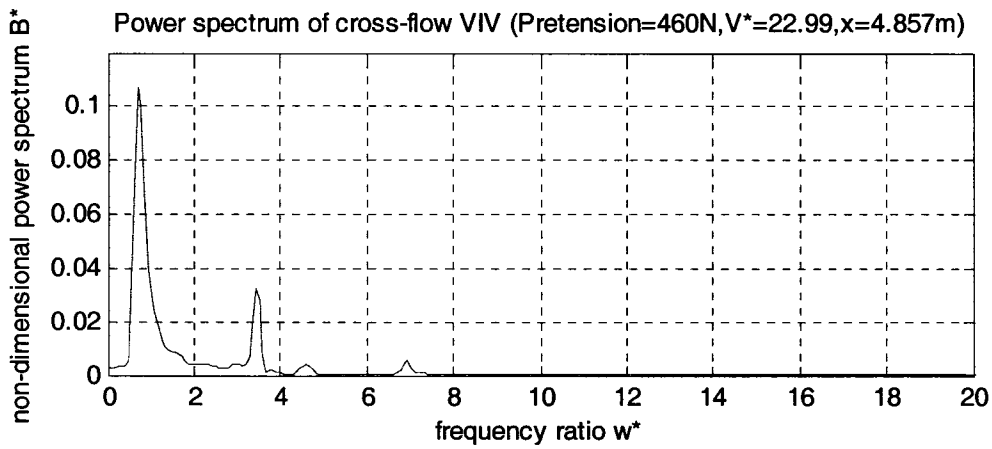


Figure 4-28(j) The cross-flow VIV power spectrum at $x=4.857\text{ m}$ in shear current produced by a 3.5 m pipe

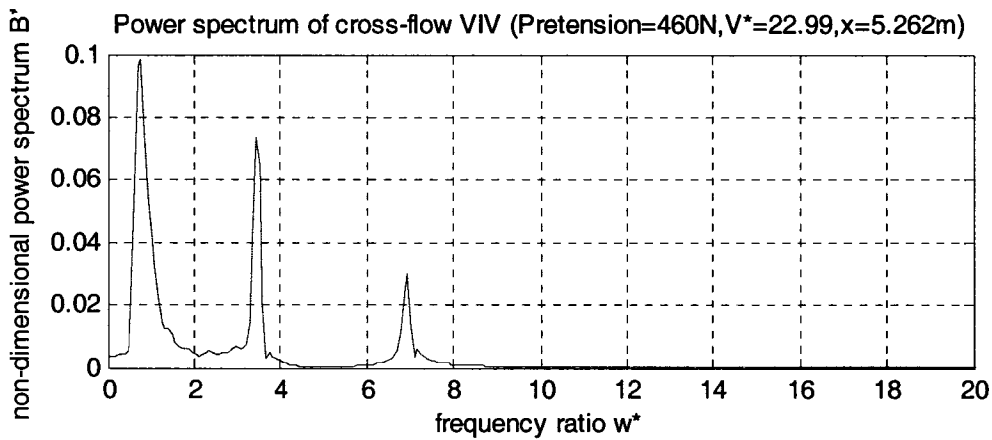


Figure 4-28(k) The cross-flow VIV power spectrum at $x=5.262\text{ m}$ in shear current produced by a 3.5 m pipe

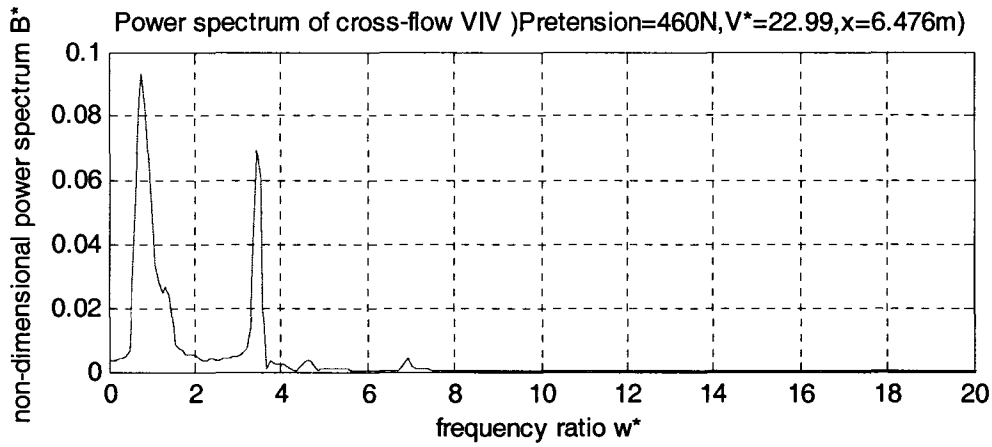


Figure 4-28(l) The cross-flow VIV power spectrum at $x=6.476$ m in shear current produced by a 3.5 m pipe

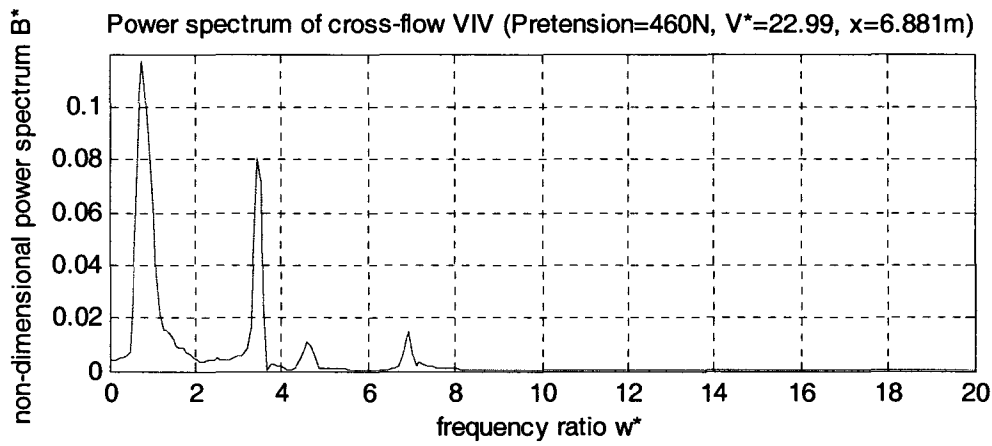


Figure 4-28(m) The cross-flow VIV power spectrum at $x=6.881$ m in shear current produced by a 3.5 m pipe

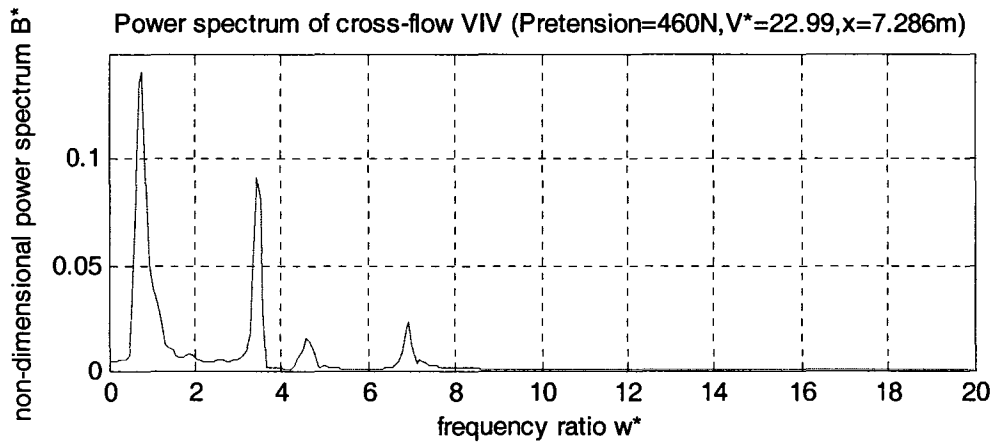


Figure 4-28(n) The cross-flow VIV power spectrum at $x=7.286$ m in shear current produced by a 3.5 m pipe

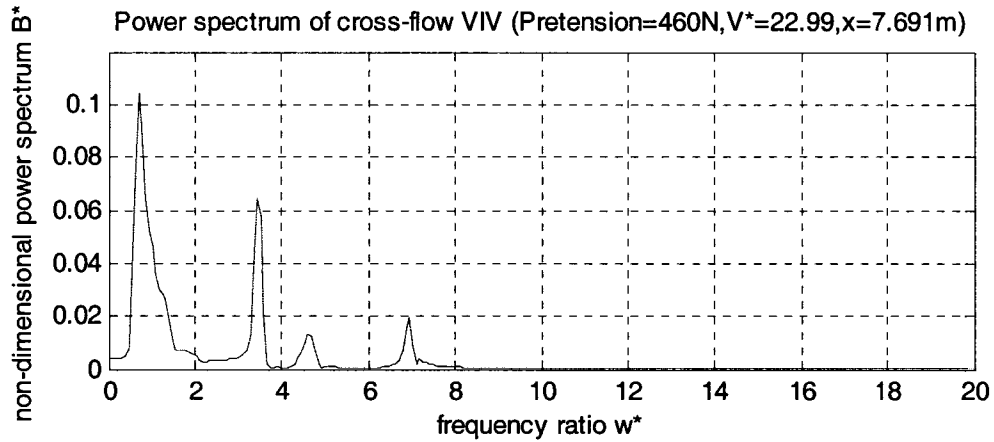


Figure 4-28(o) The cross-flow VIV power spectrum at $x=7.691$ m in shear current produced by a 3.5 m pipe

Figure 4-28 includes fifteen figures. They show the cross-flow VIV power spectra at the surviving accelerometer positions over model riser length. The horizontal axes are frequency ratio ω^* and the vertical axes are non-dimensional power spectrum B^* .

In Figure 4-28(a), there are four peaks. Frequency ratio ω^* corresponding to the peaks are 1, 3.5, 4.5, and 6.8 respectively. The strongest dominant frequency ratio is 3.5 with a peak value $B^*=0.2$. Like Figure 4-28(a), Figure 4-28(b) also has four peaks and the corresponding frequency ratios ω^* are 1, 3.5, 4.5, and 6.8 respectively. The strongest dominant frequency ratio is 6.8 with a peak value $B^*=0.1$. Three strong dominant peaks exist in Figure 4-28(c). The frequency ratios ω^* of the peaks are 1, 3.5, and 6.8 respectively. The peak value B^* ranges from 0.08 to 0.09. For three peaks in Figure 4-28(d), only the frequency corresponding to frequency ratio $\omega^*=3.5$ is dominant. Its peak value B^* is 0.34. The peak patterns in Figure 4-28(e) are similar to those in Figure 4-28(d); but the first two peak values increase. The first peak value B^* increases to 0.25, and the second peak value B^* increases to 0.7. In Figure 4-28(f), two peaks are shown. When $w^*=1$, its peak value $B^*=0.5$; when $w^*=3.5$, its peak value $B^*=0.15$. In Figure 4-28(g), there are four peaks. Among the four peaks, two peaks with equal height are dominant. The two dominant peak values for B^* are both 0.1. Four peaks appear in Figure 4-28(h). The peak values range

from 0.02 to 0.07. In Figure 4-28(i), the peak number decreases to three. The frequency ratio ω^* that the peaks correspond to are 1, 4.5, and 6.8. The dominant peak stands at $\omega^*=1$. In Figure 4-28(j), the first peak is a dominant peak in four peaks. The peak value B^* equals 1. Three clear and obvious peaks exist in Figure 4-28(k). The frequency ratio ω^* that the peaks correspond to are 1, 3.5, and 6.8 respectively. The peak values for B^* range from 0.03 to 1. There are two obvious peaks and two obscure peaks in Figure 4-28(l). The frequency ratio ω^* for the two high peaks are 1 and 3.5. Figure 4-28(m), Figure 4-28(n) and Figure 4-28(o) have a peak arrangement similar with that in Figure 4-28(l). The difference between these figures is that peak value B^* is different.

From equation 2-1, it is easy to understand that mode n natural frequency is n times the mode 1 natural frequency. Depending on the definition of ω^* shown in equation 3-22, when $\omega^*=1$, the vortex shedding frequency ω is close to the resonance frequency of mode 1. When $\omega^*=n$, vortex shedding frequency ω is close to the resonance frequency of mode n . From the majority of Figure 4-28's fifteen figures, dominant peaks appear at $\omega^*=1$. This indicates that mode 1 makes a large contribution to the whole model riser vibration in this case. When $\omega^*=3.5$, the vortex shedding frequency ω is close to the Strouhal frequencies. Although the power spectral patterns at varied positions are different, the average value of all peak frequencies for the whole model riser coincides with the value calculated from the Strouhal number.

Because reduced velocity $V^*=22.99$ corresponds to a relatively high speed, the spectra of VIV responses at all locations have multi-peaks.

4.2.4 Power spectrum comparison between different currents

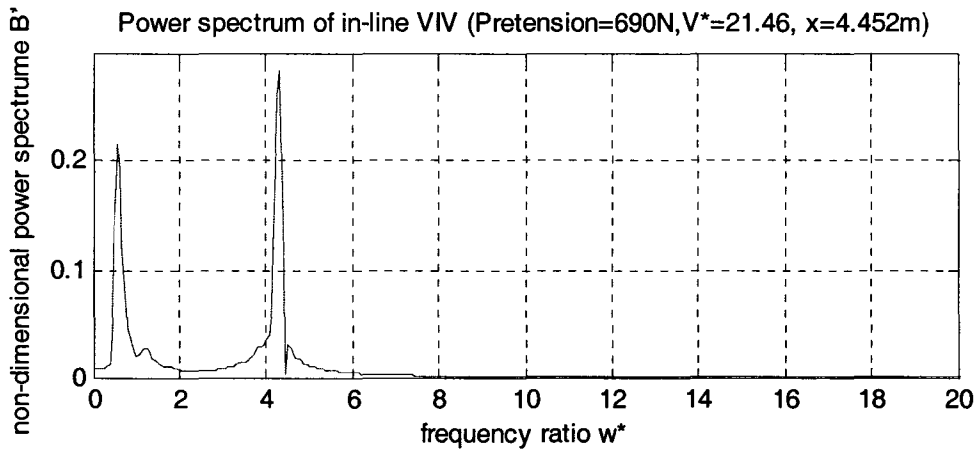


Figure 4-29 The Power spectrum of in-line VIV in shear current produced by a 4 m pipe

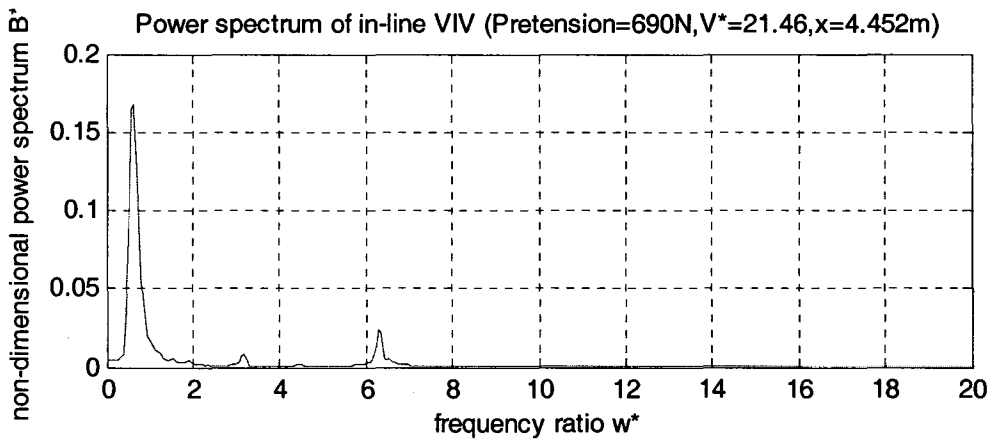


Figure 4-30 The Power spectrum of in-line VIV in shear current produced by a 3.5 m pipe

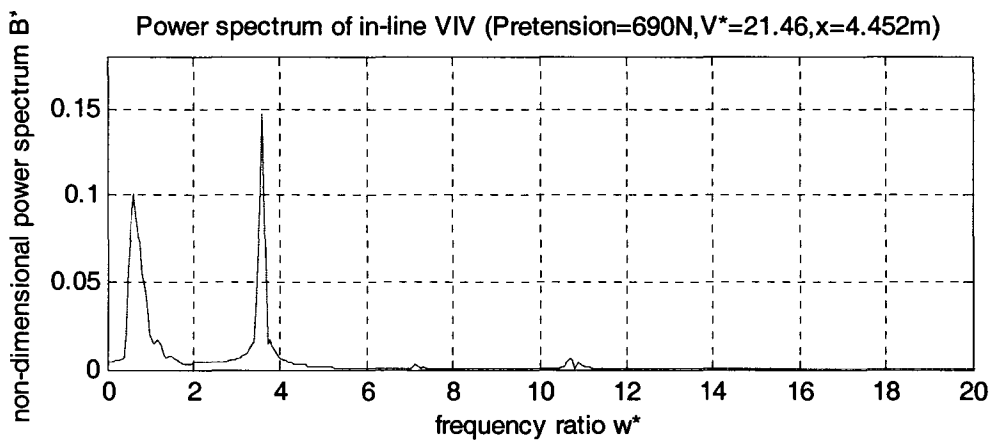


Figure 4-31 The Power spectrum of in-line VIV in uniform current

Figure 4-29, Figure 4-30, and Figure 4-31 are the power spectra for different current regimes. The spectra are vibration spectra at high reduced velocity $V^*=21.46$, so the majority of them have multi-peaks and display a broad spectral width.

4.3 Space-domain analysis

The most modes analyzed in the thesis is ten modes. So both vibration response of in-line and cross-flow are considered to contain the components from mode 1 to mode 10.

4.3.1 Modal components in the VIV response at various flow velocity

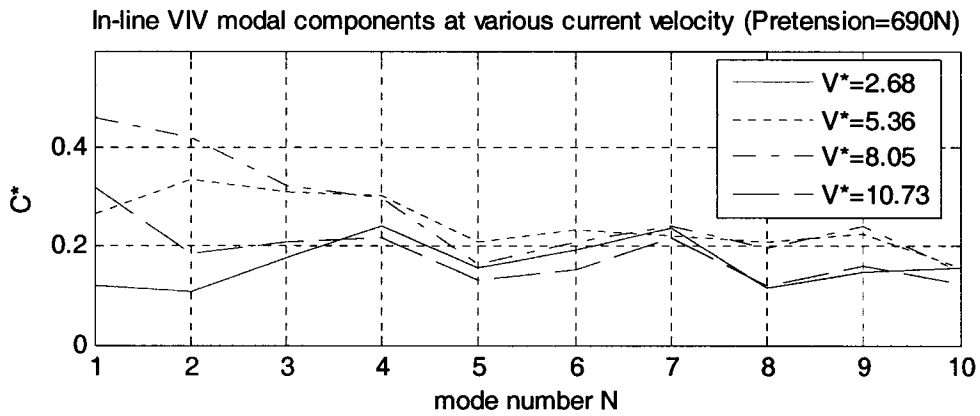


Figure 4-32(a) The in-line VIV modal component distribution in shear current produced by a 4 m pipe and reduced velocity from 2.68 to 10.73

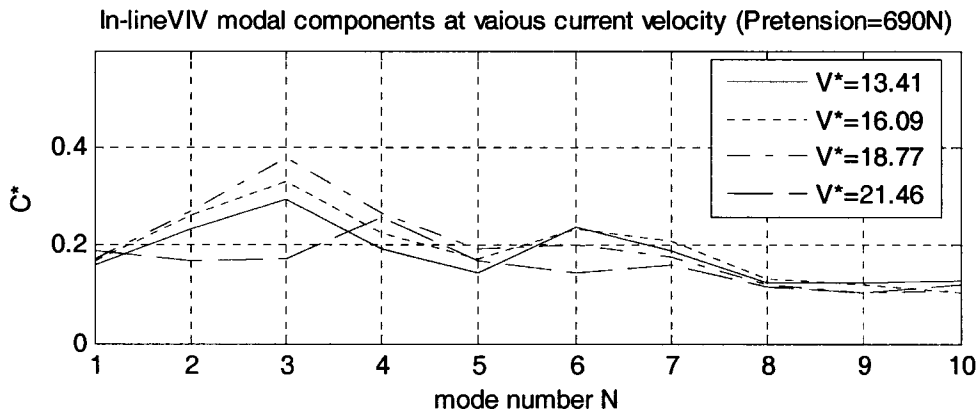


Figure 4-32(b) The in-line VIV modal component distribution in shear current produced by a 4 m pipe and reduced velocity from 13.41 to 21.46

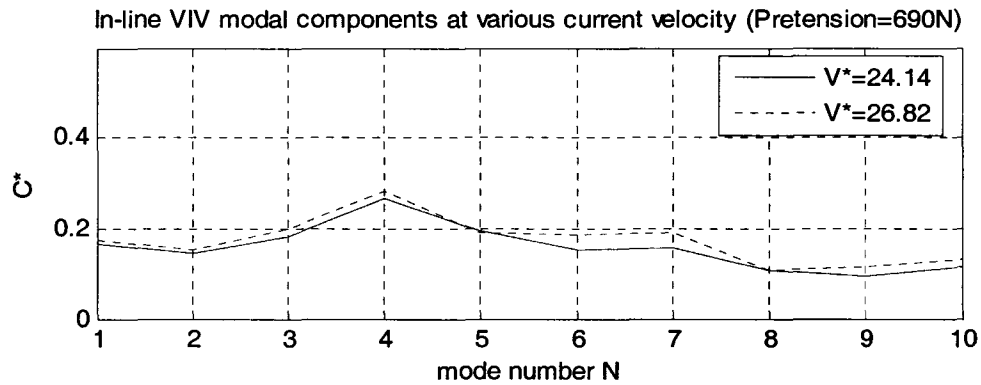


Figure 4-32(c) The in-line VIV modal component distribution in shear current produced by a 4 m pipe and reduced velocity 24.14 and 26.82

Figure 4-32 (a), Figure 4-32 (b) and Figure 4-32 (c) present in-line VIV modal component distribution at reduced velocities from 2.68 to 26.82 in shear current produced by the 4 m pipe. The horizontal axes are mode number N and the vertical axes are non-dimensional modal VIV response C^* , which is defined in chapter 3. Mode number N is from 1 to 10.

In Figure 4-32, the curves of $V^*=2.68$ and $V^*=5.36$ look relatively flat. This is because the two velocities are very low; vortex shedding frequencies which correspond to the two velocities are very low; so that they do not reach any natural frequency mode of the riser. As a result, all modes contribute similarly to the VIV response, and the mode component curve looks relatively flat without an obvious peak. When reduced velocities increase to 8.05 and 10.73, vortex shedding frequencies approach the resonance frequency of mode 1, so that mode 1 has a relatively big contribution to the VIV response at the two reduced velocities. When reduced velocity continues to increase to 13.41, 16.09, and 18.77, vortex shedding frequencies approach the natural resonance frequency of mode 3, so that mode 3 has a bigger contribution to the VIV response. When reduced velocity increases to 21.46, 24.14, and 26.82, vortex shedding frequencies approach the natural frequency of mode 4, so that mode 4 has a big contribution to the VIV response.

Modes from 5 to 10 are relatively high modes. Provided the riser VIV frequencies are near these mode frequencies, the modes have a relatively big contribution to the VIV response. In other words,

higher flow velocities are needed to make high mode vibrations contribute largely to the VIV response. In this test Rn number range, high modes such as from mode 5 to mode 10 have little contribution to the VIV response.

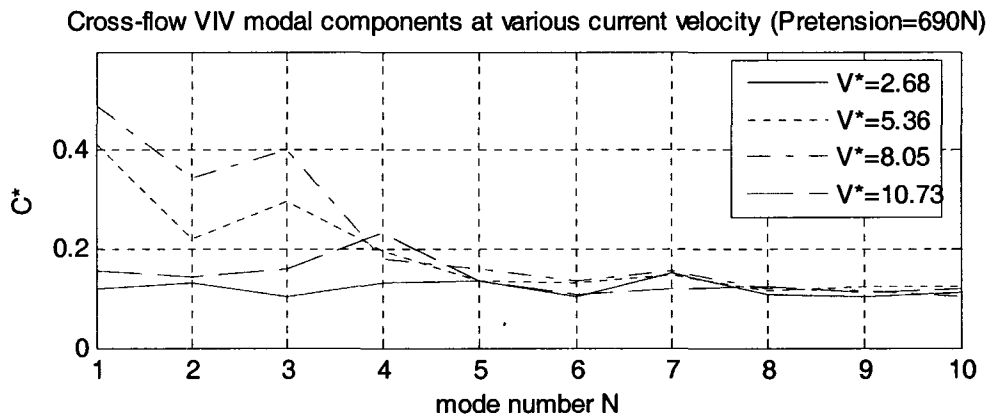


Figure 4-33(a) The cross-flow VIV modal component distribution in shear current produced by a 4 m pipe and reduced velocity from 2.68 to 10.73

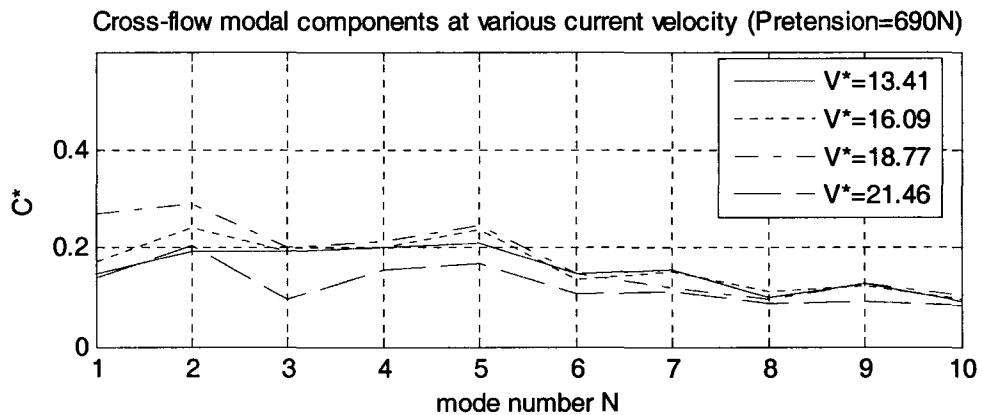


Figure 4-33(b) The cross-flow VIV modal component distribution in shear current produced by a 4 m pipe and reduced velocity from 13.41 to 21.46

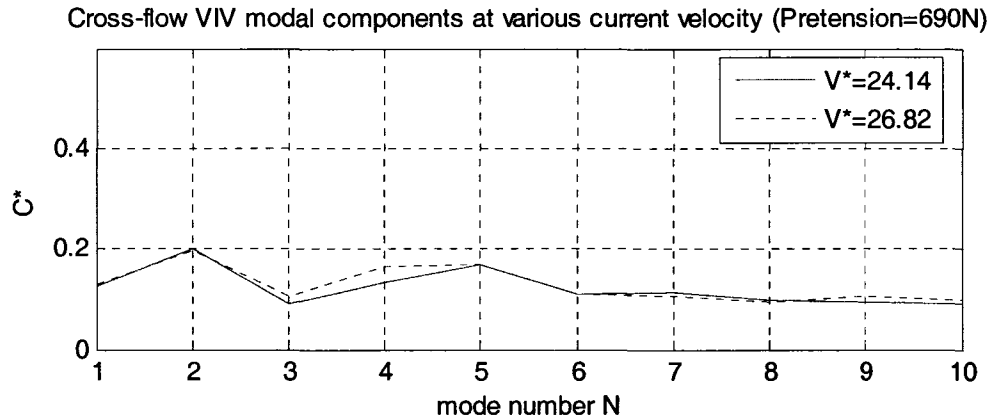


Figure 4-33(c) The cross-flow VIV modal component distribution in shear current produced by a 4 m pipe and reduced velocity 13.41 and 21.46

Figure 4-33 (a), Figure 4-33 (b) and Figure 4-33 (c) show the cross-flow VIV modal component distribution at reduced velocities from 2.68 to 26.82 in shear current produced by the 4 m pipe. The horizontal axes are mode number N and the vertical axes are non-dimensional modal VIV response C^* .

In Figure 4-33, the curve of $V^*=2.68$ is relatively flat. This is because the current velocity is too low so that the vortex shedding frequency is also too low to reach any modal natural frequency. The mode component curve does not have an obvious peak. When reduced velocities attain 5.36 and 8.05, vortex shedding frequencies approach the natural frequency of mode 1; and mode 1 has a relatively big contribution to the VIV response at the two reduced velocities. When reduced velocities increase to 10.73 and 13.41, vortex shedding frequencies do not approach any modal natural frequency again, and the mode component curves become relatively flat. When reduced velocities continue to increase to 16.09 and 26.82, vortex shedding frequencies approach the natural frequency of mode 2, and mode 2 has a bigger contribution to the VIV response at the time. High modes such as mode 5 to mode 10 have little contribution to the VIV response at any reduced velocity.

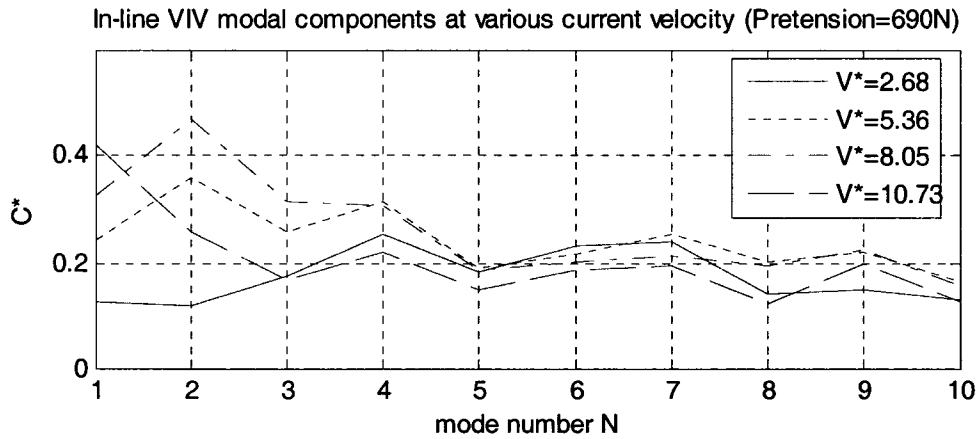


Figure 4-34(a) The in-line VIV modal component distribution in shear current produced by a 3.5 m pipe and reduced velocity from 2.68 to 10.73

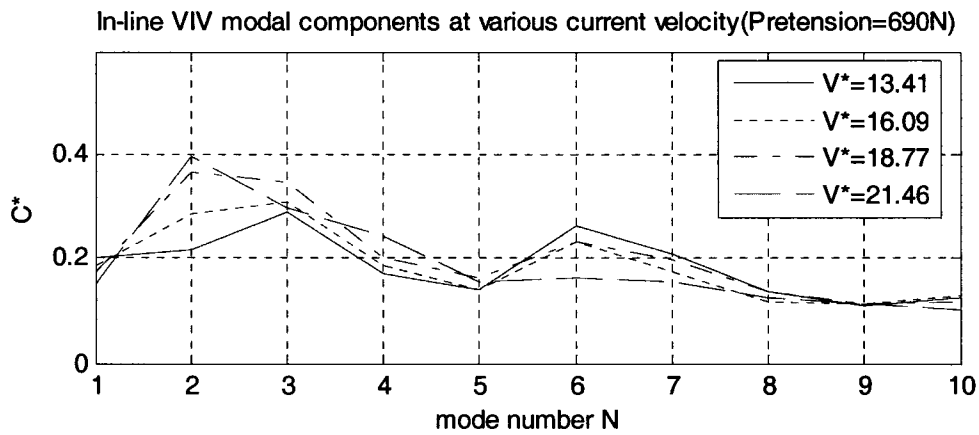


Figure 4-34(b) The in-line VIV modal component distribution in shear current produced by a 3.5 m pipe and reduced velocity from 13.41 to 21.46

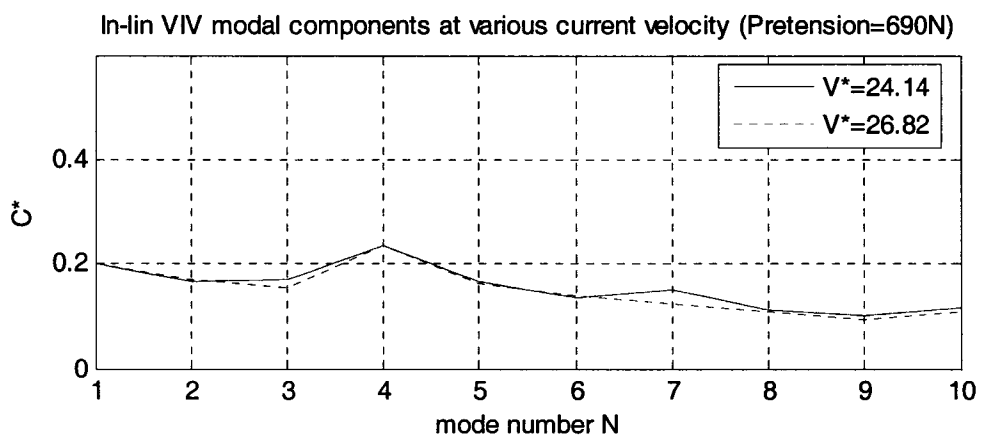


Figure 4-34(c) The in-line VIV modal component distribution in shear current produced by a 3.5 m pipe and reduced velocity 24.14 and 26.82

Figure 4-34 (a), Figure 4-34 (b) and Figure 4-34 (c) display in-line VIV modal component distribution at reduced velocities from 2.68 to 26.82 in shear current produced by the 3.5 m pipe. The horizontal axes are mode number N and the vertical axes are non-dimensional modal VIV response C^* .

In Figure 4-34, the curves of $V^*=2.68$ look relatively flat. This is because the velocity is very low so that the vortex shedding frequency corresponding to the velocity is too low to attain any modal natural frequency. The mode component curve is relatively flat. When the reduced velocity reaches 5.36 and 8.05, Mode 2 has a relatively big contribution to the VIV response. The phenomenon is a result of this particular experiment in sheared current. This is because the vortex shedding force only acts on the top half segment of the riser in this shear current; when velocity is very low, the energy excites a relatively big response for mode 2, and it is not enough to produce the resonance of mode 1, although the vortex shedding frequency approaches the natural frequency of mode 1. When reduced velocity increases to 10.73, mode 1 has a relatively large contribution to VIV response. This means that the energy is enough to excite the resonance for mode 1 at the reduced velocity and the vortex shedding frequency reaches the natural frequency of mode 1.

The vortex shedding frequency approaches a frequency between the natural frequencies of mode 2 and mode 3 when reduced velocity is 16.09 and 18.77. At the two reduced velocities, both mode 2 and mode 3 have a relatively big contribution to the VIV response.

High modes such as mode 5 to mode 10 have little contribution to the VIV response at any reduced velocity.

Cross-flow VIV modal components at various current velocity (Pretension=690N)

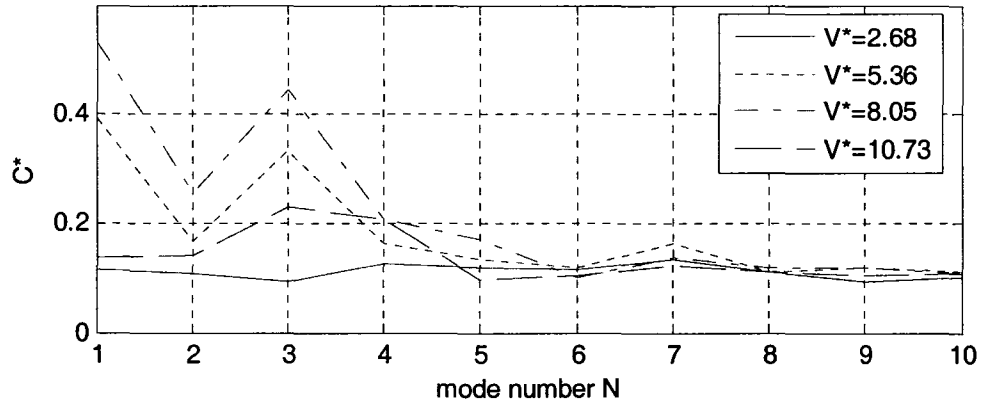


Figure 4-35(a) The cross-flow VIV modal component distribution in shear current produced by a 3.5 m pipe and reduced velocity from 2.68 to 10.73

Cross-flow VIV modal components at various current velocity (Pretension=690N)

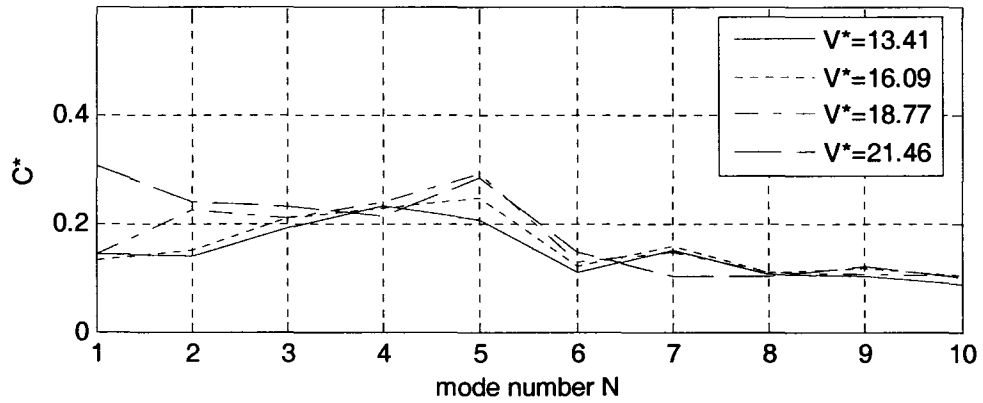


Figure 4-35(b) The cross-flow VIV modal component distribution in shear current produced by a 3.5 m pipe and reduced velocity from 13.41 to 21.46

Cross-flow VIV modal components at various current velocity (Pretension=690N)

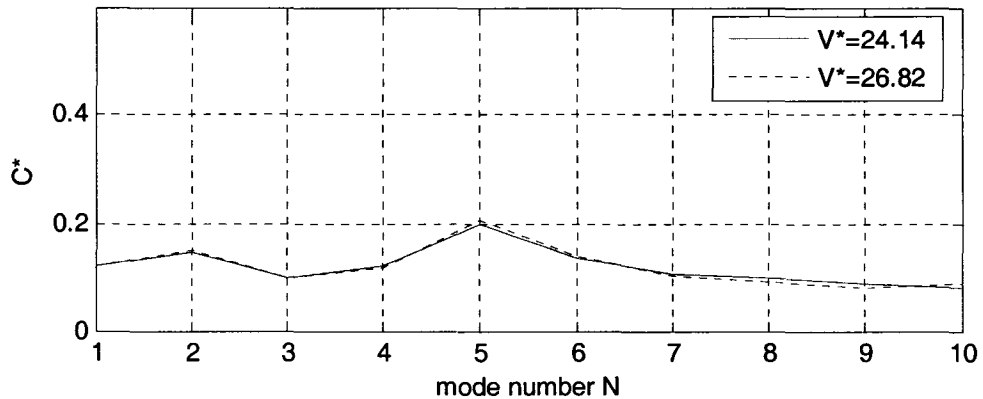


Figure 4-35(c) The cross-flow VIV modal component distribution in shear current produced by a 3.5 m pipe and reduced velocity 24.14 and 26.82

Figure 4-35 (a), Figure 4-35 (b) and Figure 4-35 (c) display the cross-flow VIV modal component distribution at reduced velocities from 2.68 to 26.82 in shear current produced by the 4 m pipe. The horizontal axes are mode number N and the vertical axes are non-dimensional modal VIV response C^* .

In Figure 4-35, the curve of $V^*=2.68$ is relatively flat. This is because the velocity is too low and the vortex shedding frequency which corresponds to the velocity is too low to excite any particular modal natural frequency. The mode component curve does not have an obvious peak. When reduced velocities attain 5.36 and 8.05, vortex shedding frequencies approach the natural frequency of mode 1; and mode 1 has a relatively big contribution to the VIV response at the two reduced velocities. When reduced velocities increase to 16.09 and up, vortex shedding frequencies approach the natural frequency of mode 5; and mode 5 has a relatively big contribution to the VIV response at the time. High modes such as mode 6 to mode 10 have little contribution to the VIV response at any reduced velocity.

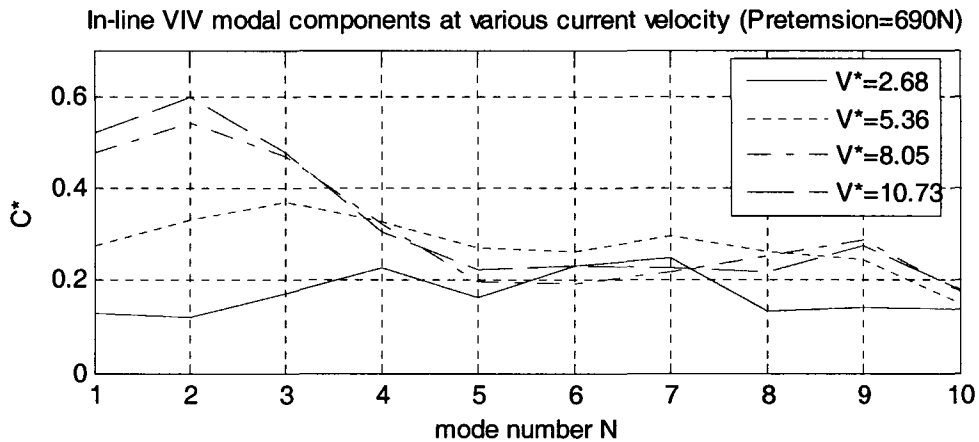


Figure 4-36 The in-line VIV modal component distribution in uniform current and reduced velocity from 2.68 to 10.73

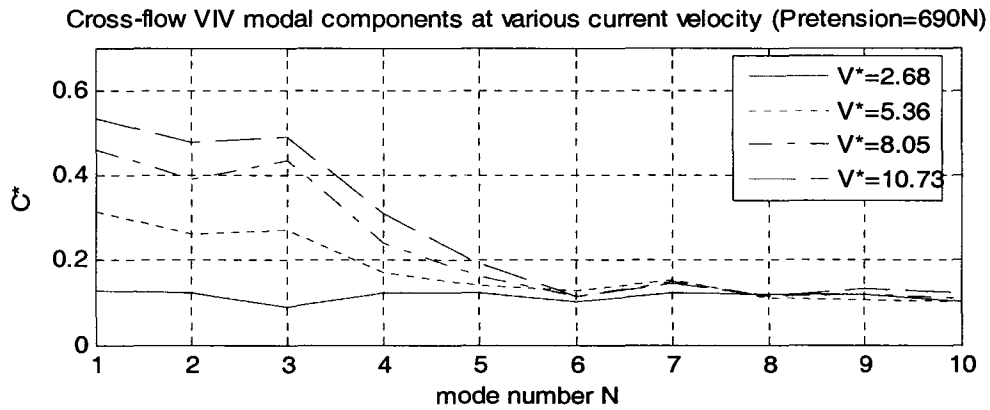


Figure 4-37 The cross-flow VIV modal component distribution in uniform current and reduced velocity from 2.68 to 10.73

Figure 4-36 to Figure 4-37 show the modal components of the in-line and cross-flow VIV responses in uniform current. At reduced velocity $V^*=2.68$, mode 1 to mode 10 contribute to vibration roughly identically. The curve of the modal component looks flat. At reduced velocity $V^*=5.36$, modal component curve of in-line VIV is still flat because vortex shedding frequency does not attain any modal resonance frequency; but the modal component curve of cross-flow VIV has a peak at mode 1. In Figure 4-36, Mode 2 has a big contribution at reduced velocity $V^*=8.05$ and $V^*=10.73$. At the two reduced velocities, Mode 1 has a big contribution as shown in Figure 4-37.

4. 3.2 Modal components vs. current velocity at various modes

From the above VIV modal component distribution figures, the curves in the following figures such as figure 4-38,etc, can be gained making reduced velocity V^* horizontal axes under each mode.

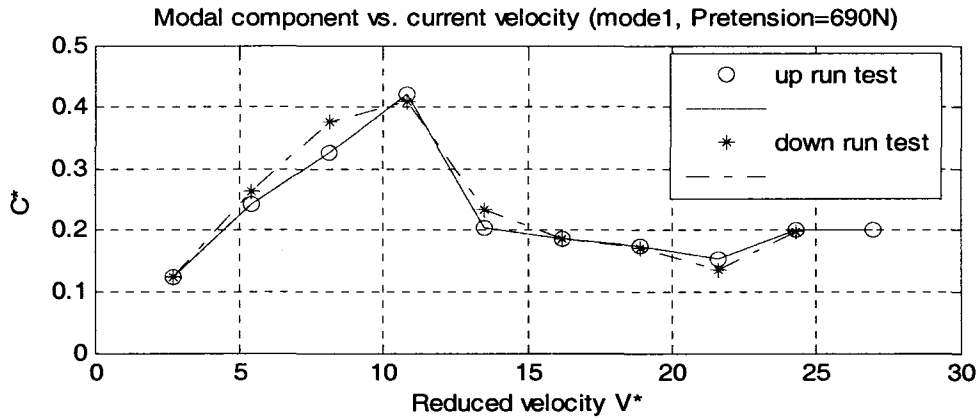


Figure 4-38 The component of in-line mode 1 in shear current produced by a 3.5 m pipe

Figure 4-38 shows the modal response for mode 1 in the in-line direction in shear current produced by the 3.5 m pipe. The pretension is 690N. The horizontal axis is reduced velocity V^* and the vertical axis is non-dimensional modal VIV response C^* . An obvious peak stands at reduced velocity $V^*=10.73$. In other words, at the reduced velocity $V^*=10.73$, the vortex shedding frequency equals the natural frequency of mode 1. Resonance in mode 1 happens. Review Figure 4-34(a), and it is found that mode 1 has the biggest contribution at reduced velocity $V^*=10.73$.

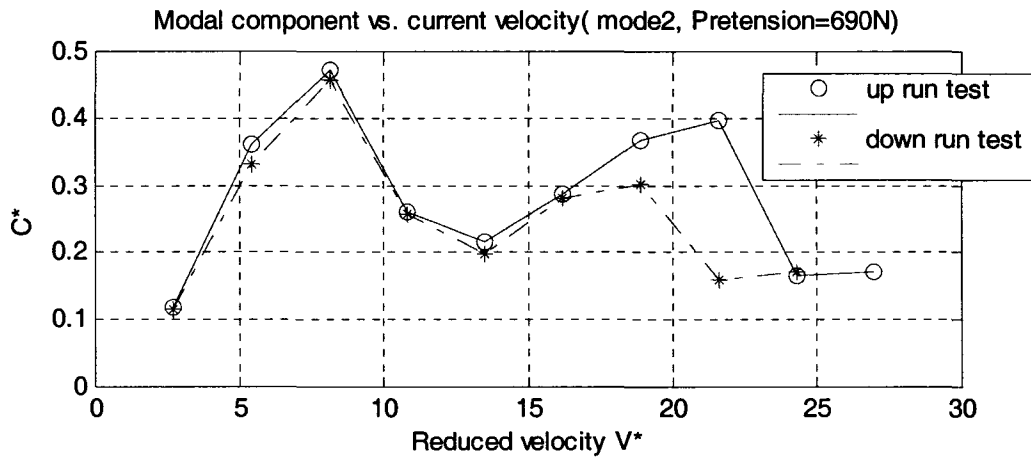


Figure 4-39 The component of in-line mode 2 in shear current produced by a 3.5 m pipe

Figure 4-39 shows the modal response for mode 2 in the in-line direction. At reduced velocity $V^*=8.05$, a peak exists. The peak value C^* is 0.45. Review Figure 4-34(a); and it is found that

mode 2 has the biggest contribution at reduced velocity $V^*=8.05$ although mode 2 is not thought to be in resonance, as discussed for Figure 4-34. Similarly, to Figure 4-39, Figure 4-40 has two peaks at a low velocity and a high velocity. When reduced velocity ranges from 16.09 to 21.46, the peaks in Figure 4-39 and Figure 4-40 imply that vortex shedding frequency is close to the natural frequency of mode 2 and mode 3 so that the two modes have a relatively big contribution to the vibration response.

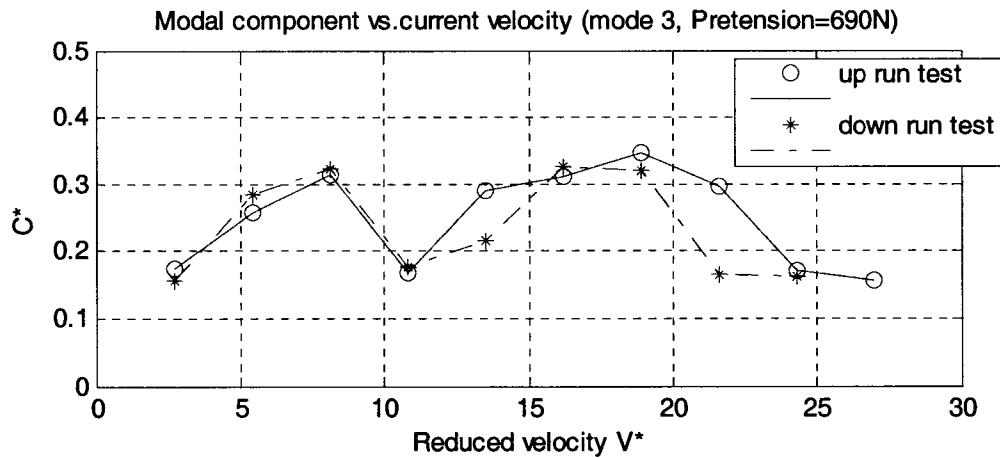


Figure 4-40 The component of in-line mode 3 in shear current produced by a 3.5 m pipe

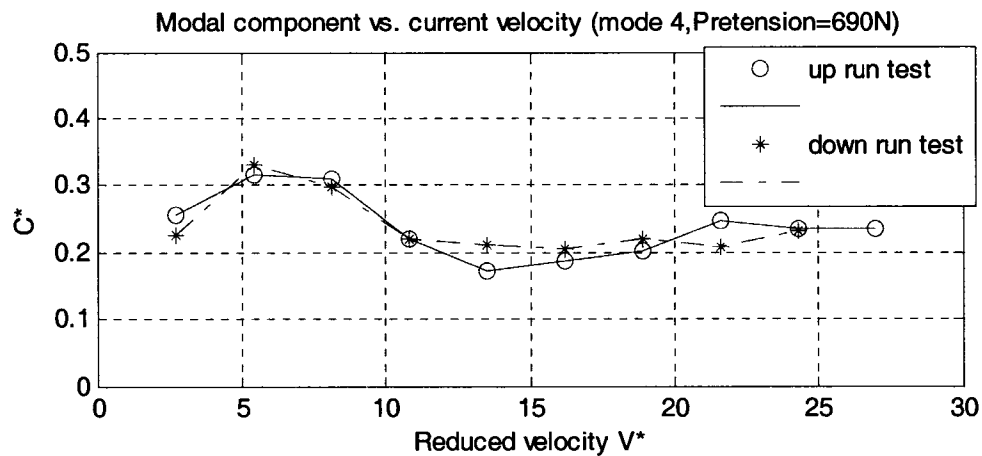


Figure 4-41 The component of in-line mode 4 in shear current produced by a 3.5 m pipe

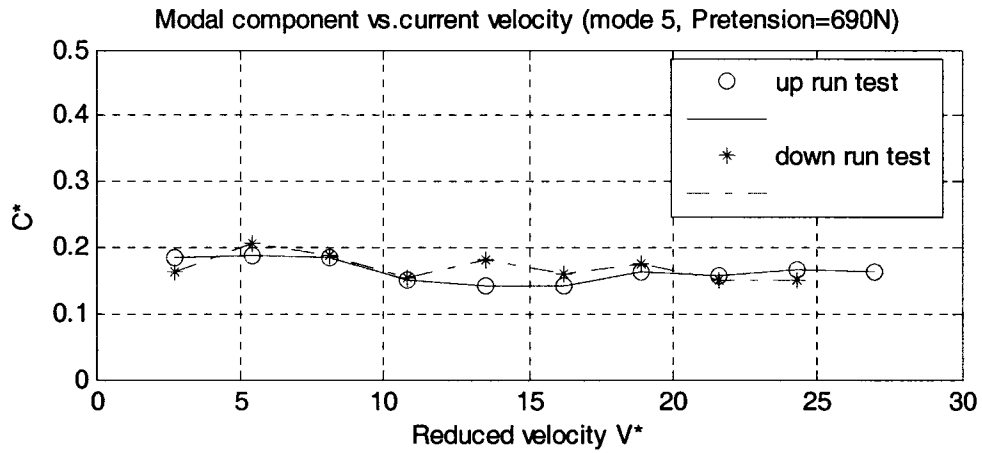


Figure 4-42 The component of in-line mode 5 in shear current produced by a 3.5 m pipe

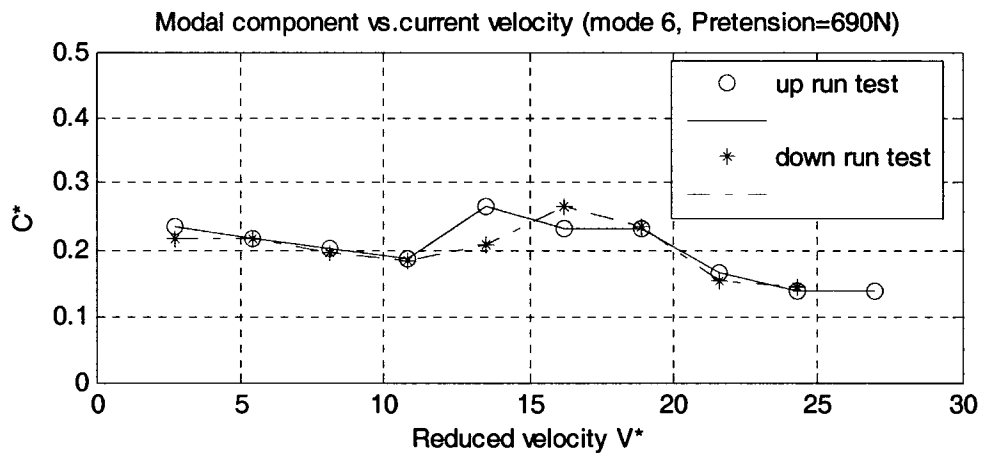


Figure 4-43 The component of in-line mode 6 in shear current produced by a 3.5 m pipe

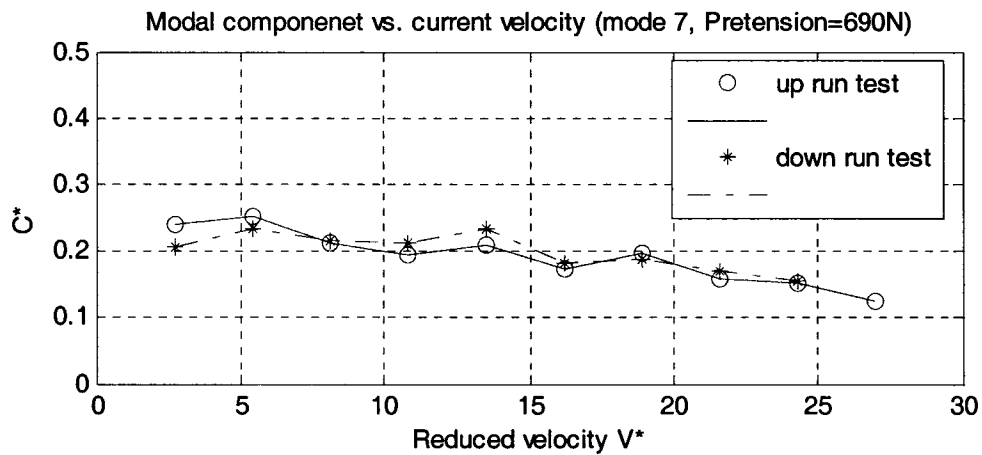


Figure 4-44 The component of in-line mode 7 in shear current produced by a 3.5 m pipe

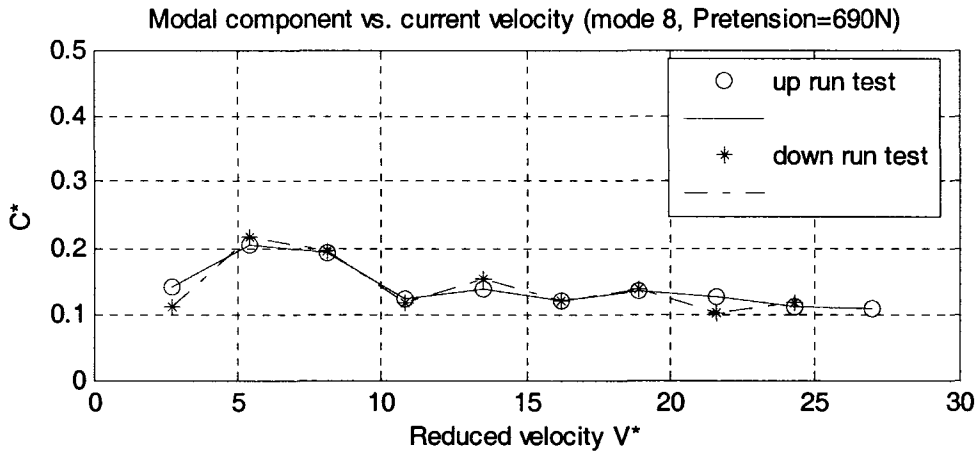


Figure 4-45 The component of in-line mode 8 in shear current produced by a 3.5 m pipe

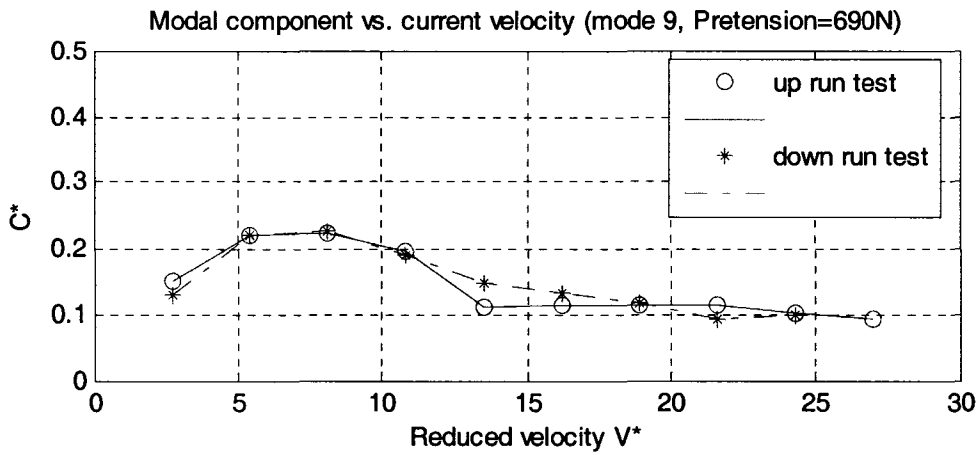


Figure 4-46 The component of in-line mode 9 in shear current produced by a 3.5 m pipe

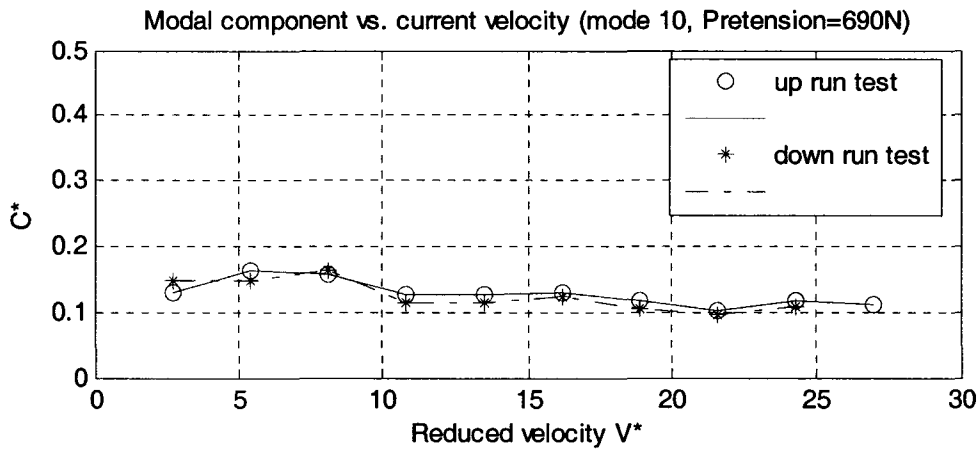


Figure 4-47 The component of in-line mode 10 in shear current produced by a 3.5 m pipe

Figure 4-41 to Figure 4-47 show the high mode component of in-line VIV vs. reduced velocity in shear current. In these figures, the curves are relatively flat; and these high modes have less contribution to the in-line vibration response.

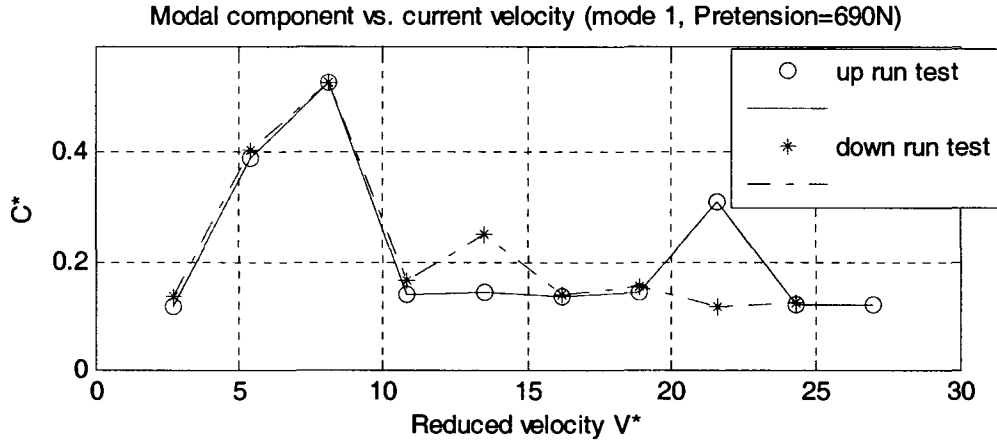


Figure 4-48 The component of cross-flow mode 1 in shear current produced by a 3.5 m pipe

Figure 4-48 shows the modal response for mode 1 in the cross-flow direction in shear current produced by the 3.5 m pipe. The horizontal axis is reduced velocity V^* and the vertical axis is non-dimensional modal VIV response C^* . An obvious peak exists at reduced velocity $V^*=8.05$. Review Figure 4-35(a), and it is found that mode 1 has the biggest contribution at reduced velocity $V^*=8.05$.

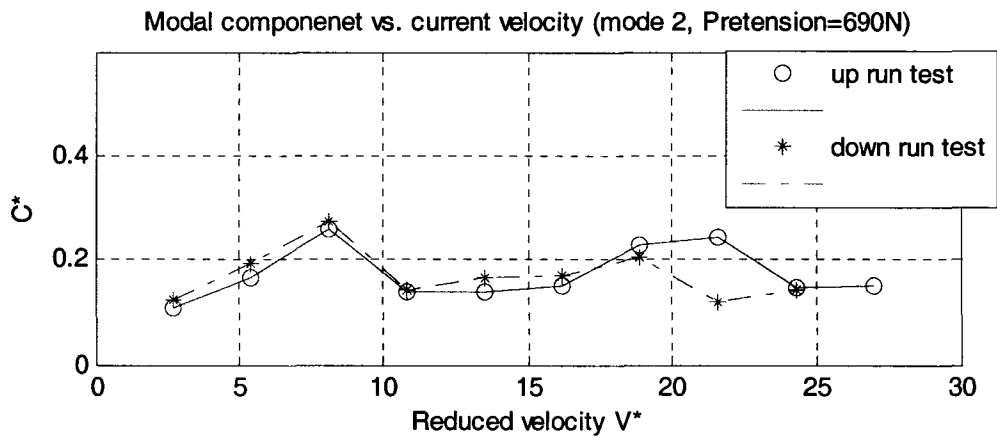


Figure 4-49 The component of cross-flow mode 2 in shear current produced by a 3.5 m pipe

Figure 4-49 shows the modal response for mode 2 in the cross-flow direction in shear current produced by the 3.5 m pipe. The curve is relatively flat. Non-dimensional modal VIV response C^* ranges from 0.15 to 0.25. At any reduced velocity, mode 2 does not provide large contribution to the VIV responses.

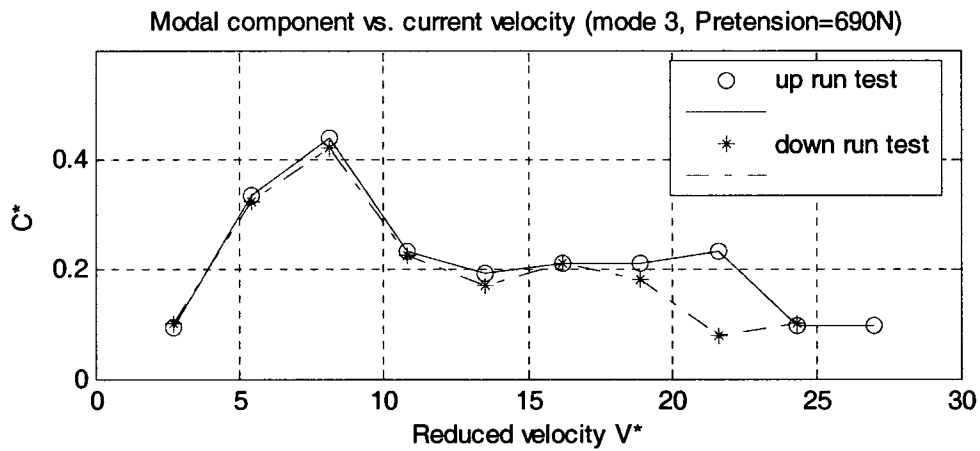


Figure 4-50 The component of cross-flow mode 3 in shear current produced by a 3.5 m pipe
 Figure 4-50 presents the modal response for mode 3 in the cross-flow direction in shear current produced by the 3.5 m pipe. A peak appears at reduced velocity $V^*=8.05$. The peak value C^* is 0.42. Although the resonance mode at the reduced velocity is mode 1, mode 3 also provides a relatively big contribution to the VIV response.

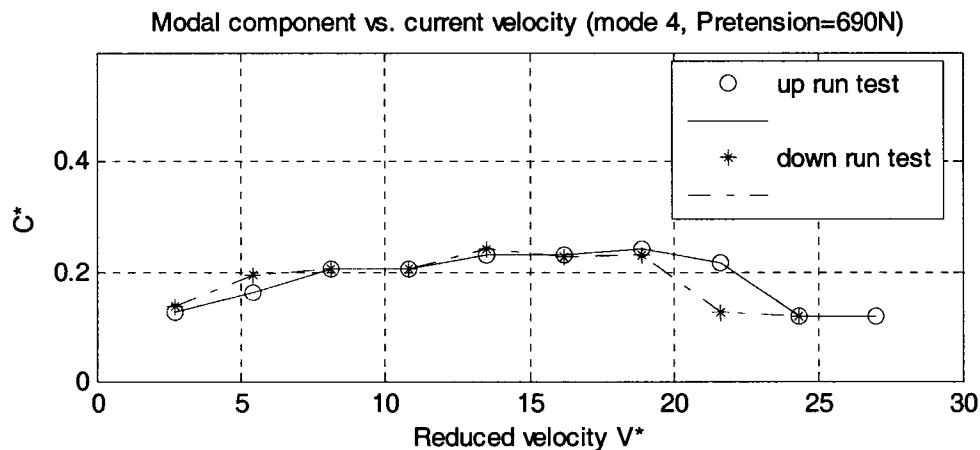


Figure 4-51 The component of cross-flow mode 4 in shear current produced by a 3.5 m pipe

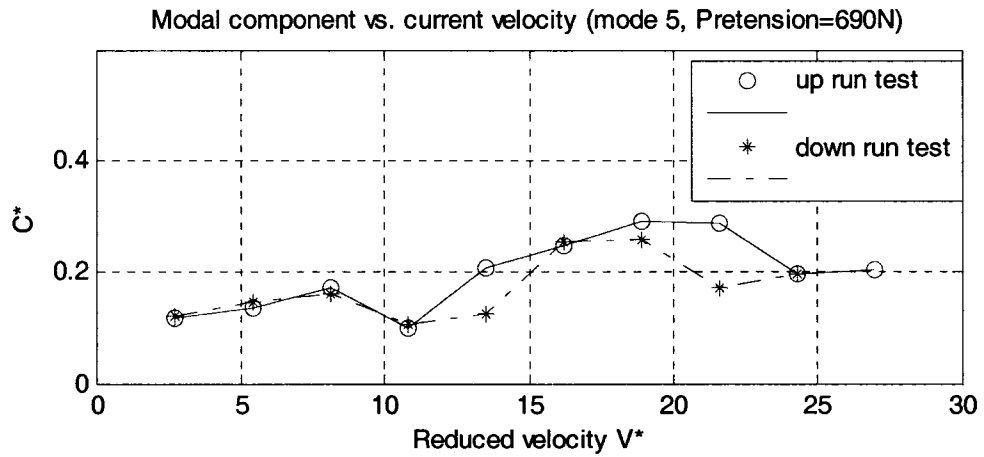


Figure 4-52 The component of cross-flow mode 5 in shear current produced by a 3.5 m pipe

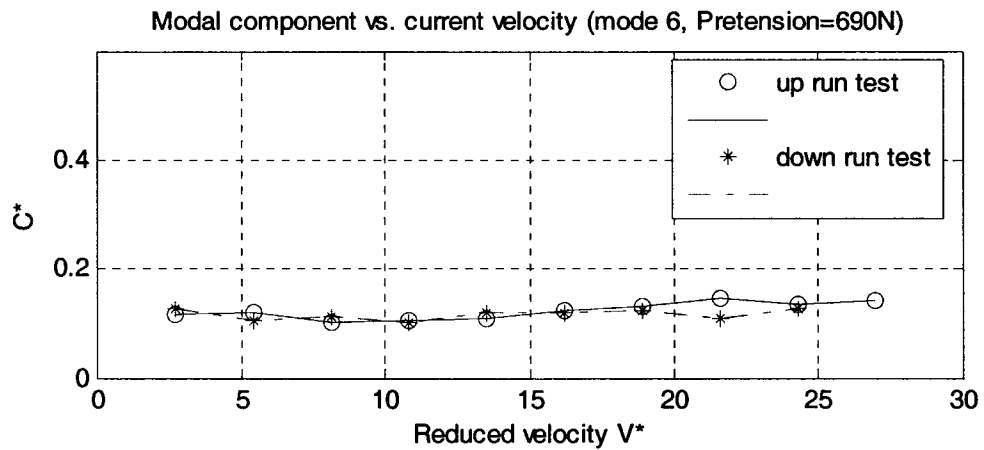


Figure 4-53 The component of cross-flow mode 6 in shear current produced by a 3.5 m pipe

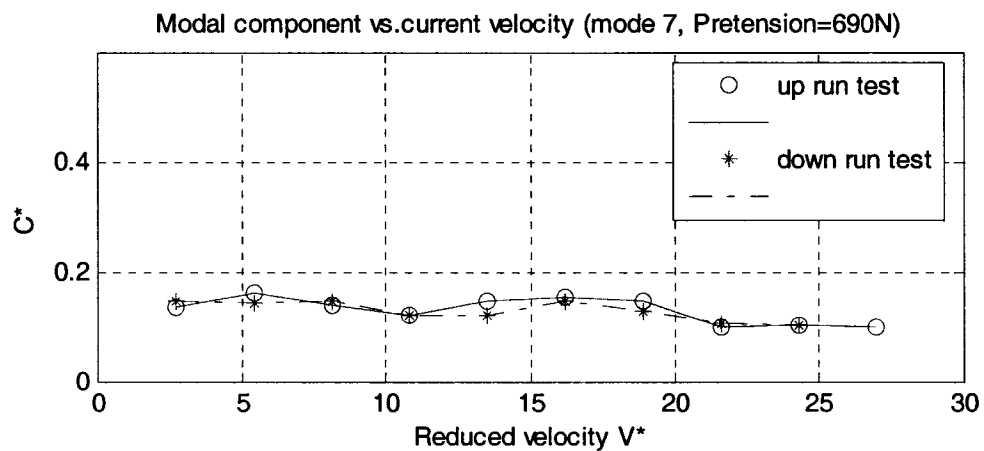


Figure 4-54 The component of cross-flow mode 7 in shear current produced by a 3.5 m pipe

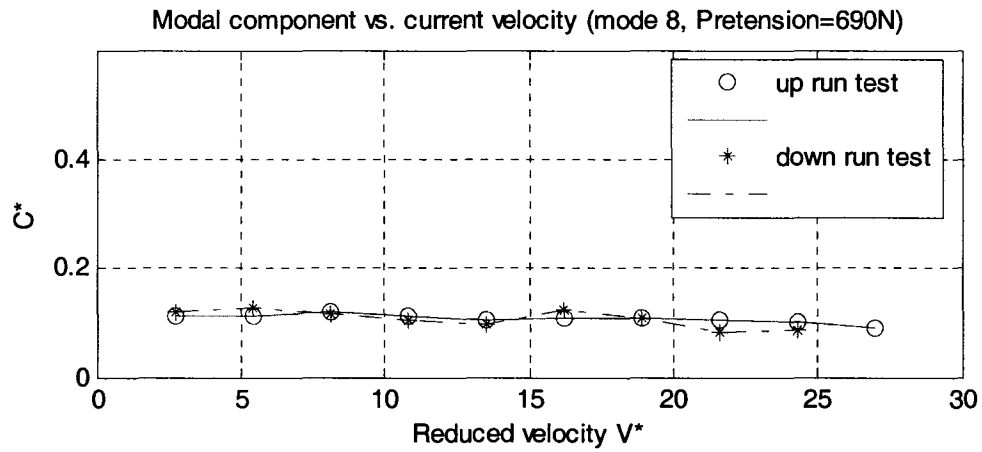


Figure 4-55 The component of cross-flow mode 8 in shear current produced by a 3.5 m pipe

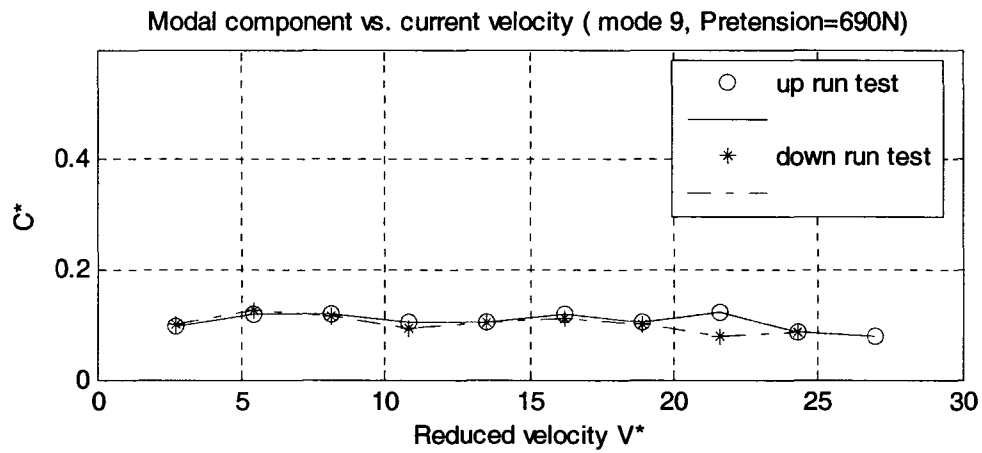


Figure 4-56 The component of cross-flow mode 9 in shear current produced by a 3.5 m pipe

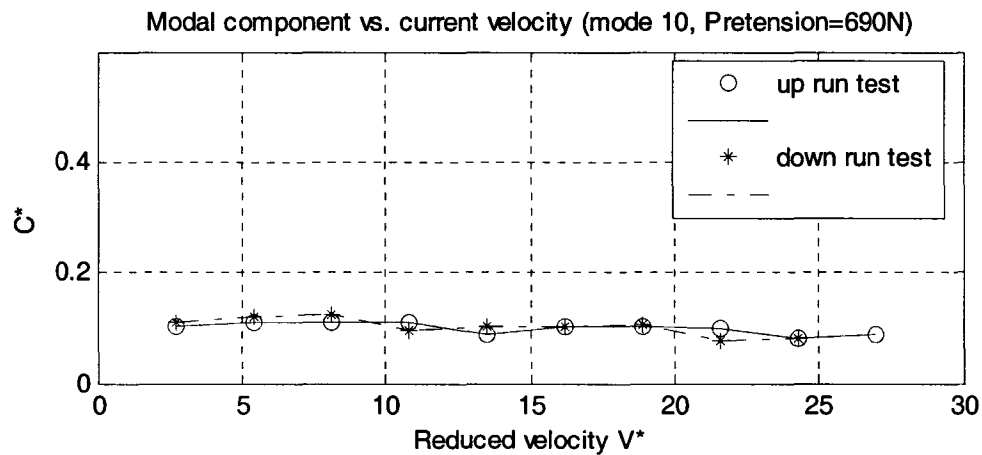


Figure 4-57 The component of cross-flow mode 10 in shear current produced by a 3.5 m pipe

Figure 4-51 to Figure 4-57 show the high mode component of cross-flow VIV vs. reduced velocity in shear current. In these figures, curves are relatively flat. These high modes have less contribution to the in-line vibration response.

4.3.3 Vibration trajectories

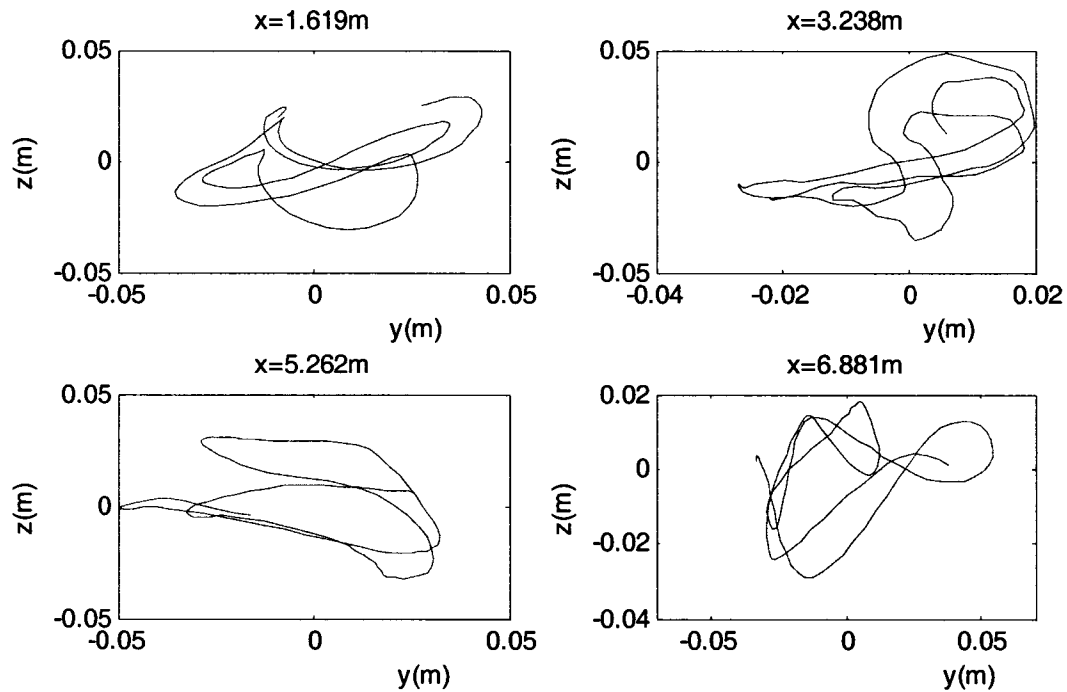


Figure 4-58 Trajectories of VIV under pretension=690 N, shear current produced by 3.5 m pipe, and reduced velocity $V^*=8.05$

Figure 4-58 demonstrates the VIV trajectories on four cross-section planes of the model riser. The four locations are $x=1.619$ m, $x=3.238$ m, $x=5.262$ m, and $x=6.881$ m. The VIV test conditions are that the model is in a shear current produced by the 3.5 m pipe, at pretension=690 N, and reduced velocity $V^*=8.05$. In the figures, the transverse axis (y-direction) indicates the in-line direction; and the vertical axis (z-direction) indicates the cross-flow direction. The units of y-axis and z-axis are metres. These figures show that VIV trajectories at various locations are different. The multi-modal VIV responses do not perform relatively regular trajectories like a single modal VIV response.

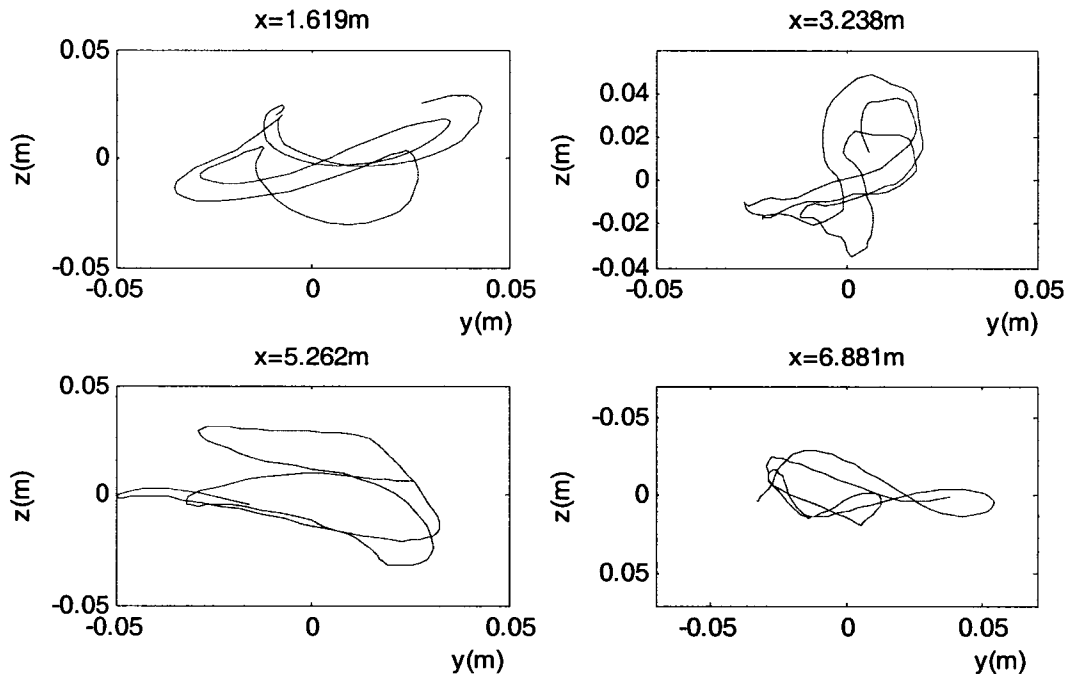


Figure 4-59 Trajectories of VIV under pretension=690 N, shear current produced by a 3.5 m pipe, and reduced velocity $V^*=16.09$

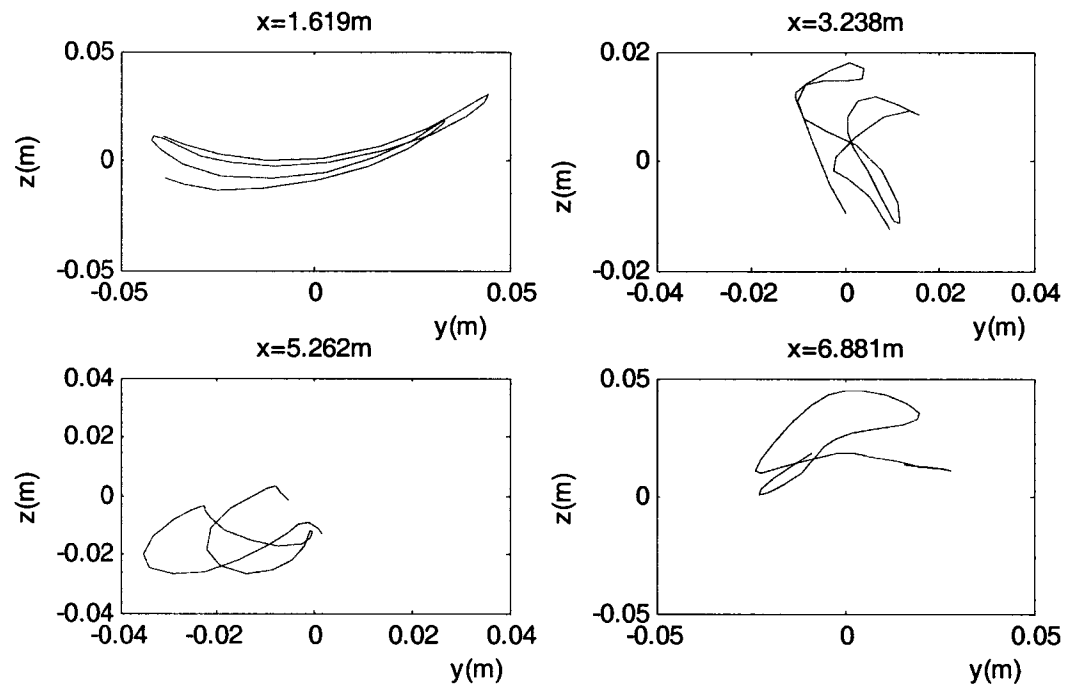


Figure 4-60 Trajectories of VIV under pretension=690 N, shear current produced by a 3.5 m pipe, and reduced velocity $V^*=18.77$

Like Figure 4-58, Figure 4-59 demonstrates the VIV trajectories on the four model riser cross-section planes too. The only difference is the difference of tested reduced velocity. In this case, the reduced

velocity V^* is 16.09. Figure 4-60 shows VIV trajectories at reduced velocity $V^*=18.77$. These trajectories are the record of the model riser motion during two or three periods.

4.4 Tension

Figure 4-61 shows average tensions versus reduced velocity under pretension=690 N in varied current. The average tensions are measured directly by the load cell during the up run tests. In the figure, the transverse axis is reduced velocity and the vertical axis is tension. The vertical axis unit is Newtons.

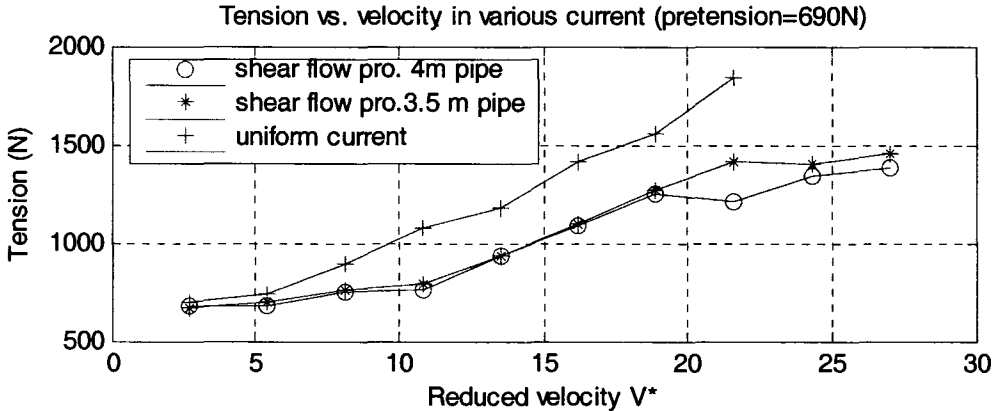


Figure 4-61 Average tension under pretension=690 N in different current

From Figure 4-61, the tension during tests can be found. For example, during the test in shear current produced by the 4 m pipe, the tension varies from 690 N to 1400 N. During the test in a shear current produced by the 3.5 m pipe, the tension varies from 690 N to 1450 N. In uniform current, the tension varies from 690 N to 1800 N. Comparing up run test curves in Figure 4-1, Figure 4-2, and Figure 4-3 with the curves in Figure 4-62, we know that tensions have relatively big values at the reduced velocities corresponding to relatively big VIV amplitudes; for instance, two peaks exist at reduced velocity $V^*=10.73$ and $V^*=16.09$. In figure 4-61, the curve for uniform current rises at the two reduced velocities.

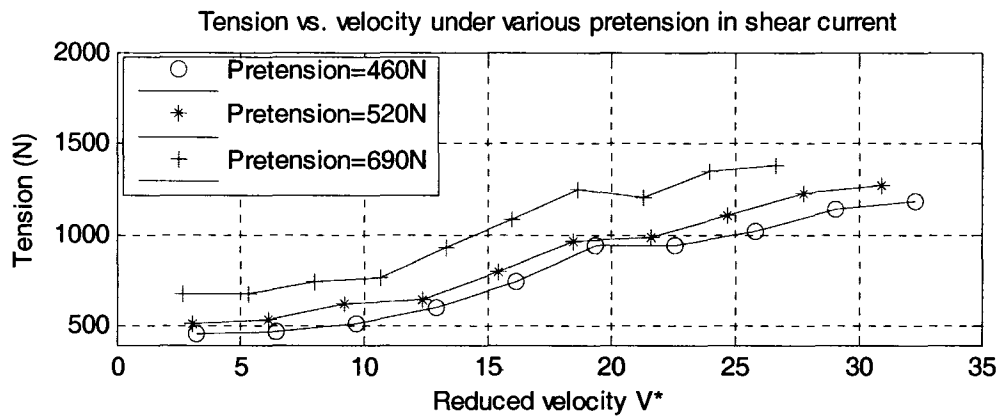


Figure 4-62 Average tension under various pretensions in shear current produced by a 4 m pipe

Figure 4-62 shows average tensions versus reduced velocity under varied pretension in shear current produced by the 4m pipe. In the figure, the transverse axis is reduced velocity and the vertical axis is tension. The vertical axis unit is Newtons. From Figure 4-62, the larger the pretension, the larger the average tension is. For tests in shear current produced by the 4 m pipe, the tension region is from 460 N to 1200 N under pretension=460 N, from 500 N to 1250 N under pretension=520 N, and from 690 N to 1400 N under pretension=690 N.

Figure 4-61 and Figure 4-62 will be a good reference to choose the load cells to measure axial tension in future tests.

4.5 Thirty minute sustained data acquisition test

A thirty minute data acquisition sustained test was carried out in a shear current produced by the 4m pipe at pretension=720 N and current velocity=0.7 m/s. The test purpose is to check on what change the VIV has when the model riser experiences a long current time. Thirty minute times can be divided into 15 time segments of 2 minutes. Table 4-2 shows the relationship between the time segment number and the time segment.

Table 4-3 Time segment number versus time

Time segment number N	Time	Time segment number N	Time
1	From 0 to 2min	9	From 16min to 18min
2	From 2min to 4min	10	From 18 min to 20min
3	From 4min to 6min	11	From 20min to 22min
4	From 6min to 8min	12	From 22min to 24min
5	From 8min to 10min	13	From 24min to 26min
6	From 10min to 12min	14	From 26min to 28min
7	From 12min to 14min	15	From 28min to 30min
8	From 14min to 16min		

The VIV of the thirty minute data acquisition sustained test was checked from two respects: amplitude and frequency. Figure 4-63 and Figure 4-64 present the in-line and cross-flow VIV amplitudes. The transverse axes are time segment number N and the vertical axes are non-dimensional vibration amplitude A^* , which is defined as the average vibration amplitude over the 2 minutes corresponding to time segment number. For example, in Figure 4-63, the A^* value for the first point is 0.42; and it corresponds to time segment number $N=1$, namely the non-dimensional vibration amplitude A^* measured from 0 to 2 minutes is 0.42. From Figure 4-63 and Figure 4-64, no sudden change happens in either in-line or cross-flow amplitude. The standard deviation of these A^* in in-line and cross-flow are respectively 0.009146 and 0.007807.

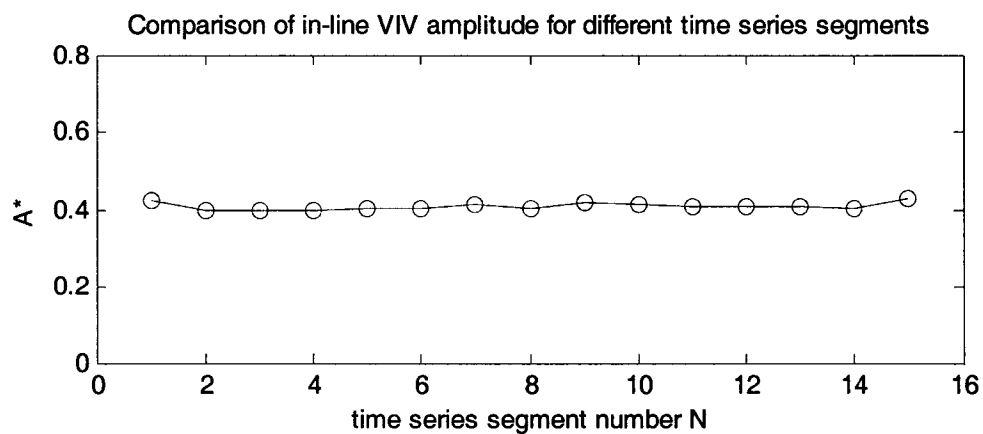


Figure 4-63 Comparison of in-line VIV amplitude of thirty minutes data acquisition sustained test

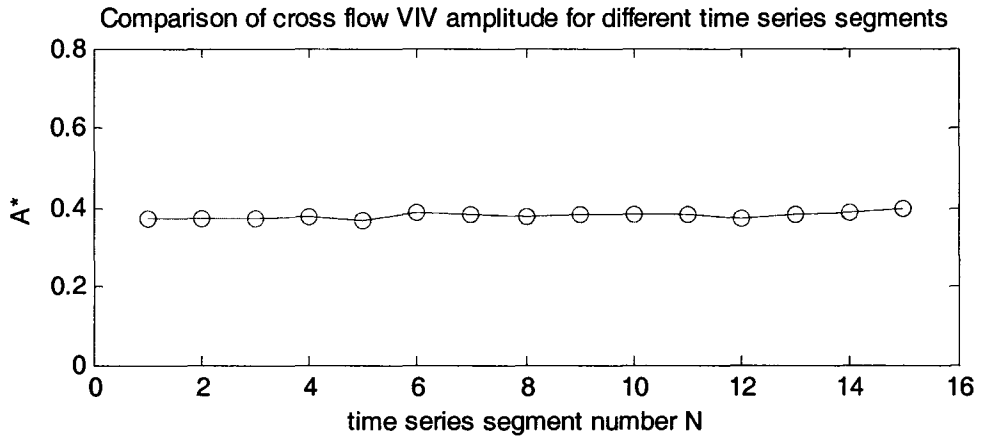


Figure 4-64 Comparison of cross-flow VIV amplitude of thirty minutes data acquisition sustained test

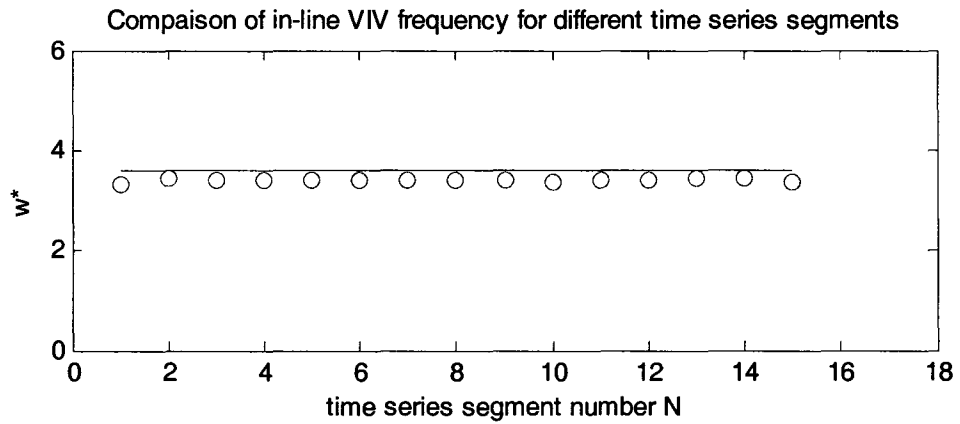


Figure 4-65 Comparison of in-line VIV frequency of thirty minutes data acquisition sustained test

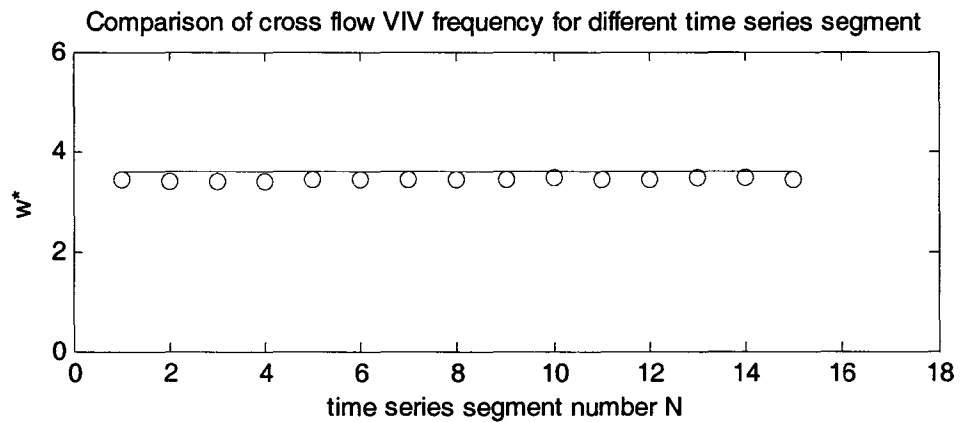


Figure 4-66 Comparison of cross-flow VIV frequency of thirty minutes data acquisition sustained test

Figure 4-65 and Figure 4-66 present the in-line and cross-flow VIV frequencies. The transverse axes are time segment number N and the vertical axes are frequency ratio ω^* . The vertical axis value ω^* denotes the average vibration frequency in the 2 minutes that correspond to time segment number. From Figure 4-65 and Figure 4-66, no sudden change happens in both in-line and cross-flow frequency.

No sudden change occurs in the amplitude and frequency; and this means that the VIV does not change when the model riser experiences a long current time.

Chapter 5

Conclusion

The following conclusions can be extracted from the tests:

1) Reduced velocity corresponding to vibration amplitude peaks remains the same for the different installation methods of the riser. The conclusion is drawn from comparing two uniform tests in the Ice Tank and the Flume Tank.

2) The results of amplitude and frequency from the up run test and the down run test basically coincide, except at a few points where there is a little difference. So-called up run tests indicate the group of tests in which current velocities keep ascending. In contrast, the group tests in which current velocities keep descending are called down run tests;

3) For a flexible riser, in-line and cross-flow peak displacements are basically the same; for example, a $0.5D$ amplitude is the average amplitude in both in-line and cross-flow; but for a rigid riser, in-line and cross-flow vibration amplitudes have different values; for example, $0.4D$ amplitude in in-line and $1.2D$ amplitude in cross-flow. [Chaplin et al., 2004]

4) The curves for the significant amplitude and the average amplitude are parallel. This explains that the ratio between significant amplitude and average amplitude for the same vibration group is one constant.

5) Increasing pretension can cause system stiffness to increase so that VIV amplitude should be reduced. The test results show that increased pretension causes the model resonance to occur at a higher current velocity; and causes the modal resonance to be stronger because of the larger vortex-shedding force at the higher current velocity.

6) At the same position, the amplitude of the in-line and cross-flow VIV versus reduced velocity are different pattern, while the amplitude curves versus reduced velocity in the sheared currents and the uniform flow are similar pattern.

7) Under the Reynolds numbers tested, vortex shedding frequencies for both significant values and average values do not change with current profile and pretension. They are compliant with the Strouhal number fitted curve. No obvious lock-in phenomena was observed in the tests.

8) Observing lock-in phenomena from significant frequency and average frequency, the result is the same. In other words, lock-in phenomena does not appear on the curve of significant frequency and the curve of average frequency simultaneously.

9) From the test results, it is observed that the natural frequency of the riser in uniform current is bigger than that in shear current. This is because the tension in uniform current is bigger than that in shear current, even though the pretensions may be identical.

10) Usually, the vibration power spectrum has a single peak or two close peaks when current velocity is low; while power spectrum has multi-peaks and there are relative big gaps between the peaks when current velocity is high.

11) The vibration power spectrum of different locations over the riser show different values and distribution. The total average value of peak frequencies coincides with the vortex shedding frequency calculated from the Strouhal number.

12) The VIV of the flexible riser is a compound of multiple modes. Every mode has a contribution to the VIV response. When the natural frequency of a mode is approached by the vortex shedding frequency, the mode will have a relatively big contribution to the VIV response. One special situation may occur in the shear current tested; namely, when current velocity is very low, the modal responses for the resonance odd mode may be smaller than those for the non-resonance even mode.

13) The VIV test results of the thirty minute data acquisition sustained test show that no sudden change occurs in the amplitude and frequency, and this means that the VIV is relatively stable when the model riser goes through a long experiment time.

Reference

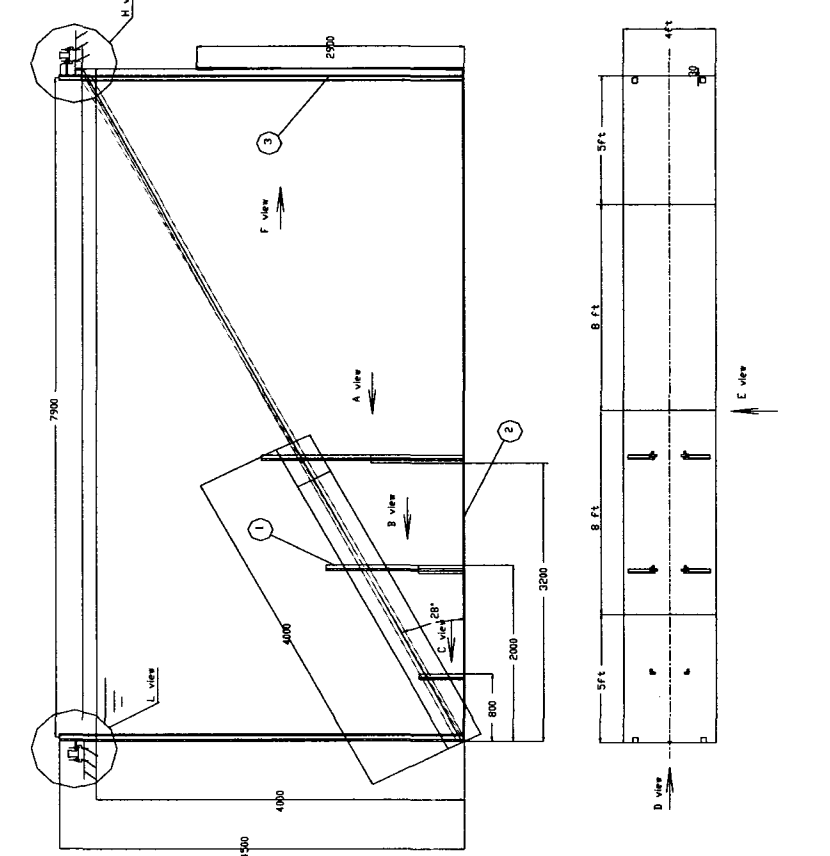
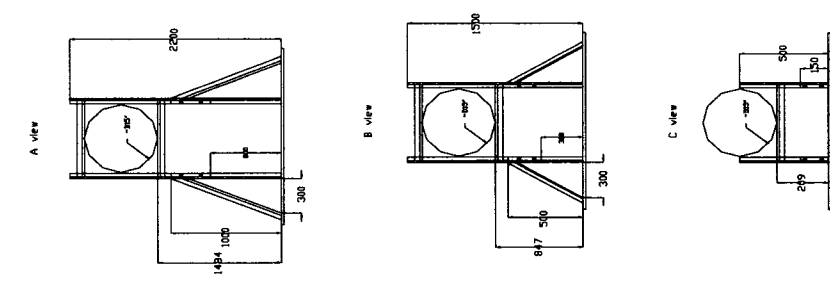
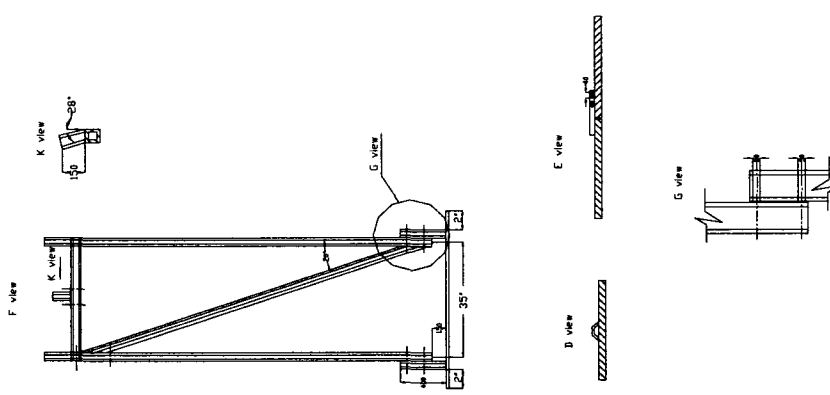
- [1] Allen, D.W. and Henning, D.L.,(2001), Prototype Vortex-induced Vibration Tests for Production Risers, Offshore Technology Conference 2001, Volume 2, OTC13114, pp499-504
- [2] Blevins, Robert D.,(1977), Flow-induced Vibration, Van Nostrand Reinhold Company, New York
- [3] Chaplin, J.R., Bearman, P.W., Huarte, F. J., and Pattenden, R. J.,(2004), Laboratory Measurements of Vortex-induced Vibrations of Vertical Tension Riser in a Stepped Current, Ecole Polytechnique ,Paris, 6-9th July 2004
- [4] Chen, S.S., Cai, Y., and Zhu, S.,(1996), Flow-induced Vibration of Tubes in Cross-Flow, Journal of Offshore Mechanics and Arctic Engineering, Nov.1996, Vol.118, pp253-258
- [5] Clough, R. W., Penzien, J., (1993), Dynamics of Structures, R. R. Donnelley & Sons Company
- [6] Fajarra, A.C., Pece, C.D., and Parra, P.P.H, (1998), Vortex Induced Vibration Experiments on a Flexible Cylinder, Proceedings of the Eighth (1998) International Offshore and Polar Engineering Conference, Montreal, Canada, Vol. III, pp393-399

- [7] Furnes, G K, Hassanein, T, Halse, K H, and Eriksen, M (1998), A Field Study of Flow Induced Vibrations on a Deepwater Drilling Riser, Offshore Technology Conference 98, Volume 2, OTC8702, pp199-208
- [8] Hong, S., Choi, Y. R., Park, J. B., Park, Y. K., and Kim, Y. H., (2001), Experimental Study on the Vortex-induced Vibration of Towed Pipes, Journal of Sound and Vibration, 249(4),pp649-pp661
- [9] Huang, Shan and Hatton, Stephen, Design Considerations of Development Using FPSO's and Flexible Risers in Mild Deep Water, www.2hoffshore.com/papers/docs/pap008.pdf
- [10] Huse, E., Kleiven, G. and Nielsen, F. G.,(1998), Large Scale Model Testing of Deep Sea Risers, Offshore Technology Conference 98, Volume 2, OTC8701, pp189-1197
- [11] Kim, Y.H. and Vandiver, J.K. and Holler, R.A., (1986), Vortex-induced Vibration and Drag Coefficients of Long Cables Subjected to Sheared Flow, Journal of Energy Resources Technology, vol.108, March 1986.
- [12] Li, Xiangqun, (2005), Identification of Linear and Non-linear Multi-Modal VIV Responses for Flexible Deepwater Risers, Ph.D. thesis, Faculty of Engineering and Applied Science, MUN, August 2005.
- [13] Lie, Halvor, Mo, Knot and Vandiver, J.Kim, (1998), VIV Model Test of a Bare- and a Staggered Buoyancy Riser in a Rotating Rig, Offshore Technology Conference 98, Volume 2, OTC8700, pp177-187
- [14] Lie, Halvae, Larsen, Carl M. and Tveit, Øyvind (2001), Vortex-induced Vibration Analysis of Catenary Risers, Offshore Technology Conference 2001, Volume 2, OTC13115, pp511-520

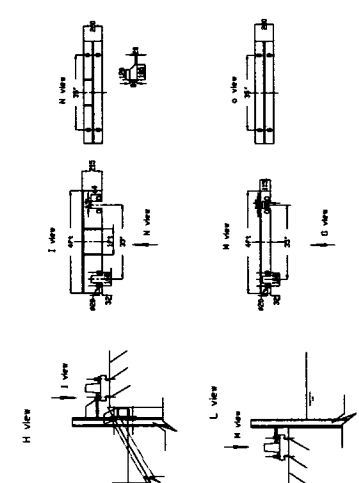
- [15] Marcollo, H. and Hinwood, J.B.,(2005), On Shear Flow Single Mode Lock-in with Both Cross-flow and In-line Lock-in Mechanisms, *Journal of Fluids and Structures*, Vol.2, issue 2, pp197-211
- [16] Sarpkaya, T., (1979), Vortex-induced Oscillations: A Selective Review, *J. Appl. Mech.* 46 (2) pp241–258.
- [17] Tim. J. Hearn, (2005), Addresses the Calgary Chamber of Commerce, http://www.imperialoil.ca/Canada-English/News/Speeches/N_S_Speech051006.asp
- [18] Vandiver, J.K., Allen, D., and Li, L. (1996), The Occurrence of Lock-in Under Highly Sheared Conditions, *Journal of Fluids and Structures*, Vol. 10, pp555-561
- [19] Vandiver, J.Kim and Chung, Tae Young, (1989), Predicted and Measured Response of Flexible Cylinders in Shear Flow, ASME Winter Annual Meeting Symposium on Flow-induced Vibration, Chicago, December 1989.
- [20] Wilde, J.J de and Huijsmans, R.H.M,(2001), Experiment for High Reynolds Numbers VIV on Riser, Proceeding of Eleventh (2001) International Offshore and Polar Engineering Conference, Stavanger, Norway, Vol.111 pp400-405

Appendix A

Design Draw for Experiment Apparatus



No.	Item	Size	Quantity	Weight	Notes
1	Angle	L3x2 1/2x1/4"			steel
2	Plate	3/8" thickness			steel
3	Trailing	312x1/4			steel



Appendix B

Strain Calculation for Experiment Apparatus

Strain calculation for supporting frame

1. pipe drag force

$$f_{d1} = \left(\frac{1}{2} \rho C_d Du^2 + \frac{1}{4} \pi \rho C_m D^2 a\right) \times L / 3$$
$$= (0.5 \times 1000 \times 1.1 \times 0.38 \times 1^2 + 0.25 \times 3.14 \times 1000 \times 1.5 \times 0.38^2 \times 0.1) \times 4 / 3$$
$$= (209 + 17) \times 4 / 3 = 298(N)$$

2. supporting frame drag force

$$f_{d2} = \left(\frac{1}{2} \rho C_d Du^2 + \frac{1}{4} \pi \rho C_m D^2 a\right) * L$$
$$= (0.5 \times 1000 \times 2.1 \times 0.08 \times 1^2 + 0.25 \times 3.14 \times 1000 \times 2.5 \times 0.08^2 \times 0.1) \times 4 \times \sin(28^\circ)$$
$$= (84 + 1.256) \times 2 = 171(N)$$

3. moment

$$M = (f_{d1} + f_{d2})l = (298 + 171) \times 1.1 / 2 = 258(N.m)$$

4. force and stress acting on vertical pole

$$F = M / d = 258 / 0.4 = 645(N)$$
$$\sigma_1 = F / A_1 = 645 / 0.00037 = 1.74 \times 10^6(N / m^2)$$

Strain calculation for supporting ear

1. steel plate weight

$$W_1 = LBh\rho = 8 \times 1.22 \times 0.0095 \times 7.8 \times 1000 \times 9.81 = 7094.8N$$

2. supporting pole weight

$$W_2 = L\rho = 4.4 \times 6 \times 13.14 \times 9.81 = 4065N$$

3. pipe weight

$$W_3 = 150 \times 9.81 = 1471N$$

4. supporting frame weight

$$W_4 = L\rho = 18 \times 7.32 \times 9.81 = 1292N$$

5. total weight

$$W = W_1 + W_2 + W_3 + W_4 = 13922.8(N)$$

6. shear stress

$$\sigma_2 = W / (lh) = 13922.8 / (0.007 \times 0.01271) = 156488704(N / m^2)$$

Appendix C

Detail derivation of formulae

According to similarity theory and Equation (3-10), the following equations can be obtained:

$$\left. \begin{aligned} \left[\frac{f_{k0}}{\rho g L D^2} \right]^{(m)} &= \left[\frac{f_{k0}}{\rho g L D^2} \right]^{(p)} \\ \left[\frac{\omega}{\omega_{nk}} \right]^{(m)} &= \left[\frac{\omega}{\omega_{nk}} \right]^{(p)} \\ \left[\frac{A_k}{\rho L D^2} \right]^{(m)} &= \left[\frac{A_k}{\rho L D^2} \right]^{(p)} \\ \left[\frac{B_k}{\rho L D \omega z_0} \right]^{(m)} &= \left[\frac{B_k}{\rho L D \omega z_0} \right]^{(p)} \end{aligned} \right\} \quad (C-1)$$

The last equation of $f_{k0} = \frac{2L}{k\pi} f_0$ in Equation (3-8) is substituted into the first equation in Equation (C-1), and the following equation can be obtained:

$$\left[\frac{\frac{2L}{k\pi} f_0}{\rho g L D^2} \right]^{(m)} = \left[\frac{\frac{2L}{k\pi} f_0}{\rho g L D^2} \right]^{(p)}$$

namely

$$\left[\frac{f_0}{k \rho g D^2} \right]^{(m)} = \left[\frac{f_0}{k \rho g D^2} \right]^{(p)}$$

Substitution of the last equation of $f_0 = \frac{1}{2} \rho C_1 D U^2$ in Equation (3-3) into the above equation gives

$$\left[\frac{\frac{1}{2} \rho C_1 D U^2}{k \rho g D^2} \right]^{(m)} = \left[\frac{\frac{1}{2} \rho C_1 D U^2}{k \rho g D^2} \right]^{(p)}$$

Simplify the above equation, and the following equation can be obtained:

$$\left[\frac{C_1 U^2}{D} \right]^{(m)} = \left[\frac{C_1 U^2}{D} \right]^{(p)} \quad (C-2)$$

Substituting Equation (3-9) into the second equation in Equation (C-1) yields

$$\left[\frac{\omega}{\sqrt{\frac{k_b \left(\frac{k\pi}{L}\right)^4 + T \left(\frac{k\pi}{L}\right)^2}{m_s + \frac{\pi}{4} \rho C_m D^2}}} \right]^{(m)} = \left[\frac{\omega}{\sqrt{\frac{k_b \left(\frac{k\pi}{L}\right)^4 + T \left(\frac{k\pi}{L}\right)^2}{m_s + \frac{\pi}{4} \rho C_m D^2}}} \right]^{(p)}$$

namely

$$\left[\frac{\omega \sqrt{m_s + \frac{\pi}{4} \rho C_m D^2}}{\frac{k\pi}{L^2} \sqrt{k_b (k\pi)^4 + TL^2}} \right]^{(m)} = \left[\frac{\omega \sqrt{m_s + \frac{\pi}{4} \rho C_m D^2}}{\frac{k\pi}{L^2} \sqrt{k_b (k\pi)^4 + TL^2}} \right]^{(p)}$$

Substituting the first equation of $A_k = \frac{L}{2} (m_s + \frac{\pi}{4} \rho C_m D^2)$ in Equation (3-8) into the above equation leads to

$$\left[\frac{\omega L^2 \sqrt{\frac{2A_k}{L}}}{k\pi \sqrt{k_b (k\pi)^4 + TL^2}} \right]^{(m)} = \left[\frac{\omega L^2 \sqrt{\frac{2A_k}{L}}}{k\pi \sqrt{k_b (k\pi)^4 + TL^2}} \right]^{(p)}$$

or

$$\left[\frac{\omega D L^2 \sqrt{\frac{2A_k}{\rho L D^2}}}{k\pi \sqrt{\rho k_b (k\pi)^4 + TL^2}} \right]^{(m)} = \left[\frac{\omega D L^2 \sqrt{\frac{2A_k}{\rho L D^2}}}{k\pi \sqrt{\rho k_b (k\pi)^4 + TL^2}} \right]^{(p)}$$

Substituting the third equation in Equation (C-1) into the above equation and simplifying it, the following equation can be obtained:

$$\left[\frac{StUL^2}{\sqrt{\rho k_b (k\pi)^4 + TL^2}} \right]^{(m)} = \left[\frac{StUL^2}{\sqrt{\rho k_b (k\pi)^4 + TL^2}} \right]^{(p)} \quad (C-3)$$

Substituting the first equation of $A_k = \frac{L}{2}(m_s + \frac{\pi}{4}\rho C_m D^2)$ in Equation (3-8) into the third equation in equation (C-1) yields

$$\left[\frac{\frac{L}{2}m_s + \frac{\pi}{8}\rho C_m LD^2}{\rho LD^2} \right]^{(m)} = \left[\frac{\frac{L}{2}m_s + \frac{\pi}{8}\rho C_m LD^2}{\rho LD^2} \right]^{(p)}$$

Simplify above equation, and the following equation can be obtained:

$$\left[\frac{m_s}{\rho D^2} + \frac{\pi C_m}{4} \right]^{(m)} = \left[\frac{m_s}{\rho D^2} + \frac{\pi C_m}{4} \right]^{(p)} \quad (C-4)$$

Substituting the second equation of $B_k = \frac{L}{2}(c_s + \frac{1}{\pi}\rho C_d D\omega z_0)$ in Equation (3-8) into the last equation in Equation (C-1) leads to

$$\left[\frac{Lc_s + \frac{L}{2}\rho C_d D\omega z_0}{2\rho LD\omega z_0} \right]^{(m)} = \left[\frac{Lc_s + \frac{L}{2}\rho C_d D\omega z_0}{2\rho LD\omega z_0} \right]^{(p)}$$

Simplify the above equation; the following equation can be obtained:

$$\left[\frac{c_s}{2\rho StUz_0} + C_d \right]^{(m)} = \left[\frac{c_s}{2\rho StUz_0} + C_d \right]^{(p)} \quad (C-5)$$



